htw saar

Nils Kleiber

Conception, modelling and dimensioning of an energy storage system for wind energy with hydro accumulators

Metropolia University of Applied Sciences &

htw saar University of Applied Sciences

Double Degree Programme

Bachelor of Engineering

Industrial Management

Bachelor's Thesis

Supervisor: Prof. Dr. Dirk Hübner

23 March 2020

Abstract

Humankind currently faces an unstoppably increasing energy demand and scarcity of resources. The associated problems of climate change and global warming have intensified the role of renewable energies, especially of wind energy, in today's energy supply. However, a critical disadvantage of renewables is their intermittent availability, which complicates the reliability of supply. As a result, energy storage technologies have become more and more important in recent times to overcome periods, when renewables do not provide power to the electrical grid.

Among the various storage methods, a research team at the University of Applied Sciences of Saarland focuses on a particularly sustainable and environmentally friendly storage solution: The decentralised storage of excess wind energy with pressurised air. Here, purely pneumatic (i.e. compressed air energy storage, CAES) and hydraulic-pneumatic storage systems are considered simultaneously. Both systems are designed, dimensioned and modelled in separate scientific studies for the research project by ensuring comparability. This work deals with the hydraulic-pneumatic approach whereby hydro accumulators are utilised to store the surplus energy.

Within the research scope, important theoretical and physical basics are illustrated for the storage concept. A first approach is provided for the dimensioning of the hydro accumulator system, which can serve as a starting point for the design of a prototype. For the dimensioned storage system, several basic models are created and simulated for evaluation and comparison purposes with the software tool AMESim. The simulation results are consistent with the outcome of the dimensioning and allow first statements about the system's efficiency and performance. The comparison with the purely pneumatic system shows that achievable energy densities of hydraulic accumulators are much lower. However, CAES systems have to challenge comparably high thermal losses during the storage process. Hydraulic accumulators are therefore most likely to achieve better efficiencies, which CAES systems could only achieve by laboriously reusing the waste heat. At the current research stage, more precise statements cannot be made, since idealised conditions have been assumed for initial simulations. For this reason, the scientific paper is structured in a way that the research team can use the provided models and collected data as a foundation for further investigations and optimisations.

Keywords: Hydro Accumulator, Energy Storage, Renewable Energy, AMESim

Table of contents

I. List of figures

II. List of tables

III. List of abbreviations

CAES	Compressed Air Energy Storage
CO_2	Carbon Dioxide
CVT	Continuously Variable Transmission
DC	Direct Current
DCV	Directional Control Valve
ESS	Energy Storage System(s)
FES	Flywheel Energy Storage
LIA	Lithium-Ion Accumulators
LOHC	Liquid Organic Hydrogen Carriers
MGB	Mechanical Gear Box
P2G	Power to Gas
PHES	Pumped Hydro Energy Storage
PHS	Pumped Hydro Storage
PRV	Pressure Relief Valve
SMES	Superconducting Magnetic Energy Storage
SNG	Synthetic Natural Gas
TES	Thermal Energy Storage
WESSPA	Wind Energy Storage System with Pressurised Air

IV. List of symbols

Symbol	Meaning	Unit
A	area, cross section	m^2; mm^2
C_{Li}	capacity of the liquid	$m^3/(N/m^2)$; l/bar
c_v	specific heat capacity	J/kgK
d	diameter	m; mm
E	bulk modulus	N/m^2; bar
E	Energy	J; kWh
f	frequency	1/s; Hz
h	height	m; mm
m	mass	kg
n	polytropic exponent	-
n	rotational speed	1/min; rev/min
p	pressure	Pa; N/m^2; bar
Δp	pressure difference, operating pressure	Pa; N/m^2; bar
P	power	W
Q	volume flow, flow rate	m^3/s; l/min
Q_H	thermal energy	J; kWh
R	gas constant	J/kgK
r	radius	m; mm
Re	Reynolds number	-
T	temperature	K
T	torque	Nm
t	time	s
U	internal energy	J; kWh
V	volume	m^3; l; cm^3
V_D	volumetric displacement	m^3/rev; cm^3/rev
ΔV	volume difference, effective volume	m^3; l; cm^3

Symbol	Meaning	Unit
v	specific volume	m^3/kg
v	average flow velocity	m/s
W'	volumetric energy density	kWh/m^3
W_c	charged energy	J; kWh
W_{diss}	dissipation work	J; kWh
W_{to}	total work	J; kWh
W_v	volumetric change work	J; kWh
z	compressibility factor	-
α	gear ratio	-
α_D	flow coefficient	-
α_g	heat transfer coefficient	W/m^2K
β	compressibility coefficient	m^2/N; 1/bar
η	efficiency	-
η	dynamic viscosity	Pa·s; Ns/m^2; cP
κ	isentropic exponent	-
ν	kinematic viscosity	m^2/s; mm^2/s
ω	angular velocity	1/s
π_{opt}	optimum pressure ratio	-
ρ	density	kg/m^3
τ	thermal time constant	s
θ	temperature	K

1 Introduction

1.1 Background – Energy demand & climate change

The earth is in a phase of rapid change. The population density of humans is increasing rapidly and the worldwide demand for energy with it. In Germany, the total energy demand for electricity in 2018 was 599TWh. To get an impression, with around 83 million inhabitants (Statistisches Bundesamt 2019), this corresponds to an annual per capita electricity demand of 7217kWh. Considering the primary energy consumption, i.e. additionally the energy consumption and losses of industry, traffic, trade and the energy sector itself, the primary energy consumption amounts to 2500TWh in 2018 (Hartbrich 2020). Europe-wide, around 18000TWh of primary energy was consumed in 2018 (Eurostat 2018).

Somehow, these immense amounts of energy must be produced. Conventional energy sources, such as coal, oil or nuclear power, fall out of favour due to their poor environmental footprint and restricted availability. However, with a share of 81.1% (2018) they still constitute a major part of the energy mix in Europe (Eurostat 2020). Therefore, humankind competes with the increasing energy demand, which in the near future can no longer be covered by conventional energy sources. This competition has a direct influence on the Earth's climate.

For this reason, climate change is one of the central issues of our time. The abatement of greenhouse gas emissions and other harmful environmental influences is omnipresent. Environmental activists, such as the movement “Fridays for Future” and the consumer trend towards “green” products, highlight society’s growing environmental awareness (UBA 2019a). At the same time, politicians attempt to reduce the influence of humanity on the ecological balance by adopting comprehensive packages of measures such as the "European Green Deal". The aim is to make Europe the first continent to become climate-neutral by 2050 (European Commission 2019, p. 2). In response, today’s industry tries to meet the changing consumer interests and the more stringent requirements by a strategical orientation towards sustainability. In this context, the electrification of the automotive sector is one of the major topics. However, there is a general acknowledgement that the energy transition, needed to curb climate change, is lagging behind at the present time.

The serious impact of the climate change on the Earth’s ecosystem cannot be denied. In 2019, the average temperature of 10.3°C was the second highest record in Germany since 1881 (Kaspar & Friedrich 2020). The European climate change service “Copernicus” recently declared the January 2020 the warmest January in Europe compared to

the 1981-2010 average (Euronews 2020). Overall, the global average temperature rises continuously (UBA 2019b). Direct consequences are, in particular, melting polar caps and rising sea levels. Weather extremes, such as droughts and floods, are becoming more frequent and do not only threaten the biodiversity and the habitat of thousands of animals and plants, but also humanity's life quality. A current example are the bush fires that have raged in Australia since September 2019 due to extreme drought and heat. The uncontrollable flames destroyed 12 million hectares of land, killed at least 29 people and forced millions to billions of animals to death (Tagesschau.de 2020).

The previously described situation has led to an increasing international interest in decarbonisation and therefore to a strong focus on renewable energies in recent decades. Comparing, for instance, the share of renewable energies in the energy mix in Germany in 2000 and 2017, it can be stated that the share had more than quintupled, from 6% to around 33%. According to the Renewable Energy Sources Act, 40 to 45 per cent of the electricity consumed in Germany should come from renewable energy sources by 2025 (FMEAE 2020). The figure below illustrates the German energy mix for gross electricity generation in 2017.

Figure 1: Gross electricity generation (in TWh) in Germany in 2017

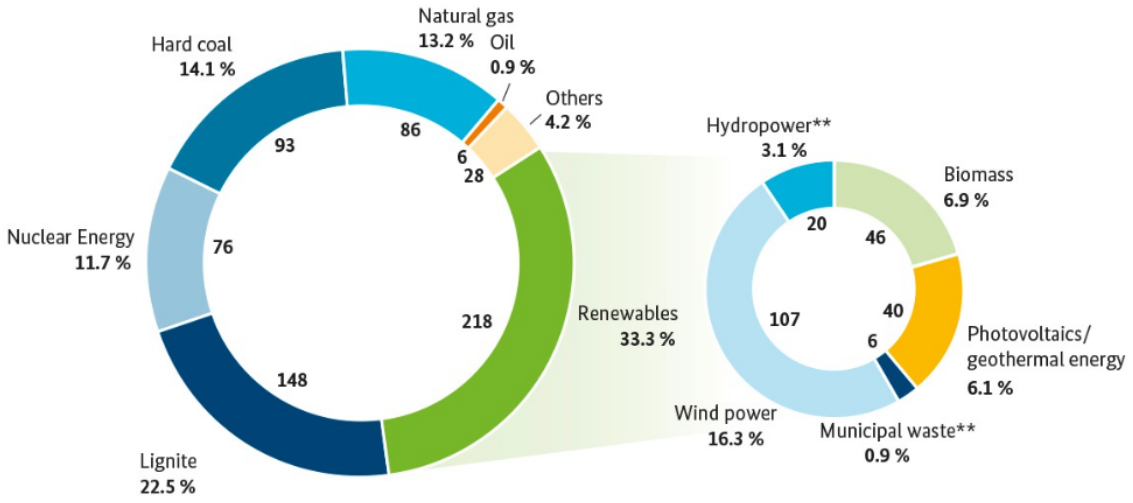

The share of geothermal energy is very low and therefore included in the share of PV
*preliminary figures, **regenerative part

Source: FMEAE last updated 2018

Having a closer look on the renewables, it can be seen that wind energy takes a crucial role in the energy transition with a total share of 16.3%. This is due to its abundant, free, and environmentally friendly characteristics.

In 2018, wind turbines already provided around 110TWh of energy, with 90.5TWh generated onshore and 19.5TWh generated offshore (FMEAE 2020). But also other renewables, like photovoltaics, experience a steep upward trend in shares in the energy portfolio. A similar positive development can be observed in other countries around the world, like China, Japan and Scandinavian countries, in order to sustainably cover future energy requirements. Nevertheless, the increasing energy supply through renewable sources is accompanied by difficulties.

The electrical grid needs to be operated on a delicate balance between demand and supply (EPA 2018). According to a spokesperson of the VGB Powertech Service GmbH in a report of the VDI newspaper, grid stability is only provided, when power generation covers the electricity demand *completely and continuously* (Wilming 2019, pp. 12-13). The consumer's power demand varies considerably within the day. That is why conventional power plants are designed to be capable of supplying peak-time demands and therefore operate with a security buffer on an adjustable constant rate (Shnaid, Weiner & Brokman 1996, p. 5). However, renewable energies are never available continuously, they are characterised by fluctuation and intermittency. Consequently, the power supply becomes more variable and thus more complex by increasing the share of renewables. The key challenge in the energy transition is to control this variability. To accomplish this, the electricity grid requires high flexibility, i.e. matching fluctuating generation with fluctuating demand in real time (ISEA 2012, p. 1). This flexibility can be provided by integrating energy storage systems (ESS) into the power transmission system. They are capable of storing amounts of energy during times of high availability and feed it back into the grid when renewable energy supply is low. Consequently, energy storage technologies will play a major role to keep the balance in the energy market and to challenge the issues of climate change and rising energy demands.

For this reason, the team of the research project "WESSPA" at the University of Applied Sciences of Saarland (htw saar) is looking for environmentally friendly solutions to store surplus wind energy decentralised. Within this framework, this scientific paper deals with the following task.

1.2 Task and motivation of this scientific paper

As part of the research project WESSPA, this work deals with the conception, modelling and dimensioning of a storage system for wind energy with hydro accumulators. Consequently, performed tasks during the scientific work are the following.

In the first step, a comprehensive research on the existent energy storage solutions, including their characteristics and working principles, provides important information regarding the current state of technology. The second chapter comprises fundamental knowledge concerning the hydro accumulator system and concept to be able to understand the subsequent simulations. Therefore, the basics of hydraulics, the working principle, types and application areas of hydro accumulators, the underlying thermodynamics of the energy storage process as well as the remaining hydraulic system components are examined. After this common knowledge base is built, the key components of the storage system are dimensioned according to a defined framework. The outcome is used as a basis to model and simulate the hydro accumulator system with the software tool AMESim. The results are documented, evaluated and compared with the findings of Jan Molter's scientific work, which deals with the purely pneumatic system.

The goal is to receive first insights in the storage's performance characteristics, technical feasibility and potential areas of application in the renewable energy sector. Moreover, the thesis provides important basic knowledge concerning the hydro accumulator technology. The results can be used in further steps of the WESSPA project including, for instance, the construction of a prototype and the investigation of experimental setups. The contribution to the development of an innovative storage solution to tackle the multi-layered problems, which were illustrated in the first part of the introduction, is the prior motivation of the author.

1.3 Research project WESSPA

The abbreviation “WESSPA“ is an acronym for "Wind Energy Storage System with Pressurized Air". Therefore, the research project at htw saar is dedicated to the development of (hydro-) pneumatic ESS, especially, for the application in wind turbines. The initial idea is to modify the unused space in the tower of the wind turbine to a local storage reservoir for air. The air is compressed either with compressors or by integrating hydraulic components. After that, it gets stored and is used on demand to drive a generator to produce electricity in the final step (Hübner 2019, p. 2).

The project is being carried out in cooperation with a working group of the htw saar (consisting, inter alia, of Prof. Dr.-Ing. Dirk Hübner and Prof. Dr.-Ing Frank Ulrich Rückert), Dr. Karsten Kühn (Festo Lernzentrum Saar GmbH), the "Institut Physikalische Prozess Technik" (htw saar) and the "WI Institut" (htw saar). The project is scheduled in several stages. The initial phase, at the time of this thesis, comprises the conception, modelling and comparison of different WESSPA concepts using the software AMESim. In the second step, the most promising storage concept will be realised in a prototype. It will be analysed and measured in combination with a prototype of a wind turbine which is currently under construction. The measurements will be carried out in the wind tunnel of the htw saar. Based on these data, a profitability analysis will be conducted and the practicability in large-scale applications will be investigated. The results of the project will be documented and published in form of a scientific work (Hübner 2019, pp. 8-9).

To tackle the theoretical and practical questions, the project is mainly executed at the wind laboratory of the htw saar. Particularly, the 75KW “Göttinger wind tunnel”, which has been installed in 2015, plays an important role for the examination of the prototype (Labor Windenergietechnik htw saar n.d). With it, detailed data can be obtained in realistic settings, which can then be compared with the previous simulations results. Figure 2 illustrates the initial idea of the research project as well as the wind tunnel.

As already mentioned in the task section, this thesis investigates the energy storage by utilising hydro accumulators. For this reason, the labelled components, responsible for energy conversion and recovery, vary depending on the storage concept (cf. Figure 2). For example, in case of a hydro accumulator system, hydraulic components like a pump or a hydraulic motor would replace the pneumatic engine.

Figure 2: WESSPA concept and wind tunnel at htw saar

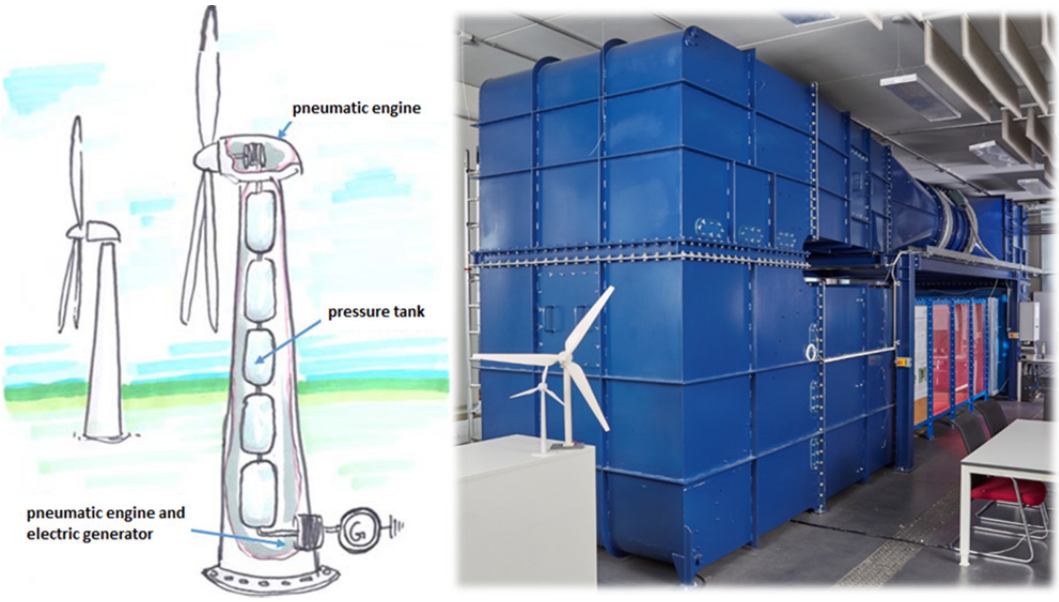

Source: Hübner 2019, p. 7 & Labor Windenergietechnik htw saar n.d.

1.4 State of energy storage technologies

Energy storage represent the process of energy conversion from mostly electrical energy to a storable form, reserving it in various mediums and converting it back into electrical energy when needed (Luo et al. 2015, p. 511). To guarantee a proper evaluation of ESS, the following question needs to be answered: “What characterises good energy storage solutions?” Despite their ability to smooth supply fluctuations, good ESS should operate on a long-lasting and sustainable base. The aim is not only to produce “green” energy but also to store this energy environmentally friendly. High efficiencies of the storage system, quick response times, adequate energy to power ratio, as well as a good storage capability, defined by energy and power density, are other indicators for attractive storage solutions (Sabihuddin, Kiprakis & Mueller 2015, pp. 175-176; ISEA 2012, pp. 10-11). In the best case, the installation and operation happens on low maintenance and costs. Further, decentralised utilisation, e.g. coupling the storage technology directly to the wind turbine, improves the interaction between renewables and the grid (Bocklisch 2014, p. 63).

Because of that, ESS have multiple value propositions by offering a subset of supportive activities. For instance, the storage technology can provide frequency or voltage control when fluctuations endanger the system’s balance. After a system failure, the ESS can provide energy to restart the system (black start capability). Furthermore, peaks can be shaved and loads can be levelled through the utilisation of ESS (European Commission 2017, pp. 6-7; ISEA 2012, pp. 4-5). These so called *ancillary services*, i.e. all services needed to ensure the integrity and the stability of the electrical grid, can increase the overall systems efficiency (ISEA 2012, p. 3).

There is already a large number of different ESS in use and under development today. Basically, they can be distinguished by the type of energy that is stored (e.g. mechanical, chemical, electrical energy). Figure 3 illustrates a possible classification scheme of known storage solution at the present time.

Figure 3: Classification of energy storage technologies

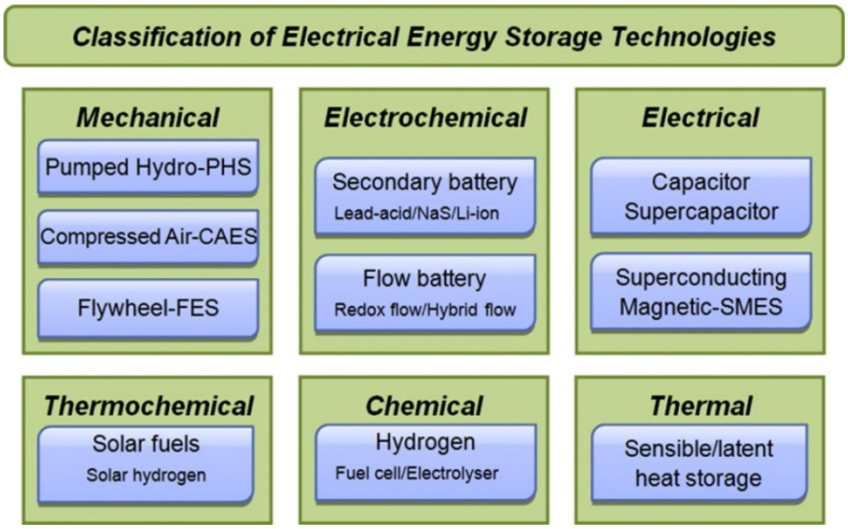

Source: Luo et al. 2015, p. 514

According to the International Renewable Energy Agency (IRENA), the total installed storage worldwide was approximately 176 gigawatts (GW) of power in 2017. Almost half (48%) of it was installed in only 3 countries – China (32.1 GW), Japan (28.5 GW) and the United States (24.2 GW). Among this, Pumped Hydro Storage (PHS) still has by far the largest share with 169 GW, accounting for 96% of the total power capacity (2017, pp. 21&29). To get an understanding of the different storage concepts, a technology brief is provided in the following section.

Mechanical Energy Storage

Pumped Hydro Energy Storage (PHES), already commercialised in the 1890s, is the most mature large-scale ESS. Energy is stored as gravitational potential energy by pumping water between two reservoirs with different heights (IRENA 2017, p. 50). Having a long lifetime and reasonable efficiency (70-80%), the main application areas for PHES are bulk energy storage and energy shift during peak and off-peak periods (Rehman, Al-Hadhrami & Alam 2015, pp. 588-589). Detrimental is, however, the low energy density and more important the geographical dependence as well as the serious interference with nature (IRENA 2017, p. 52; ISEA 2012, p. 19). Moreover, increasing shares of renewables force the conventional PHS to become less rigid. Recently, the Max Bögl Wind AG, for instance, integrated water reservoirs into wind parks as a pilot project in Germany, having a storage capacity of 70 MWh, in order to provide flexible and decentralised grid support (Max Bögl 2017).

Figure 4: Working principle of mechanical energy storage technologies

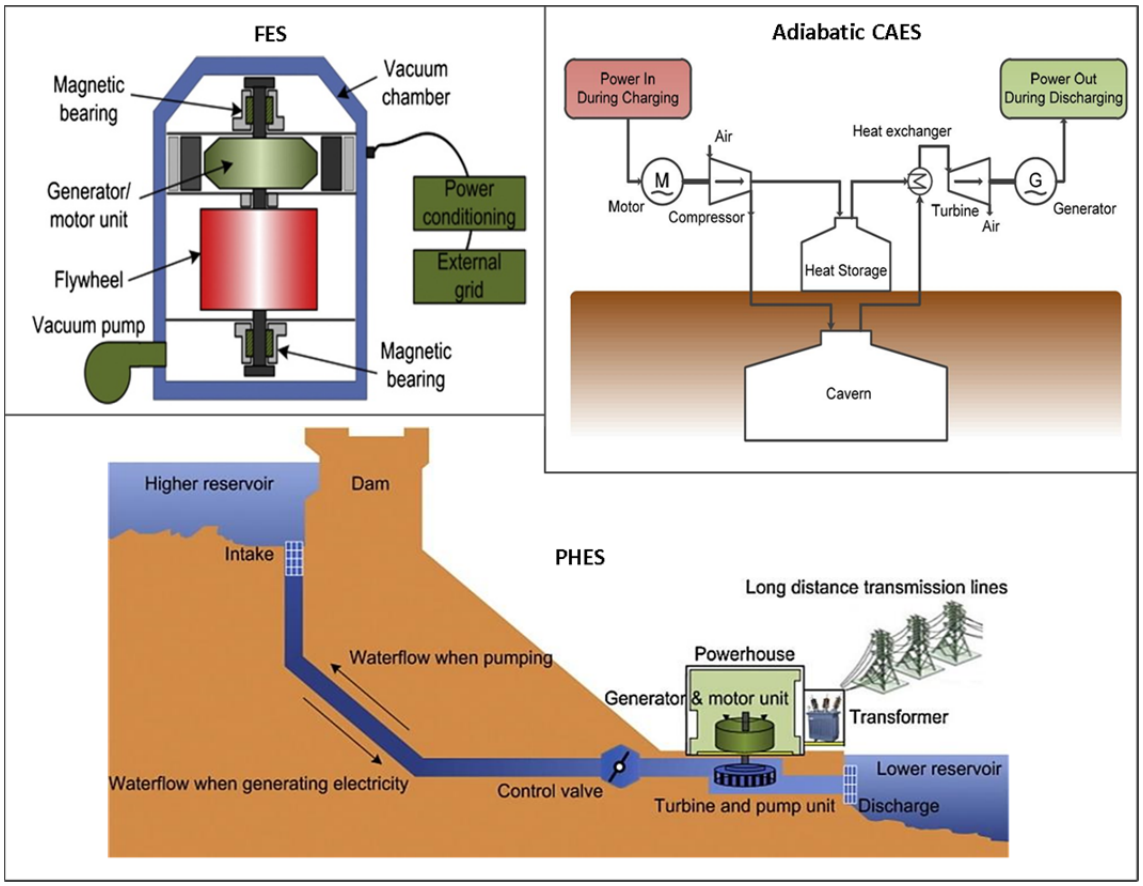

Source: Luo et al. 2015, pp. 514-516 & ISEA 2012, p. 21

Another way to store mechanical energy is in form of rotational kinetic energy. *Flywheel Energy Storage* (FES) systems accelerate and brake a rotating mass and thus store energy dependent on the rotary speed and moment of inertia. A motor-generator unit either charges the flywheel or discharges it and uses the delivered torque to provide direct current (DC) (IRENA 2017, p. 58). FES systems are characterised by high efficiencies (~90%), short response times and high power density (Arani et al. 2017, pp. 9-12). Nevertheless, the main disadvantage is a high discharge rate due to friction losses which makes FES primarily applicable for short-term and high power supplies (ISEA 2012, pp. 24-25).

Compressing air stores energy in form of potential elastic energy. *Compressed Air Energy Storage* (CAES) systems take advantage of this phenomenon by utilising compressors that store the energised air into a natural or manmade reservoir (e.g. salt caverns or pressure vessel). The pressurized air can then be reused to drive an air or gas-air turbine and hence generate electricity (Shnaid, Weiner & Brokman 1996, p. 5). Today's mostly known CAES concepts are either diabatic or adiabatic. While diabatic systems do not harness waste heat that is generated during air compression, adiabatic CAES store this heat in thermal storages and reuse it at the expansion step (where the air significantly cools down) with the aim to increase overall efficiency (up to 70%).

Hence, conventional CAES systems generally use fossil fuel to reheat the air in a combustion chamber to drive the turbine while adiabatic systems operate emission-free (IRENA 2017, p. 54; Wang et al. 2017, p. 6). Currently, there are two large-scale CAES plants connected to the grid: a 321MW plant in Huntorf (Germany) and an 110MW plant in McIntosh (US). Both run diabatically with a round trip efficiency of around 40-55% (Wang et al. 2017, p. 10; Uniper SE n.d.). Adiabatic CAES, however, is still under development. First pilot projects, like the ADELE-project in Staßfurt (cancelled 2015) (RWE Power 2010) or the Swiss ALACAES in Biasca (Geissbühler et al. 2018; Jorio 2016) have been enrolled to investigate the technical feasibility. Nevertheless, thermal storage remains the major challenge for reasonable commercial use. The advantages of CAES are mainly the freely available storage medium, a sophisticated level of knowledge for used sub-components and above all the excellent ecological footprint. Furthermore, the space requirements are significantly lower than for PHES systems (Wang et al. 2017, p. 3; ISEA 2012, p. 23). Nevertheless, further development, with the focus on decentralisation and an increase in efficiency and flexibility, is necessary to find serious benefits for the changing needs of energy transition.

Electrochemical Energy Storage

Commonly known as *batteries* (i.e. primary batteries) or *accumulators* (i.e. secondary or rechargeable batteries), electrochemical energy storages are probably the most popular but also most multifaceted storing solutions. Specific requirements led to the development of many different types, like lead-acid, sodium-sulphur and lithium-ion batteries, whereby the main difference lies in the material selection of the basic components of the battery: the electrodes (i.e. anode and cathode), the separator and the electrolyte (IRENA 2017, p. 65). In general, accumulators use the electrical potential difference between the anode and cathode to store and release energy through chemical oxidation and reduction reactions between the electrodes and the electrolyte (Liu, Neale & Cao 2016, p. 110). Compared to other battery technologies, lithium-ion accumulators (LIA) have the advantage of simultaneously great power and energy density characteristics. Furthermore, LIA have an excellent lifetime and efficiency (IRENA 2017, p. 64). That is why LIA experienced an immense development over the past few years. The enhanced performance on decreasing costs made the accumulator technology economically attractive, not only for conventional portable electronic devices, but also for stationary and automobile application fields. Besides the dominance in the electric vehicle market, accumulators are likely to play an important role in the stabilisation of the power transmission system fed by renewables (Chang 2019, p. 1; IRENA 2017, p. 71). However, the major disadvantage remains the poor ecological footprint compared to other ESS. The mining of required raw materials, like lithium and cobalt, the production process as well as the recycling is still premature and environmentally

questionable. For instance, a study by a Swedish research group mentioned that a 100kWh accumulator, as used for electric cars, has caused 15-20 tons of carbon dioxide (CO_2) before its first use (Leiva 2017).

It should be mentioned that *flow batteries* (e.g. vanadium redox flow batteries) also count to the electrochemical ESS. They basically differ from conventional batteries by having the electro-active material dissolved in electrolyte solutions .The electrolytes are stored in tanks separated by a cell stack (i.e. reaction unit), which is responsible for electricity generation (IRENA 2017, p. 86). While the power and energy capacity is coupled in “normal” accumulators, flow batteries have the advantage that energy capacity and power is independently scalable by varying the storage tank volume and by adjusting the reaction unit. Overall, this defines an ideal characteristic for long-term storage of surplus energy (Park et al. 2016, p.1; ISEA 2012, p. 38).

Chemical Energy Storage

Storing chemical energy is mostly associated with *Power to Gas* (P2G) concepts, which is one of the major topics in the energy transition these days. In the VDI report “Dauerbrenner”, Stephan Eder and his colleagues call the year 2020 “the year of hydrogen” (Eder, Hartbrich & Reckter 2020a, p. 1). Using surplus renewable power to break down water into hydrogen and oxygen (i.e. electrolysis) and therefore having a green and versatile energy carrier, makes hydrogen a highly potential alternative for the climate protection (Ogawa, Takeuchi & Kajikawa 2018, pp. 1-2). Mainly discussed application areas are the long-term storage of renewable energies, the direct combustion of hydrogen to provide heat for domestic or industrial needs (e.g. replacement of coking coal in the steel industry) as well as the inversion of the chemical reaction via fuel cells, which provides electricity for all kinds of energy consumption like gird support, transportation, etc. (Eder, Hartbrich & Reckter 2020b, pp. 20-21; IRENA 2018, p. 7). Moreover, hydrogen allows the interconnection between the electricity, gas and fuel infrastructure (Wraneschitz 2020, p. 11; ISEA 2012 p. 36). For example, hydrogen, produced with renewables, can be directly fed into the natural gas grid to a certain extend. Furthermore, it can also be processed to methane (“methanation” process) by adding carbon dioxide. Then, it can be fed into the gas grid without limitation or be alternatively stored as synthetic natural gas (SNG) for later use (IRENA 2018, pp. 16-17; Schaaf et al. 2014, p. 3). Research and development focuses on ways to store the valuable energy source safely (solid/liquid storage, LOHC, etc.), to improve efficiencies of the conversion chain (currently only ~40%) and to speed up the expansion and integration of the P2G solution (Bocklisch 2014 pp. 65-66; IEA 2005, pp. 71-77).

Electrical Energy Storage

Exceptional high power demands can be covered with short-term electrical storage solutions like *Supercapacitors* or *Superconducting Magnetic Energy Storage* (SMES) devices. Both technologies are mainly applied to maintain power quality and uninterruptible power supply (Sabihuddin, Kiprakis & Mueller 2015, pp. 201-202; ISEA 2012, p. 26; Tixador 2008, pp. 9-10). The reason for this is their characteristically high power density but low energy density combined with short response times. Typically, high costs of materials or peripheral devices lead to high energy installation costs, i.e. price per installed energy (€/kWh) (ISEA 2012, pp. 27-29; Tixador 2008, p. 5). SMES systems store energy in a magnetic field by connecting a current source to a superconducting coil. The superconductive state is achieved with expensive cyro-cooling to very low temperatures (-249°C – -138°C). In direct contrast, supercapacitors apply a voltage source in order to store energy in a static-electric field between electrodes and the ions in an electrolyte (ISEA 2012, p. 26; Tixador 2008, pp. 1-2).

Thermal Energy Storage (TES)

Generally, thermal energy can be stored in three different ways. Sensible heat TES stocks thermal energy by heating (or cooling) a liquid or solid storage medium (e.g. water, concrete). Less common but emerging is energy storage as latent heat (e.g. from solid state to liquid state) and through chemical reactions (IEA-ETSAP & IRENA 2013, p. 3). TES systems can be utilised to store energy for heating and cooling applications as well as for power generation. Particularly, waste heat from industrial processes or from renewable power plants can efficiently be reused with TES, which consequently help minimising process losses and environmental impacts (IEA-ETSAP & IRENA 2013, p. 1). Especially, the concentrating solar power is an important driving sector for TES-power applications, where almost all new plants are equipped with TES solutions (IEA-ETSAP & IRENA 2013, p. 18). Here, thermal storage is mostly based on molten salt where solar power heats a pre-liquefied salt mixture up to 550°C and therefore stores sensible energy that can later be used to generate steam which drives a turbine to produce electricity (Pfleger et al. 2015, p. 1488). However, other ESS can also benefit from TES like the adiabatic CAES. Major barriers related to TES are the costs and efficiencies of the storage medium and heat insulations as well as the complexity and controllability of the storage process, which is especially high for latent heat and chemical reaction TES systems (IEA-ETSAP & IRENA 2013, pp. 14&18).

To sum up, chapter 1.4 provides an overview of existent ESS, which are predominantly in focus when talking about the integration of renewable energies. Since this thesis deals with hydro accumulators as a storage technology, the concept of this storage system is illustrated separately in chapter 2.

2 Hydro accumulator system and concept

Basically, a hydro accumulator system is a *hydraulic-system.* A system can be defined as a group of multi-domain components which are interacting in predefined system boundaries and are therefore generating outputs dependent on the system's attributes (i.e. system's characteristics, inputs). These outputs may then affect the system's surrounding (Roddeck 2016, pp. 26-27). Hydraulic systems consist of a set of components (e.g. pumps, motors, pipes, turbines), allowing the system the transmission of signals, forces and energy by the use of hydraulic liquids. The transmission is realised by pressurising the liquid (*hydrostatic*) or by using the kinematic energy of the liquid (*hydrodynamic*) (Matthies & Renius 2014, p. 2). The hydro accumulator system belongs to the hydrostatic approach. The two main parameters of hydraulic systems are, on the one hand, the *volume flow* Q and, on the other hand, the *pressure* p. Today, hydraulic systems are mainly distinguished in stationary, mobile and aerospace hydraulics dependent on diverse system requirements such as power to weight ratio (Murrenhoff 2014, pp. 15-20). The high power density, the easy and reliable overload protection as well as the good controllability of the dynamics facilitate the implementation of hydraulic systems in various areas, e.g. the machine and plant engineering, the aerospace and automobile industry. However, challenges like hydraulic resistances, friction and leakage leading to efficiency losses still require continuous development of the described systems (Murrenhoff 2014, p. 27).

Chapter 2 provides basic knowledge concerning the underlying system with its most important characteristics and components, as well as the thermodynamic essentials to understand the storage process. This is necessary to be able to model and simulate on an appropriate level of expertise in the following step.

2.1 Hydro accumulators

Hydraulic accumulators or hydro accumulators, as the key component of the storage system, are already well understood and applied in various operation fields (Korkmaz 1982, pp. 5-9; Bauer 2016, p. 197). This chapter provides an overview of the working principle, the most common types as well as an insight in conventional and novel application areas.

The *general working principle and function* of a hydro accumulator can be summarised as follows. The hydro accumulator is a system component that is able to hold a limited volume of liquid under pressure and release it back into the hydraulic system when required (Murrenhoff 2014, p. 305). Due to the poor compressibility of liquids, the hydraulic liquid itself is not a suitable energy carrier. Therefore, a second material is used to store the system's energy. The hydraulic accumulator is charged by pumping the

liquid into the accumulator, displacing the material that is responsible for holding the performed work, and is discharged by allowing the liquid to exit the accumulator (Watter 2017, p. 166; Bauer 2016, p. 197; Korkmaz 1982, p. 1). In other words, by applying a hydro accumulator in a system, excess energy can be temporarily stored for later use through work exchange between the liquid and the storage material. This makes hydro accumulators attractive regarding the application as an energy storage device integrated in a wind power system.

2.1.1 Types of hydro accumulators

Today, there are various types of hydro accumulators available. Figure 5 depicts how the existent technologies can be classified.

Figure 5: Classification of hydro accumulators

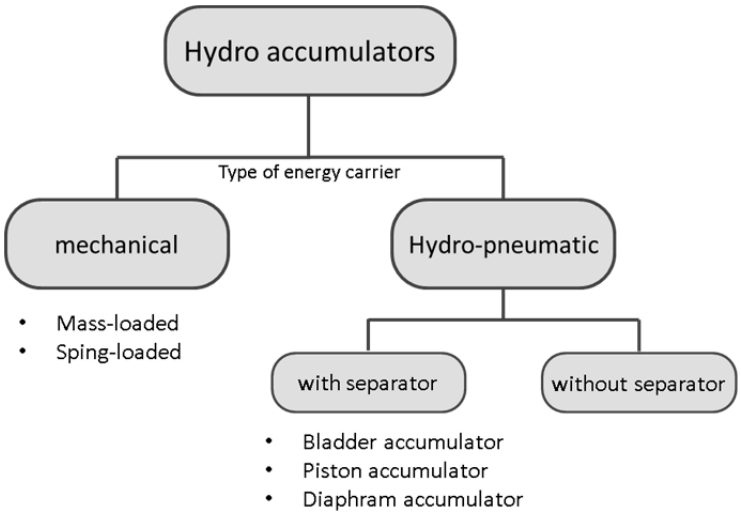

Source: based on Cosford 2014; Korkmaz 1982, p. 10

Hydro accumulators can basically be sub-divided in mechanical accumulators and hydro-pneumatic accumulators. Mechanical accumulators can operate either mass-loaded or spring-loaded.

Mass-loaded accumulators utilise a large mass to pressurise the fluid by taking advantage of the gravity force (Cosford 2014). Although, the mass-loaded accumulator is the only hydro accumulator that is able to operate at constant pressure, this type of accumulator is rather bulky and the required mass takes up much space. Consequently, this accumulator configuration is barely used these days (Bauer 2016, p. 198).

Spring-loaded accumulators store energy as potential energy by compressing a spring. Poor energy to spring-mass ratios and the unintended settle-effect of springs deteriorate the storage quality and stability which is the reason why spring-loaded accumulators are also rarely used (Bauer 2016, p. 198; Korkmaz 1982, p.10).

The described disadvantages of mechanical accumulators mainly shifted the research and development to the hydro-pneumatic accumulators which are by far the most implemented hydro accumulators in modern industries (Bauer 2016, p. 199). Hence, the mechanical hydro accumulators will not be further considered, but only the hydro-pneumatic accumulators.

Hydro-pneumatic accumulators (further simply referred to as hydro accumulators) generally comprise a pressure resistant housing (shell) having a dry side, i.e. gas chamber, which contains the pre-stressed gas (mostly nitrogen) and a wet side, i.e. liquid chamber, containing the hydraulic liquid (Cosford 2014; Murrenhoff 2014, p. 305). The liquid side is connected to the hydraulic line while the pressurised gas provides the compressive force on the liquid. During the charging step, the hydraulic liquid is pumped in the liquid chamber and compresses the gas even further. Thus, hydro accumulators are able to store energy quantities into a gas as potential energy to release them in times of demand through the exchange of work between gas and liquid (Carr 1975, p. 4).

Hydro accumulators are further distinguished in accumulators with or without a separator. Separators are applied to avoid mixing of the gas and the liquid during operation. Dependent on the hydraulic liquid and gas in use, appearing dissolving effects, cf. Henry's Law (Watter 2017, p. 17), can contaminate the hydraulic liquid and therefore disturb the storage process. The most common hydro accumulators, distinguished by the used separator, are illustrated in the figure below.

Figure 6: Types of hydro accumulators with separator

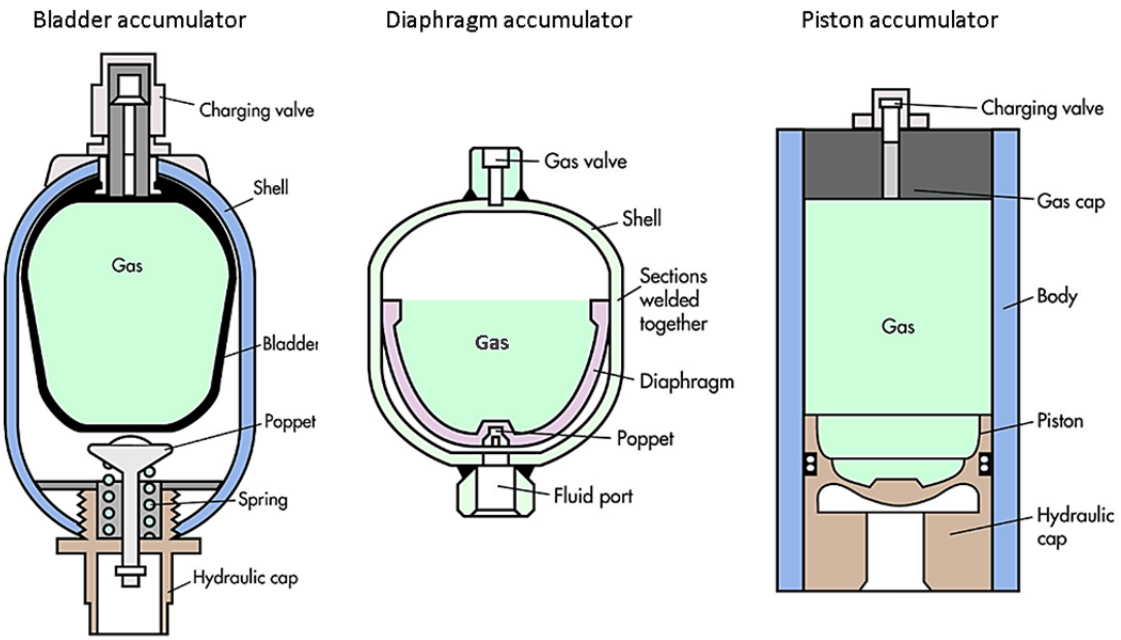

Source: Cosford 2014

The *bladder accumulator* separates its two chambers with an open or closed bladder usually made out of synthetic rubber, such as Nitrile. This type of accumulator operates fast responding and on low-maintenance but has restrictions regarding the operating pressures due to the durability of the elastomer (Murrenhoff 2014, p. 305; Korkmaz 1982, p. 14). The bladder is fixed into a cylindrical shell with hemispherical caps at either end. A poppet prevents the bladder to get pushed through the fluid port when the accumulator gets fully discharged. Bladder accumulators operate with pressure ratios not higher than 3 or 4, with total volumes between 0.2l and 450l and a flow rate of up to 140l/s (Murrenhoff 2014, pp. 305-306).

Similar to the bladder accumulator, the *diaphragm accumulator* or *membrane accumulator* utilises a flexible diaphragm to separate the liquid and the gas. The shape of the housing can be cylindrical or spherical with either welded or screwed halves. Screwed bladder accumulators compress the membrane between the top and the bottom shell, whereas the welded type has a diaphragm bonded in the middle. The threaded construction has the advantages that maintenance is possible (e.g. separator exchange) and higher pressures (<750bar) can be applied. Due to the fixation of the membrane, the welded construction only allows medium pressures (<250bar). Furthermore, a welded design does not allow maintenance but comes with a significant cost advantage compared to the threaded type. Diaphragm accumulators are characterised by much lower total volumes (<2l) but higher pressure ratios (up to 10:1) than bladder accumulators. They tend to have a long service life and high energy densities because of the spherical shape (Cosford 2014; Murrenhoff 2014, p. 306, Korkmaz 1982, pp. 17-18).

In a *piston accumulator*, gas and liquid are separated by a "flying piston" that moves freely in a honed cylinder capped on both ends. The pressure ratio is not restricted by the deformation of the bladder or diaphragm, so that higher ratios can be realised (Matthies & Renius 2014, p. 177). Moreover, the piston accumulator is able to operate at high pressures (<800bar) and large storage volumes (<1200l) (Murrenhoff 2014, p. 306). However, the dynamics of the piston accumulator are worse than of the two other designs because of the piston’s mass and friction (Bauer 2016, p. 199). Slowly moving and short pistons are vulnerable to the “stick-slip-effect”. For this reason, the piston of the generic type must be relatively long compared to its diameter and the flow rate of the liquid must be calculated so that the piston moves with approximately 2 to 3.5 m/s. The piston design requires high maintenance efforts and is the costliest compared to the other accumulator types (Runkel 2014, p. 6; Murrenhoff 2014, pp. 306-307).

2.1.2 Operational parameters and system requirements

The following illustration shortly demonstrates the typical *operational parameters* and states of charge of the hydraulic accumulator, using the piston type as an example:

Figure 7: Operation of hydro accumulators

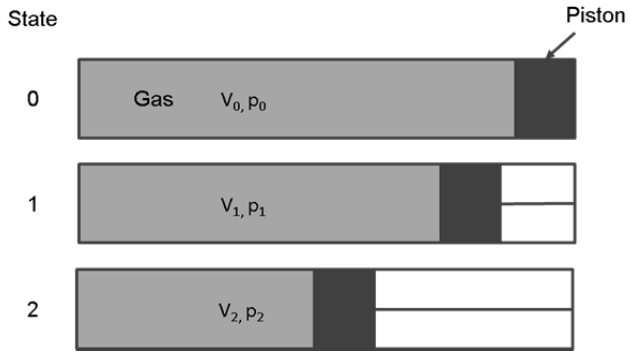

Source: based on Murrenhoff 2014, p. 309

At state 0, the accumulator is fully discharged. The gas has the maximum volume V_0 at a defined pre-charge pressure p_0. The operating state 1 defines the lower operating pressure p_1 in the hydraulic component with V_1 as the related volume. The highest operating pressure p_2 by the gas volume V_2, represents a fully charged hydro accumulator (state 2). There might also be a state 3 determining the system pressure p_3, where a safety valve opens in order to prevent damage. The *operating pressure range* is given by $\Delta p = p_2 - p_1$ and the *operating pressure ratio* by p_2/p_1. During compression, an *effective volume* of $\Delta V = V_2 - V_1$ (indices reversed for expansion) can be added to or taken from the accumulator (Murrenhoff 2014, p. 310). Dividing the highest operating pressure p_2 by the pre-charge pressure p_0 defines the accumulator's *maximum pressure ratio*. Examined temperatures can be distinguished into the temperature of the gas and the temperature of the surrounding (e.g. the hydraulic liquid). The temperature at state i is expressed with T_i or with the Greek letter θ_i ("Theta"). θ_{max} and θ_{min} determine the maximum and the minimum *operating temperature*, which is mainly restricted through material properties and the application area (Korkmaz 1982, p. 21).

The most important requirements of the hydro accumulator are high energy densities, low maintenance, high reliability and good dynamics regarding the volume flow (Matthies & Renius 2014, p. 176). Moreover, safety regulations are mandatory since operating with high pressures and power densities devote attention in order to prevent accidents (Murrenhoff 2014, p. 307). In Europe, the pressure device guideline 97/23/EG is authoritative for design, construction and dimensioning of hydro accumulators as a pressure device (Watter 2017, p. 173; Murrenhoff 2014, p. 307).

2.1.3 Conventional and novel application areas

Conventional hydro accumulators, for small-scale hydraulic circuits, are technically mature. Primarily, they are utilised in hydraulic systems to take on supportive tasks. Typical assignments are in particular (Watter 2017, pp. 167-168; Murrenhoff 2014, p. 305; Matthies & Renius 2014, p. 175):

- emergency supply during system breakdown
- reduction of pulsation by damping pressure surges
- compensation of leakages
- hydro-pneumatic vehicle suspension
- coverage of temporarily high power demands
- energy absorption during recuperation (e.g. braking vehicles)

However, the turnaround in energy policy and the increased demand of flexible energy storage solutions opened up new application opportunities for hydro accumulators.

In the years 2009 to 2016, the companies Robert Bosch GmbH and PSA Groupe (Peugeot and Citroën) developed a pneumatic hybrid prototype “PSA Air Hybrid” that was able to store braking energy by compressing gas (nitrogen) in a 20 litre pressure tank. Figure 8 shows a picture of the prototype and the general working principle.

Figure 8: PSA – Hybrid air prototype and working principle

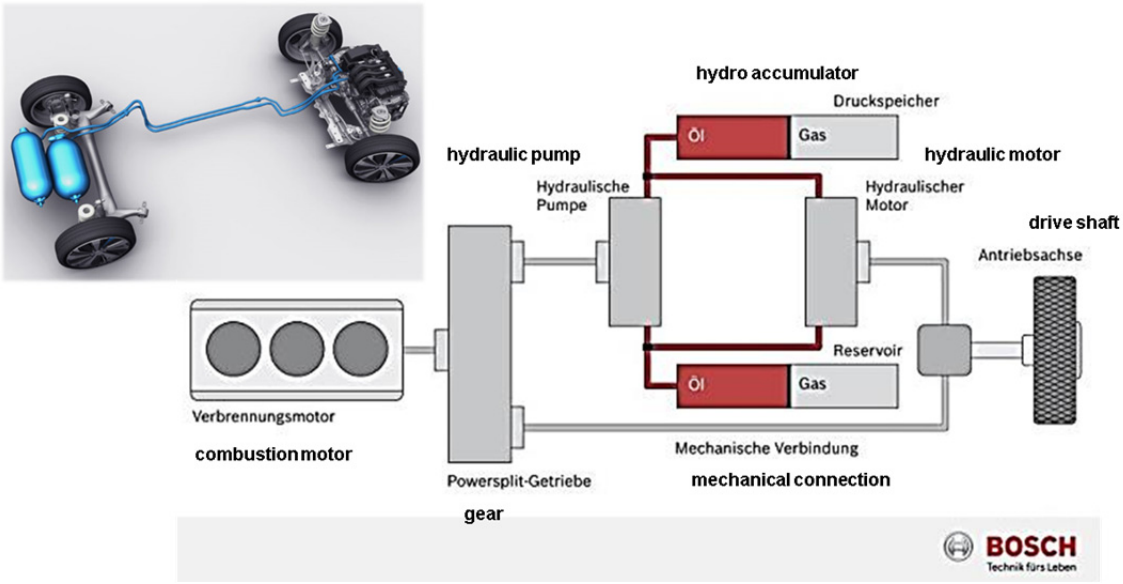

Source: PSA Groupe 2016 & Wiesinger 2015

Two hydraulic pumps were in operation to compress the nitrogen up to 350bar leading to a total power of the hydraulic drive of around 41HP. Hypothetically, the vehicle was able to drive 400m with 60km/h just by using the hydro accumulator as an energy source. Especially for intercity use, the hydro accumulator technology tends to be high-

ly promising to lower fuel consumption and therefore the environmental impact of hybrids. In fact, PSA claims that the hybrid achieves up to 80% zero-emission-operation in city traffic, reducing the CO_2 emissions by almost 50%. Unfortunately, the project was discontinued in 2016 and the hydro accumulator was replaced by an electric hybrid drive (Gomoll 2014; Grünweg 2014).

Recently, experts try to figure out ways to utilise hydro accumulators for large scale storages. Especially for offshore renewables, the hydro accumulator seems to have high potential by using freely available water as the hydraulic liquid. In fact, the hydro accumulator competes with several other open-loop hydraulic storage concepts. Examples are “Buoyant Energy Storage” (University of Innsbruck n.d.), “Ocean Renewable Energy Storage (ORES)” (Slocum et al. 2013) and “Energy Bags for underwater CAES” (Pimm, Garvey & Jong 2014), which are widely discussed in the open literature, but not described in more detail in this paper. The major challenges are the integration in the existent power transmission system, the construction of large scale pressure reservoirs and the interface between the hydraulic circuit and fluctuating power source.

As an example, Buhagiar and Sant try to face the challenge of pressure variations dependent on the state of charge of the hydro accumulator (2017, p. 283). They investigate and model a novel hydro-pneumatic accumulator of a wind turbine for large-scale offshore energy storage. The model consists of a compressed air chamber, integrated into the tension leg platform of the power plant, which functions as an absorber of pressure fluctuations to keep the pressure of the gas during the (dis-) charging process nearly constant. The buffer is connected to the hydro accumulator which is located in the gravity foundation of the wind turbine. By pumping seawater into or allowing the seawater to exit the accumulator, energy is stored and released decentralised under relatively constant conditions (Buhagiar & Sant 2017, pp. 283-286).

Figure 9: Novel hydro-pneumatic accumulator for offshore energy storage

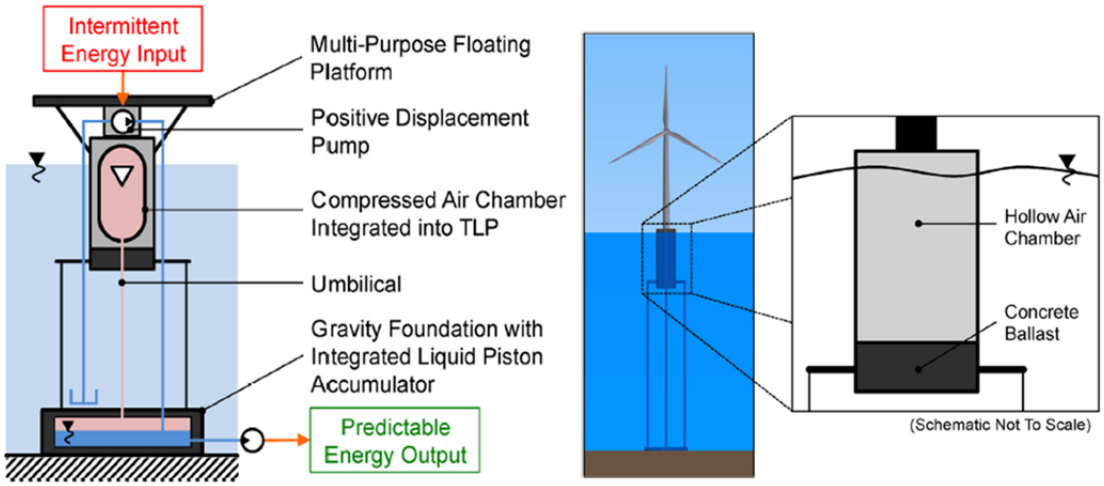

Source: Buhagiar & Sant 2017, p. 286

Another example, published in the journal “Applied Sciences”, shows how Liejiang Wei et al. model and simulate a closed hydraulic wind turbine system with an integrated bladder accumulator to validate efficiency and performance during fluctuations of wind power. They implement a control scheme that provides constant electrical power output regardless of wind speed and load power. The simulation results indicate that hydro accumulators can significantly support the integration and control of intermittent wind power (2018, pp. 1&16). But also several other works deal with initial findings regarding the control and storage of wind energy through hydraulic transmission systems (i.e. hydraulic wind turbines) including hydro accumulators (Liu et al. 2017; Fan, Mu & Ma 2016; Vaezi & Izadian 2014).

It can be concluded that the potential of hydro accumulators is identified. Scientists are concentrating on creating important foundations for the large-scale practical implementation. However, summarising the current state of development, it can be said that large-scale hydro accumulator systems are still in their initial stages. Theoretical investigations are made but wide range practical use remains open. Consequently, much more research and development is required to make the hydro accumulator technology commercially available for this type of application. Therefore, the research project WESSPA is an opportunity to gain more insights of the process parameters and applicability of hydro accumulator systems. It is important to mention that hydro accumulators, combined with small-scale renewable power plants (wind turbines, photovoltaics, etc.), have also the potential to be utilised in domestic areas. These storage systems would have much smaller dimensions and could provide supportive activities on site to lower the energy demand from the electrical grid. In the best case, the integration of hydro accumulators leads to self-sufficient and self-sustaining households, which are independent of the grid’s power.

2.2 Thermodynamics of the storage process

The investigation of a hydraulic accumulator from the thermodynamic point of view permits detailed insights into the energy storage process. Moreover, basic thermodynamic principles allow the calculation and specification of various parameters of interest, like the maximum amount of energy that the accumulator is able to store or the development of pressure and temperature. The following section illustrates the underlying thermodynamic aspects in order to get a deeper understanding for the simulation. The change and the interrelation of the state variables (pressure, volume, temperature), as well as the process variables, i.e. the volumetric change work (W_v) and the thermal energy (Q_H) are taken into account and exemplified with a short calculation.

The gas side of the hydro accumulator can be seen as a closed thermodynamic system (Korkmaz 1982, p. 26). Cerbe & Wilhelms define a closed system as a system with predefined boundaries where no mass transfer occurs. Therefore, the system is characterised by a fixed quantity of substance (2013, p. 46), i.e. the mass of the storage medium (gas) remains the same. The system is able to exchange work and heat with its surrounding as well as storing it (Korkmaz 1982, p. 26). The hydraulic liquid and the gas perform work on each other, by following the first law of thermodynamics, during the energy storage process:

$$dU = dQ_H + dW_{to} = dQ_H + dW_v + dW_{diss} \qquad 2.2\text{-}1$$

Here dU is the change of the internal energy of the system when it absorbs or releases energy as heat dQ_H or as work dW_{to}. Energies supplied to the system are counted positive, discharged energies are counted as negative (Stierstadt 2018, p. 71). The total change of work dW_{to} consist of the change of volumetric change work dW_v and the change of dissipation work dW_{diss}. While dW_v determines the reversible amount of usable energy, dW_{diss} considers occurring friction and other system immanent losses. Dissipation work is always counted positive and represents the unusable (irreversible) amount of the total work (Cerbe & Wilhelms 2013, pp. 53-54).

During the charging process, the liquid performs work on the gas by compressing it which means energy is stored as W_v in the gas. During discharging, the gas expands and releases the stored energy and therefore performs work on the hydraulic liquid. Furthermore, heat transfer occurs when the temperature of the gas deviates from the ambient temperature. A higher temperature of the gas than the temperature of the surrounding components (e.g. hydraulic fluid or storage tank) would result in a heat transfer Q_H, meaning an energy exchange, from the hot gas to the colder components, for instance.

In order to keep the calculation of the thermodynamics lucid, a few simplifying assumptions have to be made.

Assumptions

The first assumption is that ideal behaviour is assumed for the gas of the hydro accumulator. Under this condition the *thermal equation of state* of the ideal gas can be applied (Cerbe & Wilhelms 2013, p. 33):

$$p\,V = m\,R_i\,T \qquad 2.2\text{-}2$$

Equation 2.2-2 can also be displayed volume specific:

$$p\,v = R_i\,T \qquad \text{2.2-3}$$

p pressure of the gas [Pa or N/m^2], 1 bar ≙ 10^5 Pa ≙ 10^5 N/m^2

V volume of the gas [m^3]

v specific volume of the gas [m^3/kg]

m mass of the gas [kg]

R_i specific gas constant [J/kgK]

T temperature of the gas [K]

The thermal equation of state is only accurate for state changes within low pressure, small specific volume and normal temperature ranges. That means, for example, the equation becomes less accurate in changes of state with high pressures and low temperatures. Hence, the assumption of an ideal gas might be extended in further steps by adding a *compressibility factor* z to avoid gross calculation errors (Watter 2017, p. 168; Korkmaz 1982, p. 42).

$$z = \frac{p\,V}{m\,R\,T} \qquad \text{2.2-4}$$

By introducing the compressibility factor, the thermal equation of state still can be used to describe real gas behaviour. The factor depends on pressure and temperature, can mostly be obtained from scientific tables and can be set equal to “1” for low pressures (≙ ideal gas) (Watter 2017, p. 168).

Second, the hydraulic liquid, used in the hydraulic system, is assumed to be incompressible. That means that the volume remains constant with different pressures. Consequently, the gas is the only substance that stores potential energy. This assumption is based on the *ideal liquid*, which can be described as massless, frictionless and incompressible (Murrenhoff 2014, p. 29).

$$C_{Li} = \frac{dV}{dp} \approx \frac{\Delta V}{\Delta p} = \frac{V}{E} = V \cdot \beta \quad = \mathbf{0} \qquad \text{2.2-5}$$

C_{Li} capacity of the liquid [m^3/(N/m^2) or l/bar]

ΔV volume difference [m^3 or l]

Δp pressure difference [N/m^2 or bar]

E bulk modulus [N/m^2 or bar]

β compressibility coefficient [m^2/N or 1/bar]

(Watter 2017, p. 69; Murrenhoff 2014, p. 60)

In real hydraulic applications the utilised high pressure ranges often do not allow the assumption of incompressibility so that the hydraulic capacity needs to be taken into account. Furthermore, the friction and mass of the liquid have an additional impact on

the performance of a hydraulic system and should be included in further calculations. However, these impacts are not considered for this moment.

Another prerequisite is the pressure equality between the gas side and the liquid side of the hydro accumulator. Depending on the type of the hydro accumulator this is not always the case. For instance, the piston in the piston accumulator underlies friction and mass inertia during motion, which leads to pressure differences between liquid and gas (Korkmaz 1982, p. 12).

From the thermodynamic point of view, the preceding assumptions define that energy is not converted into dissipation energy ($W_{diss} = 0$) in the closed system during the energy storage process. In other words, the hydro accumulator operates without friction, having the volumetric change work and the thermal energy as the only way to convert energy (reversible process).

The final assumptions are made in relation to the changes of state of the storage medium. The different states of a storage process and its operational parameters were already described in the previous chapter (cf. Chapter 2.1.2). The energy storage process can be visualised in a *p-V-diagram* (Figure 10).

Figure 10: p-V-diagram of the charging process

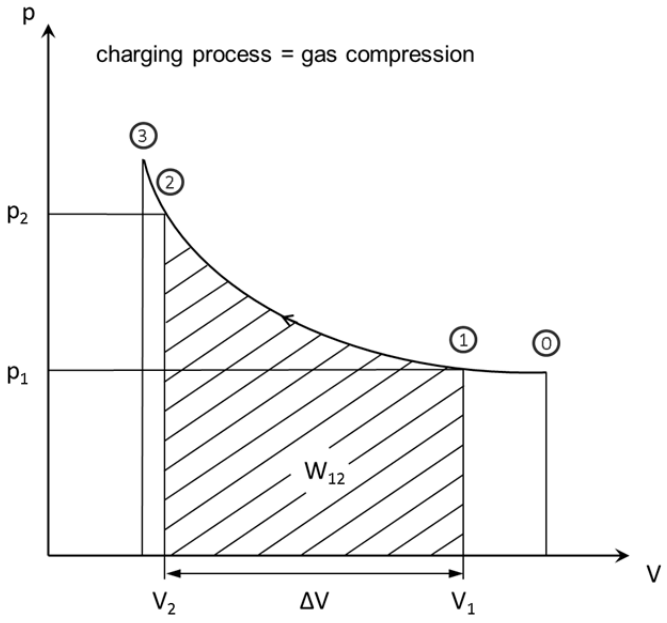

Source: based on Murrenhoff 2014, p. 309

The performance of a hydro accumulator depends on the underlying change of state of the gas (Murrenhoff 2014, p. 310). With the assumption of an ideal gas (2.2-2), the compression (or the expansion) can be generalised by the polytropic equation:

$$pV^n = const. \qquad 2.2\text{-}6$$

By setting the polytropic exponent n according to the following values, the different changes of state can be represented (Bauer 2016, p. 200; Matthies & Renius 2014, p. 178; Cerbe & Wilhelms 2013, p. 110):

$n = 1$ With $pV^1 = const.$ the change of state is *isothermal*. The accumulator is operated over a long time period, giving enough time for a complete heat exchange between the gas and its environment. As a result, the gas temperature remains constant while energy is exchanged.

$n = \kappa$ With $pV^\kappa = const.$ the change of state is *isentropic*. In this case, the (dis-) charging process happens quickly, so that no heat exchange and dissipation occur (adiabatic & reversible change of state).

$n = \infty$ With $pV^\infty = const.$ the volume remains constant. *Isochoric* change of state occurs, for instance, when a charged accumulator is shut off from the system, followed by a longer rest period during which partial or complete temperature equalisation with the environment takes place.

The isentropic exponent κ ("kappa") depends on the pressure, temperature and type of the gas. For example, the isentropic exponent of air or nitrogen under standard conditions is $\kappa = 1.4$ (Cerbe & Wilhelms 2013, pp. 103&517). In the context of this thesis, kappa is assumed to be constant during the storage process.

Isothermal and isentropic are idealistic changes of state. In fact, the change of state takes place between both with $1 < n < \kappa$, resulting in a polytropic change of state. That means heat is neither completely given off nor completely hold in the system during the storage process. Figure 11 visualises the different changes of state.

Figure 11: Changes of state of hydro accumulators

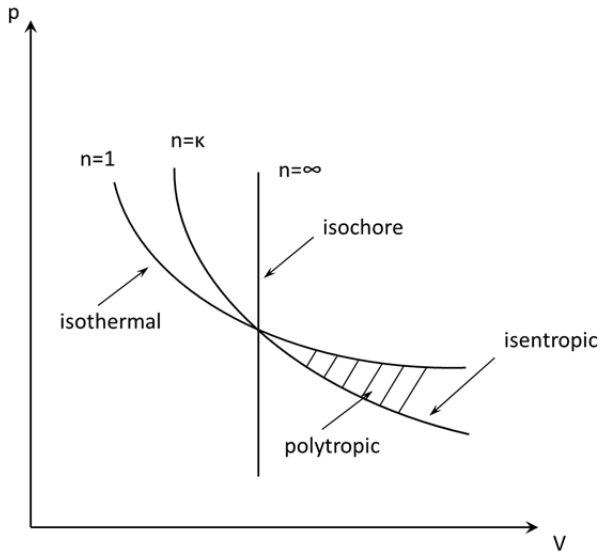

Source: based on Korkmaz 1982, p. 27

The following calculation example helps to understand the different impacts of the possible changes of state on the storage results. The main parameters of interest are:

First, the amount of (volumetric change) work of the hydro accumulator, further declared as W_{v12} (Cerbe & Wilhelms 2013, p. 53):

$$W_{v12} = -\int_{1}^{2} p\, dV \qquad \text{2.2-7}$$

It specifies the amount of usable energy that the accumulator is able to store or, in other words, the amount of work that the accumulator is able to perform due to stored energy. The area underneath the line of the different changes of state in the p-V-diagram represents the volumetric change work W_{v12} (cf. Figure 10).

Second, the amount of replaceable effective volume that the hydro accumulator is able to provide (Korkmaz 1982, p. 30):

$$\begin{aligned} &\text{during compression:} \quad \Delta V = V_2 - V_1 \\ &\text{or expansion:} \quad \Delta V = V_1 - V_2 \end{aligned} \qquad \text{2.2-8}$$

The effective volume is used to drive a pump or a hydraulic motor reusing the stored energy for generating electricity. The higher the provided volume, the better is the potential energy yield.

2.2.1 Calculation example

To keep it simple, the pre-charge state 0 is set to the lower operating state 1 in the following calculation (cf. Chapter 2.1.2). Consequently, the accumulator has only two operating states: discharged (i.e. pre-charge state 1) and charged (state 2). An accumulator with a volume of $\mathrm{V_{Acc}} = 1\mathrm{m}^3$ is used. Air at ambient temperature ($\mathrm{T_1} = 293\mathrm{K} = 20°\mathrm{C}$) will be compressed by the hydraulic liquid up to the higher operating pressure of $p_2 = 200bar$. The volume of the gas at the pre-charge stage is set equal to the accumulator volume ($\mathrm{V_1} = \mathrm{V_{Acc}} = 1\mathrm{m}^3$). Questions that will be answered are:

- How much energy can be stored through work exchange in case of an isothermal and isentropic change of state (W_{v12})?
- How much effective volume can be provided in the case of an isothermal and isentropic change of state (ΔV)?

The pre-charge pressure p_1 should be set to get a maximum of the volumetric change work and a maximum of the effective volume.

Isothermal change of state

The equation for the volumetric change work in case of an isothermal compression ($T_1 = T_2$) is given with (Cerbe & Wilhelms 2013, p. 99):

$$W_{v12} = -\int_1^2 p\, dV = p_1 V_1 \ln\left(\frac{p_2}{p_1}\right) \qquad \text{2.2.1-1}$$

It can be seen that the maximum of W_{v12} depends on the size of the storage tank and the applied pressures. In order to find the maximum of the volumetric change work the following differential equation, with respect to p_1, needs to be solved:

$$\frac{dW_{v12}}{d\left(\frac{p_2}{p_1}\right)} = 0 \qquad \text{2.2.1-2}$$

$$\Leftrightarrow V_1 \ln\left(\frac{p_2}{p_1}\right) - p_1 V_1 \frac{1}{\left(\frac{p_2}{p_1}\right)} \frac{\mathrm{p_2}}{{\mathrm{p_1}}^2} = V_1 \ln\left(\frac{p_2}{p_1}\right) - V_1 \frac{p_1^2}{p_2} \frac{p_2}{p_1^2} = 0$$

$$\Leftrightarrow V_1 \left(\ln\left(\frac{p_2}{p_1}\right) - 1 \right) = 0 \quad | \, \mathrm{V_1} = \mathrm{const.}$$

$$\Leftrightarrow \ln\left(\frac{p_2}{p_1}\right) = 1 \;\Leftrightarrow\; \frac{p_2}{p_1} = e = \pi_{opt} \qquad \text{2.2.1-3}$$

It is illustrated that for an isothermal change of state, the maximum volumetric change work can be absorbed / released with an optimum pressure ratio of $\pi_{opt} = \boldsymbol{e} \approx \mathbf{2.718}$.

In this case the optimal pre-charge pressure p_1 of the hydro accumulator is:

$$p_1 = \frac{p_2}{\pi_{opt}} = \frac{p_2}{e} = \frac{200bar}{2.718} \approx \boldsymbol{73.58bar}$$

$(73.58bar = 73.58 \cdot 10^5 \frac{N}{m^2} = 73.58 \cdot 10^5 \frac{J}{m^3})$

With $V_1 = 1m^3$, the volumetric change work for the isothermal compression is equivalent to (2.2.1-1& -3):

$$W_{v12} = p_1 V_1 \ln(\pi_{opt}) = 73.58 \cdot 10^5 \frac{J}{m^3} \cdot 1m^3 \cdot \ln(e) \approx 7.36\ MJ \qquad \text{2.2.1-4}$$

$$\triangleq \boldsymbol{2.04kWh}$$

$$W_{v12} = \frac{1}{e}\, p_2 V_1 \approx \mathbf{0,368} \cdot 200 \cdot 10^5 \frac{N}{m^3} \cdot 1m^3 \approx 7.36\ MJ \qquad \text{2.2.1-5}$$

$(1J = 1Ws = 0.001kW \frac{1}{3600} h = \frac{1}{3.6 \cdot 10^6} kWh \approx 2.78 \cdot 10^{-7} kWh \Rightarrow 1MJ = 0.278\ kWh)$

For better comparability, the stored energy can also be declared as *volumetric energy density*, i.e. the amount of energy stored per unit volume. In this case, the result is the same since the storage volume is 1m^3:

$$W' = \frac{W_v}{V} \qquad \text{2.2.1-6}$$

W' volumetric energy density [kWh/m^3]

Therefore, W' for isothermal change of state yields (2.2.1-4& -5& -6):

$$W' = \frac{W_{v12}}{V_1} = p_1 \ln(\pi_{opt}) = \frac{1}{e}\, p_2 \qquad \text{2.2.1-7}$$

$$\Rightarrow W' = \frac{2.04kWh}{1m^3} = \mathbf{2.04}\,\frac{\boldsymbol{kWh}}{\boldsymbol{m^3}}$$

Concerning the calculation above, the results show that with an optimal pressure ratio and a final pressure of 200bar, the hydro accumulator with 1m^3 storage volume absorbs around 2.04kWh of energy. This would be the same amount of energy that could be released during expansion in an ideal system. To get a first impression, that would roughly be the amount of energy that is necessary to run a vacuum cleaner for two hours which seems not much. To improve the volumetric change work, either the system's storage pressure or storage volume must be increased. Higher storage pressures can be realised by choosing an appropriate accumulator type.

Common piston accumulators, for instance, are able to realise pressures up to 800bar (cf. Chapter 2.2.1). Another opportunity is to increase the storage volume by connecting multiple hydro accumulators and integrate them into a modular system and hence adding up the volumetric change work.

The replaceable effective volume can be calculated with equation 2.2-8, the polytropic equation 2.2-6 and $n = 1$ for isothermal change of state:

$$p_1 V_1 = p_2 V_2 \Leftrightarrow V_2 = \frac{1}{e} \cdot V_1 = \frac{1m^3}{e} \approx \mathbf{0.368}\boldsymbol{m^3}$$

$$\Delta V = V_2 - V_1 = 0.368m^3 - 1m^3 \approx -0.632m^3 = \mathbf{-632}\ \boldsymbol{l}$$

The volume of the gas is reduced by 632 litres. This is the volume which is taken by the hydraulic liquid. In this ideal system, the hydro accumulator would be able to provide 632 litres of working liquid, to operate a hydraulic motor during the discharging process.

The heat exchange during the charging process is given with the first law of thermodynamics (cf. 2.2-1, with $dT = 0 \rightarrow dU = 0$) (Cerbe & Wilhelms 2013, p. 100):

$$Q_{H,12} = -W_{v12} = -p_1 V_1 \ln\left(\frac{p_2}{p_1}\right) \approx -\mathbf{2.04\ kWh} \qquad \text{2.2.1-8}$$

Consequently, the released (or absorbed) heat is equivalent to the volumetric change work during the energy storage process. In this case, isothermal compression transfers 2.04kWh of thermal energy from the gas to its surrounding ("-"≙ released energy / heat). Especially the hydraulic liquid can support heat removal because of its characteristically high specific heat capacity (Murrenhoff 2014, p. 95).

Isentropic change of state

The equation for the volumetric change work in case of an isentropic compression ($Q_{H,12} = 0, W_{diss,12} = 0, n = \kappa$) is given with (Cerbe & Wilhelms 2013, p. 105):

$$W_{v12} = -\int_1^2 p\, dV = \frac{p_1 V_1}{\kappa - 1}\left(\left(\frac{p_2}{p_1}\right)^{\frac{\kappa-1}{\kappa}} - 1\right) \qquad \text{2.2.1-9}$$

Solving the differential equation 2.2.1-2 for 2.2.1-9 returns the optimal pressure ratio for the isentropic change of state (Watter 2017, p. 170):

$$\pi_{opt} = \frac{p_2}{p_1} = \kappa^{\left(\frac{\kappa}{\kappa-1}\right)} \qquad \text{2.2.1-10}$$

With air having $\kappa = 1.4$ as an ideal isentropic exponent, π_{opt} is:

$$\pi_{opt} = \frac{p_2}{p_1} = \kappa^{\left(\frac{\kappa}{\kappa-1}\right)} = 1.4^{\left(\frac{1.4}{1.4-1}\right)} \approx \mathbf{3.247} \qquad \text{2.2.1-11}$$

Hence, the maximum volumetric change work for an isentropic change of state can be reached with an optimum pressure ratio of $\pi_{opt} \approx \mathbf{3.247}$.

In this case, the optimal pre-charge pressure p_1 of the hydro accumulator is:

$$p_1 = \frac{p_2}{\pi_{opt}} = \frac{200bar}{3.247} \approx \mathbf{61.6bar} = 61.6 \cdot 10^5 \frac{J}{m^3}$$

With $V_1 = 1m^3$, the volumetric change work for the isentropic compression is equivalent to (2.2.1-9& -11):

$$W_{v12} = \frac{p_1 V_1}{\kappa - 1}\left(\pi_{opt}^{\frac{\kappa-1}{\kappa}} - 1\right) = \frac{61.6 \cdot 10^5 \frac{J}{m^3} \cdot 1m^3}{1.4 - 1}\left((3.247)^{\frac{1.4-1}{1.4}} - 1\right) \qquad \text{2.2.1-12}$$

$$\approx 6.16\ MJ \triangleq\ \mathbf{1.71\ kWh}$$

$$W_{v12} = \frac{1}{3{,}247}\, p_2 V_1 \approx \mathbf{0{,}308} \cdot 200 \cdot 10^5 \frac{N}{m^3} \cdot 1m^3 \approx 6.16\ MJ \qquad \text{2.2.1-13}$$

2.2.1-12& -13 can be displayed as volumetric energy density according to 2.2.1-6:

$$W' = \frac{W_{v12}}{V_1} = \frac{p_1}{\kappa - 1}\left(\pi_{opt}{}^{\frac{\kappa-1}{\kappa}} - 1\right) = \frac{1}{3{,}247}\, p_2 \qquad \text{2.2.1-14}$$

$$\Rightarrow W' = \frac{1.71\ kWh}{1m^3} = \mathbf{1.71}\ \boldsymbol{\frac{kWh}{m^3}}$$

In comparison to the isothermal compression, it can be seen that the maximum volumetric change work is lower with an isentropic change of state. More precisely, the maximum amount of energy that can be stored is around **19.3%** higher with an isothermal change. Therefore, the aim should be to configure the hydro accumulator system so that it operates slowly, i.e. isothermally, in order to store or release more energy (Murrenhoff 2014, p. 314).

Likewise the isothermal case, the replaceable effective volume can be calculated with the equation 2.2-8, the polytropic equation 2.2-6 and $n = \kappa = 1.4$ for the isentropic change of state:

$$p_1 {V_1}^{\kappa} = p_2 {V_2}^{\kappa} \Leftrightarrow V_2 = \left(\frac{1}{\pi_{opt}}\right)^{\frac{1}{\kappa}} \cdot V_1 = \left(\frac{1}{3.247}\right)^{\frac{1}{1.4}} \cdot 1m^3 \approx \mathbf{0.431}\boldsymbol{m^3}$$

$$\Delta V = V_2 - V_1 = 0.431m^3 - 1m^3 \approx -0.569m^3 = \ \mathbf{-569}\ \boldsymbol{l}$$

The isentropic change of state results in a volume reduction of the gas of only 569 litres (632 litres in the isothermal change of state). Consequently, the replaceable effective volume is roughly 10% lower than the volume provided by isothermal compression.

Since the heat exchange $Q_{H,12}$ during isentropic compression is zero, the temperature of the air rises according to the following equation (Cerbe & Wilhelms 2013, p. 104):

$$\frac{T_1}{T_2} = \left(\frac{V_2}{V_1}\right)^{\kappa-1} \qquad \text{2.2.1-15}$$

$$\Rightarrow T_2 = T_1\left(\frac{V_1}{V_2}\right)^{\kappa-1} = 293K \cdot \left(\frac{1m^3}{0.431m^3}\right)^{1.4-1} \approx 410.3K = \mathbf{137.3}\boldsymbol{°C}$$

The fast isentropic compression leads to a temperature rise of the gas of around 117°C. The faster the charging process, the closer is the change of state to the isentropic which leads to more heat that remains in the system over short time periods. As a consequence, the material durability or the process stability could be diminished. For instance, if water is used as hydraulic liquid and the temperature of the gas is far over 100 degrees, the water might evaporate close to the separator having an adverse impact on the stability of the system parameters. This also applies to the discharging process, where the gas temperature can drop to very low values, which would also have

negative effects on system components and the overall storage process. Consequently, the system should be designed so that temperature extremes are avoided.

If the hydro accumulator is shut off from the system, the system balances through temperature equilibrium. As mentioned in section 2.2, this change of state can be defined as isochoric. In the example, the air has the following state variables after the isentropic compression step:

$T_2 \approx 410K, \qquad p_2 = 200bar, \qquad V_2 \approx 0.43m^3$

The parameter of interest is the final pressure p_3 of the air after it has reached the ambient temperature:

$T_3 \approx 293K, \qquad V_2 = V_3 = 0.43m^3, \qquad p_3 = ?$

The following equation provides the solution (Cerbe & Wilhelms 2013, p. 91):

$$\frac{p_2}{p_3} = \frac{T_2}{T_3} \qquad \text{2.2.1-16}$$

$$\Rightarrow p_3 = p_2 \left(\frac{T_3}{T_2}\right) = 200bar \cdot \left(\frac{293K}{410K}\right) \approx \mathbf{142.9bar}$$

The pressure of the air after the isochoric equalisation is roughly 57bar lower than right after the isentropic compression. That means the hydro accumulator is able to perform less work which reduces the efficiency of the full storage cycle.

The volumetric change work released from the hydro accumulator would be, in the case of an isothermal expansion back to the pre-charge pressure ($p_4 = p_1 = 61.6bar$) (2.2.1-1):

$$W_{v34} = p_3 V_3 \ln\left(\frac{p_4}{p_3}\right) = 142.9 \cdot 10^5 \frac{J}{m^3} \cdot 0.43m^3 \cdot ln\left(\frac{61.6bar}{142.9bar}\right)$$
$$\approx -5.17MJ \triangleq \mathbf{-1.44kWh}$$

The calculation shows that only 1.44kWh ("-"≙ released work) can be "restored" for energy generation after the isochoric system balancing, while charging the accumulator consumed 1.71kWh of energy. The amount of reusable energy would be even lower for an isentropic expansion (≈ -3.28MJ ≙ -0.91kWh). The result is an "energy loss" of roughly 16% (or even 47% for isentropic expansion) comparing input and output of the volumetric change work. These results highlight again that it is more efficient to operate hydro accumulators over longer time periods, i.e. isothermal operation.

The calculation example helps to understand the physical basics of the hydro accumulator's storage process on the easiest basis. The following chapter shortly describes the remaining system components of the hydro accumulator system. It is the last step to have an overall understanding of the storage concept and system.

2.3 Further system components

The hydro accumulator, as the key component of the investigated storage system, was already described in detail in section 2.1. However, there are other important components involved in the process. Their main working principle and role for the hydro accumulator system will be illustrated by following the energy conversion process:

Figure 12: General setup of the hydro accumulator system

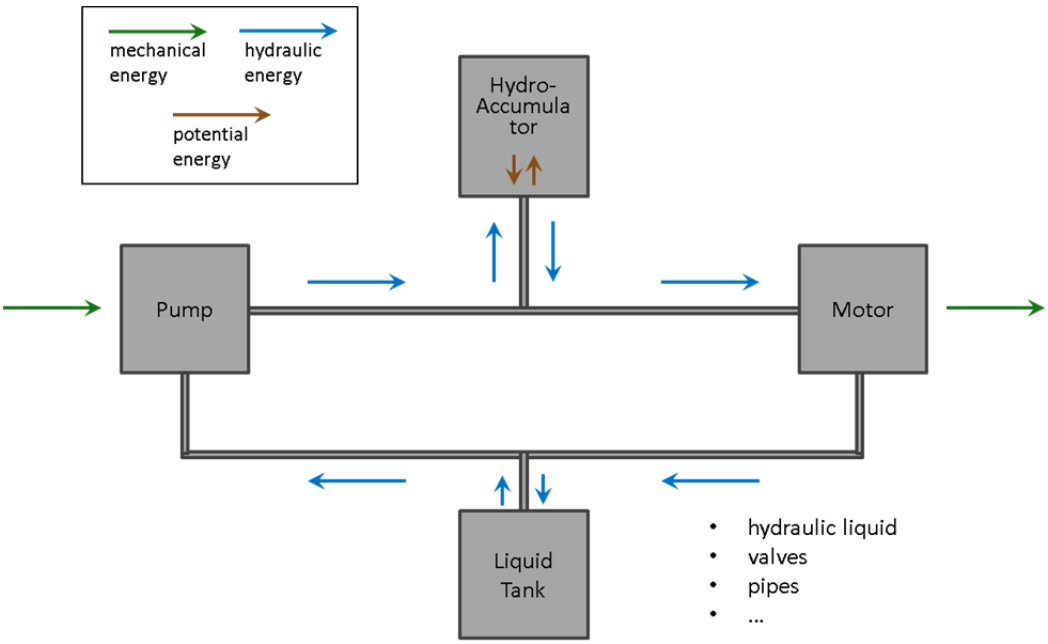

When wind is blowing, the rotor blades of the wind turbine are accelerated and convert the kinematic energy of the wind into mechanical energy, i.e. rotational energy of the shaft (Hau 2016, p. 85). This mechanical energy is the input for the hydro accumulator system (directly or indirectly). It is used to drive a pump; the first system component.

Hydrostatic pumps are displacement machines and enable the transformation of mechanical energy into hydraulic energy (Murrenhoff 2014, p. 153). They energise the hydraulic liquid by displacing it from the low-pressure suction side of the pump (pump inlet) to the high-pressure side (pump outlet). Therefore, the increase of hydraulic energy is manifested as the difference of the liquid's pressure and velocity before and after the pump (Watter 2017, p. 92). Pumps exist in various designs. Examples are the gear, diaphragm, piston and vane pump (Watter 2017, pp. 92-96). One key parameter of the pump is the volumetric displacement V_D, which defines the amount of liquid that a pump is able to deliver per revolution (Watter 2017, p. 96). Dependent on the design, the pump can provide a variable or fixed volume flow Q, i.e. a specific amount of liquid per time, to the hydraulic system (Bauer 2016, p. 75). Besides hydro pumps, there are also continuous-flow machines (e.g. turbine) which can provide the hydraulic energy. In contrast to hydrostatic displacement machines, these components operate with much higher flow rates and on lower pressures (Bauer 2016, p. 73). Since high pressures are

required for the hydro accumulator system, flow machines are not taken into consideration in the remainder of the study.

The *hydraulic liquid*, responsible for energy transmission in the system, is also called the working medium. Further, the liquid takes on other tasks, like the lubrication of bearing areas or the dissipation of heat (Bauer 2016, p. 49). Its characteristics significantly influence the system's performance. Especially the liquid's viscosity, density and temperature resistance determine factors like friction, leakage and heat development (Murrenhoff 2014, pp. 103-109). The majority of hydraulic systems are operated with mineral oils (Murrenhoff 2014, p. 96). However, using water as an alternative working medium seems attractive for sustainable energy storage because it is almost freely available, non-hazardous, can be applied in open-loop systems and is economically degradable. Hence, water is initially utilised as the hydraulic liquid in this thesis. If it turns out that this selection leads to problems (e.g. dissolving effects), the water can still be replaced by oil in later steps.

After passing the pump, the energised liquid is distributed through the hydraulic system via *hydraulic pipes* or *hoses*, which interconnect, for instance, the pump with the hydro accumulator. Pipes are rigid connecting elements, while hoses are made of elastic materials (i.e. flexible connection). Further, the word "pipe" is used as a substitute for both types of connecting elements. The length, shape, diameter and the material of the pipes affect the pressure and velocity of the liquid. For example, the pipe friction, i.e. friction between the pipe wall and the liquid, results in internal pressure losses, which reduce the hydraulic energy (Bauer 2016, pp. 13-15).

To control the power flow, several *valves* need to be utilised in the hydro accumulator system. 'Valves are components to influence the direction and amount of flow and of pressure.' (Murrenhoff 2014, p. 221). The following valves are integrated into the storage system:

Figure 13: Types of integrated valves

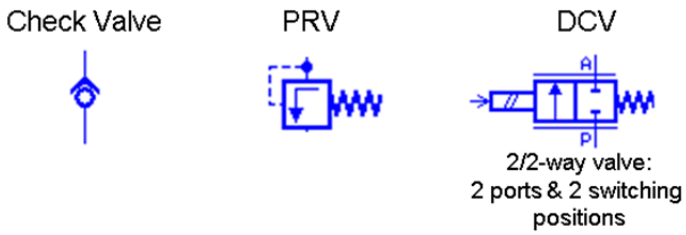

Source: Siemens Industry Software NV 2017

Table 1: Types and function of integrated valves

Valve	Function
Check Valve	The check valve restricts the liquid to flow in only one direction. It is generally located after the pump outlet since liquid might flow from the high-pressure side back into the pump. That would drive the pump in the opposite direction and could cause serious damage (Wei et al. 2018, pp. 5-6).
Pressure Relief Valve (PRV)	The PRV is a pressure control valve. It is applied as a safety valve because it limits the maximum working pressure in the system. It is, for instance, installed in bypass to the pump, in order to release amounts of liquid when pressures become too high (Wei et al. 2018, p. 7; Murrenhoff 2014, p. 254).
Directional Control Valve (DCV)	DCVs control the direction of flow of the liquid in the hydraulic system by open and block specific flow paths. They can be distinct by the number of ports and switching positions that are available (Murrenhoff 2014, p. 243). DCVs are applied to separate the charging and discharging lines.

Besides the valves, several *sensors* are integrated into the storage system to monitor, steer and regulate important system variables such as pressure, shaft velocity and volume flow. Somehow, the required liquid must be supplied and excess liquid must be stored in the hydraulic system. For this purpose, a *liquid tank* is applied. It can simply be a closed metal tank or, for example, an open liquid reservoir for large-scale applications (Bauer 2016, p. 67).

While the liquid transfers the energy through the system, the gas in the hydro accumulator is responsible for the energy storage. The properties of the *storage gas* affect the outcome of the storage process. As mentioned before, conventional hydro accumulators mainly use nitrogen. For first examinations, dry air (further referred to as air) is used as the storage medium because it has several advantages that are illustrated at the end of this chapter. “Dry” means that solved water contents are excluded from consideration, which normally affect the air’s characteristics during operation. Dry air is a mixture of several gases including 78% nitrogen, 21% oxygen and 1% other different gases of which argon is the main component (Hering, Martin & Stohrer 2017 p. 447).

When the accumulator discharges, the potential energy of the gas converts back to hydraulic energy, which then gets carried via the liquid to the *hydraulic motor*. The motor unit, as the final component of the hydraulic storage system, works according to the same principles as the pump but the other way around. That means hydraulic energy is converted back to mechanical energy which, in the next step, can be used to drive a generator and, consequently, create electricity. As it is for pumps, there are many dif-

ferent designs available for hydraulic motors. It is also possible to have a device that works bidirectional, i.e. as pump and as motor (Murrenhoff 2014, p. 155).

Classification of the hydro accumulator system

Comparing the hydro accumulator system with the storage technologies that were illustrated in the introduction, it can be seen that the storage concept is similar to CAES. In both cases, pressurised air is used as the fundamental storage medium. Thus, hydro accumulators can be classified as a "sub-concept" of CAES. However, in CAES systems, air is used both as a working and storage medium, whereas hydro (-pneumatic) accumulator systems utilise a liquid as the working medium (Wietschel et al. 2015, p. 217). This allows the hydraulic systems to transmit higher forces with high efficiency, compared to solely pneumatic systems, because gases have comparably low densities and are therefore much more compressible (Bauer 2016, p. 5; Wietschel et al. 2015, p. 217). Pneumatic systems, like CAES, also have to challenge high amounts of thermal energy generated during compression and expansion. Using a liquid as the working medium has the advantage that heat can be managed more easily. On the one hand, the heat capacity of water is much higher than the heat capacity of air, which reduces temperature changes when energy is absorbed or released (see Chapter 3.2.1 for more details). On the other hand, hydro accumulators can be (dis-) charged over longer time periods so that heat can be exchanged more continuously with the environment (Wietschel et al. 2015, p. 217).

As a roundup of the theoretical background, the advantages and disadvantages of the hydro accumulator system are summarised in the table below.

Table 2: Advantages and disadvantages of the hydro accumulator system

Advantages	Disadvantages

• characteristics of the storage & working medium (air & water):
  ○ (nearly) free & limitless availability
  ○ non-hazardous & non-toxic
  ○ economically degradable
• very low ecological footprint → environmentally friendly ESS
• most system components are technically mature → wide range of choice
• direct & decentralised integration in renewable power generation units (like wind
	• low volumetric energy density → small amount of energy stored per volume
	• space-consuming for large storage capacities
	• hydro accumulators are still immature for large scale-applications
	• discontinuity of the (dis-)charging process due to pressure variations over time → challenges in system regulation and control

Advantages	Disadvantages
turbines) possible → high potential for the energy transition • versatile application areas: small- to large-scale, bulk energy storage, ancillary services, etc. • scalable storage capacity (modular design) → flexibility & adaptability • no irreversible capacity losses (cf. conventional accumulators) • long-lasting ESS (with regular maintenance)	• high maintenance efforts and costs dependent on the type of the accumulator

At this point of the thesis, the overall hydro accumulator system is well understood regarding its functionality, its components, its main characteristics and its state of development. The following chapter investigates the system taking more practical perspectives into consideration.

3 Dimensioning & simulation of a hydro accumulator system

3.1 Introduction of the LMS AMESim Software

LMS AMESim is a simulation software (student edition of the Simcenter Amesim) provided by Siemens Industry Software Inc. It represents a multi-domain platform that covers the entire development process of mechatronic systems. The software enables engineers to quickly model, analyse, asses and optimise the performance of technical solutions in early stages of the design cycle (Siemens Industry Software Inc. 2019).

Figure 14: Architecture of AMESim

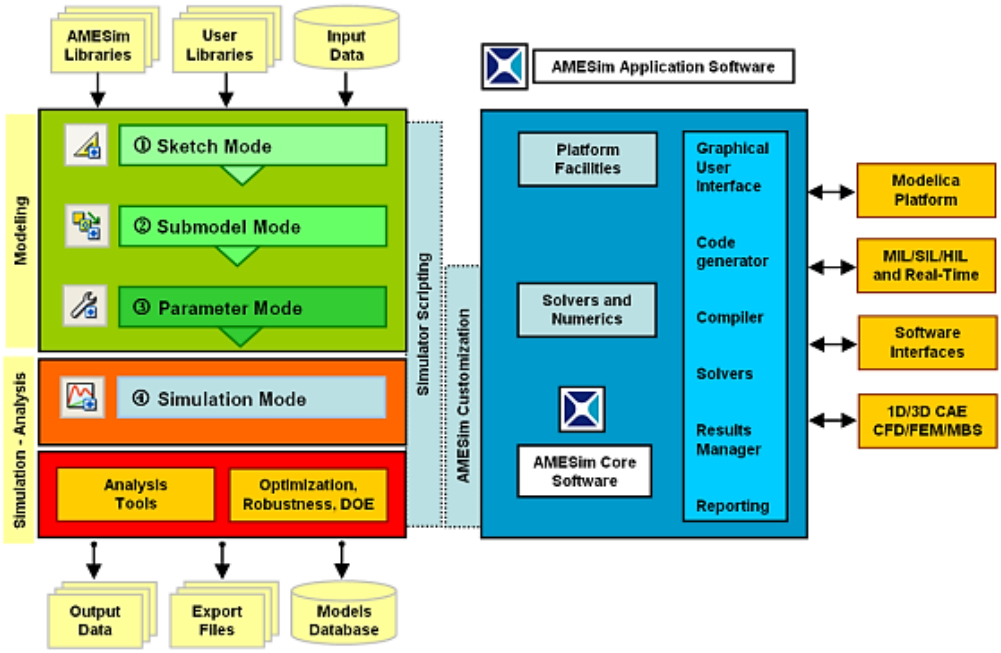

Source: Siemens Industry Software NV 2017

The programme is handeled through an intuitive grafical user interface with four general working modes (cf. Figure 15):

- Sketch mode
- Submodel mode
- Parameter mode
- Simulation mode.

With the *sketch mode,* the user builds up the model for the desired system by making use of an extensive library, which contains pre-defined components as icons for different physical domains (e.g. mechanical, electrical and hydraulic). The components are linked by connecting the inputs of one icon to the outputs of another icon.

Figure 15: Graphical user interface of AMESim

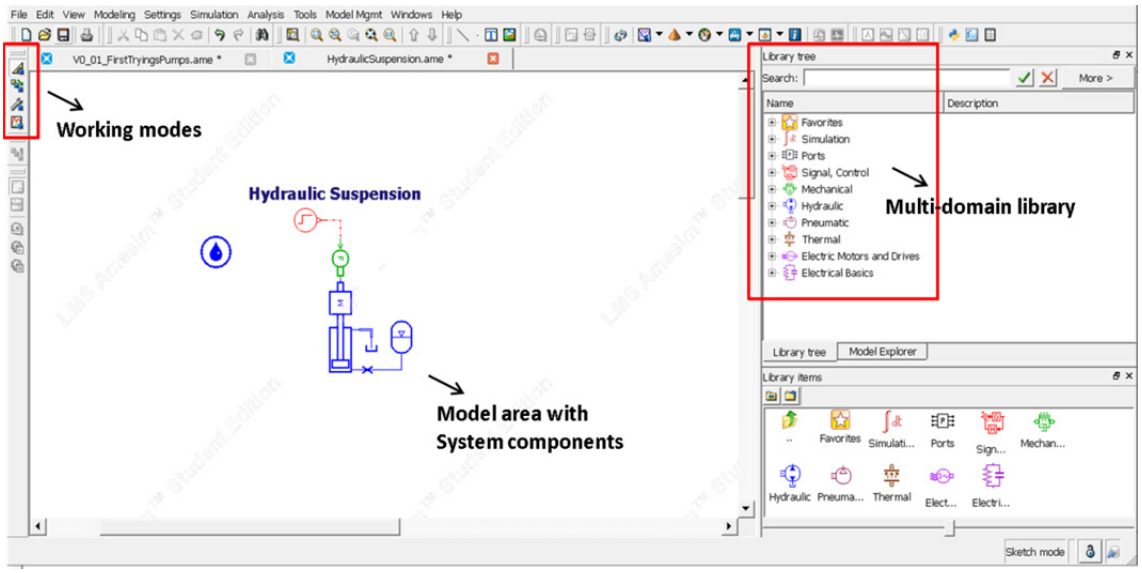

Source: Siemens Industry Software NV 2017

When the model is created, the user has to select the underlying equations of the components in the *submodel mode*. Thus, the selected submodel defines the dynamic behaviour of a component and the superior system during the simulation. For example, a hydraulic pipe can be used to connect a fluid tank and a pump. As a submodel, a direct connection could be selected which would represent an ideal dimensionless connection between the two other components. Furthermore, the hydraulic line could be submodeld by taking realistic compressibility and friction characteristics of the used liquid into account. In this case, corresponding hydraulic equations are selected for the pipe to consider pressure losses and flow behaviour.

Subsequently, the *parameter mode* feeds the model with realistic values by defining the size and characteristics of the used components in more detail. For the pipe, the dimensions can be selected in terms of length, diameter, wall thickness, etc.

Figure 16: AMESim: Parameter setting and plotting of simulation results

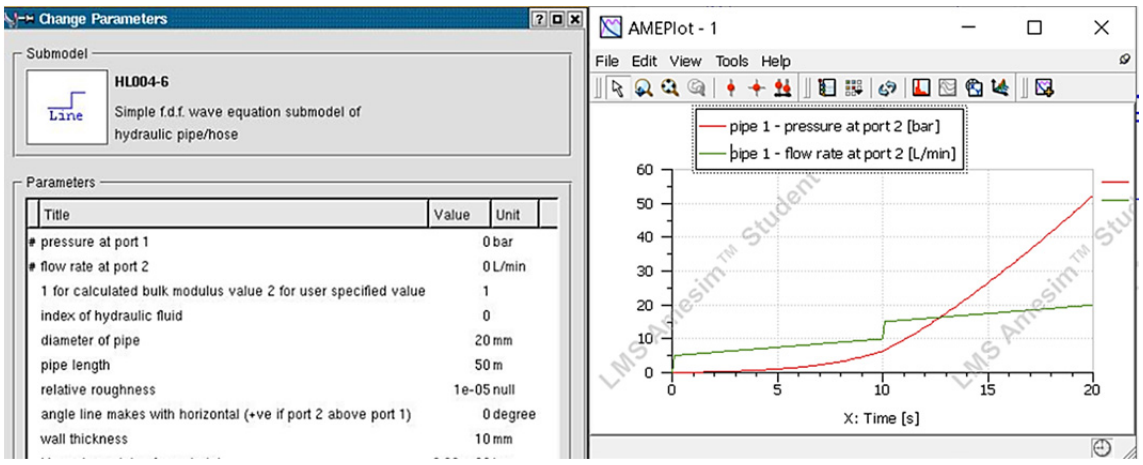

Source: Siemens Industry Software NV 2017

After the parameter setting is finished, a simulation run is initiated in the *simulation mode.* The result is a detailed calculation of the system's behaviour and its parameters over a defined time period. Graphs can be plotted to visualise the results to optimise the model iterative (cf. Figure 16)

Additionally, the program offers a wide range of extra functions and features. Analysis tools like animation, table editor or dashboard support the assessment process. Software interfaces allow data transfer and interaction with other simulation and engineering tools like CAD, CFX, MATLAB, etc. Numerous solvers and simulator scripting functions enable a professional usage for high standard industrial needs.

3.2 Framework and observed parameters

3.2.1 Framework for the dimensioning & simulation

The basic model of the hydro accumulator system is set up according to a predefined framework. The framework is the application environment, where the storage system operates with a set of initial assumptions.

More precisely, this is the interface between the power supply and demand of the system. As the power source, the wind turbine prototype of the WESSPA project is used. Furthermore, an electric load, i.e. a generator, determines the power demand during discharging. Both are initially seen as *constant* power source and consumer, having the following characteristics:

Table 3: Characteristics of the system's power source and consumer

Wind Turbine Prototype (at optimal operating point)		**Generator**	
Power P_{wt} (P_{in}) [W]	500	Power P_g (P_{out}) [W]	500
Rotational speed n_{wt} [rev/min]	300	Frequency f_g [1/s; Hz]	50

Thus, the hydro accumulator system has a constant power input during the charging step and a constant power demand during discharging. While the constant power demand is a realistic assumption, the constant power input remains an initial simplification. Normally, the provided power varies with the intermittent wind speed. Hence, the model should be extended by a variable input in further steps of the research project. Nevertheless, for initial examinations of the storage system, it is more transparent to keep the input values constant. Besides the interfaces, there are additional specifications made for the hydro accumulator system, which are described in the following.

The charge time t_c of the storage system is set to 30min. That is assumed to be long enough to have a nearly isothermal process, i.e. isothermal change of state of the storage medium (air). In the hydro accumulator, the higher operating pressure p_2, i.e. storage pressure, is aimed to be 100bar. According to the optimal pressure ratio for isothermal change of state (2.2.1-3), the lower operating pressure is nearly 37bar. Generally, it is recommended to have a gas pre-charge pressure that is 10% lower than the lower operating pressure (Korkmaz 1982, p. 20). Therefore, the pre-charge pressure p_1 of the air will be equal to 35bar. For the sake of simplicity, this pressure will also be the initial pressure in the hydraulic system, so there is no need to distinct the pre-charge state and the lower operating state of the hydro accumulator (cf. Chapter 2.2.1). Further, the assumption of pressure equality between working and storage medium is maintained. Consequently, the air pressure is always equal to the pressure at the high pressure-side of the hydraulic system.

The pump and the motor of the hydraulic system are ideal fixed displacement units which are controlled torque-dependent with a mechanical gear box (cf. Chapter 3.4.1). Ideal means that an efficiency of 100% is assumed (Murrenhoff 2014, p. 218):

$$\eta_t = \eta_{vol} \cdot \eta_{hm} \qquad = \mathbf{1} \tag{3.2.1-1}$$

η_t total efficiency of the displacement unit

η_{vol} volumetric efficiency

η_{hm} hydraulic-mechanical efficiency

The volumetric efficiency takes volumetric losses like internal and external leakage into account, while hydraulic-mechanical losses are determined by various friction phenomena (Murrenhoff 2014, pp. 213&216). This assumption can be replaced with more realistic values in later steps of the simulation. Furthermore, the pressure at the low-pressure side of these units is, at first, set to zero. Normally, low static pressures should be avoided in hydraulic systems since this can cause solved air to escape from the liquid and form cavities, which implode when the pressure suddenly increases (Kalide 2005, p. 35). This phenomenon is called “cavitation”.

‘Consequences are a faulty behaviour of transport, noise generation as well as increased wear with insufficient lubrication.’(Murrenhoff 2014, p. 113). In later steps of the project, the low-pressures should be adapted in a way that cavitation is prevented.

The working and storage medium, applied in the storage system, are water and dry air. The advantages of this selection were already highlighted in section 2.3. Both have an initial temperature equivalent to the ambient temperature: $T_{wa,1} = T_{air,1} = 293K\ (20°C)$.

The water is assumed to be incompressible (as it was done in Chapter 2.2). This is close to reality, considering that water has a bulk modulus of around 20,000bar.

That refers to a volume change of only 1% when it gets pressurised from 1bar up to 200bar (Sigloch 2017, p. 6). When applying higher pressures or changing the liquid, the compressibility might be taken into account. Besides, other parameters of interest, necessary for the simulation, are the liquid's density and (dynamic) viscosity. In reality, these parameters are a function of the liquid's temperature and pressure (Murrenhoff 2014, pp. 44&108). However, these values are assumed to be constant (cf. Table 4).

The initial supposition of ideal gas behaviour is maintained (cf. Chapter 2.2). The properties for the air, applied in the hydro accumulator, are initially selected according to the standard conditions: ambient temperature (20°C) and pressure (1bar). Important values are the specific heat capacity at constant volume ($c_{v,air}$) and the specific gas constant (R_{air}). The gas constant is required to determine the state variables (e.g. volume and pressure) of the air during operation (cf. 2.2-2). The specific heat capacity is an important parameter regarding the heat development at the accumulator. It depends on and rises with the temperature of the gas. That is why an average value for the existent temperature range during operation should normally be applied ($c_{vm}|_{t_1}^{t_2}$) (Cerbe & Wilhelms 2013, pp. 75-76). Since almost isothermal state change is assumed, it is not necessary to calculate an average and $c_{v,air}$ is set according to standard conditions: 718J/kgK (Sigloch 2017, p. 463). This means that 718J of energy is required to raise the temperature of 1kg of air by 1K. In other words, the smaller the heat capacity of a medium, the higher the change of temperature for the same amount of added energy. In comparison, water has a much greater heat capacity of 4187J/kgK (Sigloch 2017, p. 463), which makes it capable of storing high amounts of energy without significant temperature changes.

The properties of interest for the water and the air are summarised in the table below (according to previous specifications).

Table 4: Properties of the applied working and storage medium

Water		**Air**	
Temperature $T_{wa,1}$ [K]	293	Temperature $T_{air,1}$ [K]	293
Density ρ_{wa} [kg/m^3]	1,000	Specific heat capacity $c_{v,air}$ [J/kgK]	718
Bulk Modulus E_{wa} [bar]	20,000*	Gas constant R_{air} [J/kgK]	287
Dynamic viscosity η_{wa} [cP]	1.002	Isentropic exponent κ	1.4
(η [Pa·s, Ns/m^2], 1cP = 1"centipoise" = 10^{-3} Pa·s) *can be used without notable influences on the simulation results			

Source: Sigloch 2017, pp. 6, 454, 455, 463

The predefinitions, made in the framework, will be used as the basis for the dimensioning of the key components (Chapter 3.3). Assumptions for design parameters will be made as realistic as possible, so that the simulation model and the correlation of several system parameters can be examined properly. In later steps, the basic model can be varied, optimised and scaled up to greater dimensions.

To ensure comparability with other storage technologies and proper assessment of the simulation model, the following parameters of interest will be in focus.

3.2.2 Observed parameters

Discharge time t_d

Contrary to the charge time, which is set to 30min, the discharge time depends on the amount of requested power and on the actual amount of energy that is stored in the hydro accumulator before discharging. It defines the time period where the hydro accumulator discharges from the higher operating pressure back to pre-charge pressure. The more energy is available, the longer the storage system will be able to drive the constant generator unit at defined power. The amount of stored energy is reduced by losses, occurring during operation, which consequently reduce the discharge time.

t_c charge time [s] (with $t_c = 30min = 1800s$)

t_d discharge time [s]

Efficiency η_s

The total efficiency of a system is the ratio of energy output to energy input of one storage cycle:

$$\eta_s = \frac{E_{out}}{E_{in}} = \frac{P_{out} \cdot t_d}{P_{in} \cdot t_c} \qquad 3.2.2\text{-}1$$

η_s total efficiency of one storage cycle

E_{out} & E_{in} energy output and energy input [kWh]

P_{out} & P_{in} power output and power input [W]

t_d & t_c discharge time and charge time [s]

The higher the efficiency, the better the storage technology is capable of storing and releasing amounts of energy without losses (e.g. waste heat, hydraulic and mechanical friction, etc.). The efficiency can also be determined for the charging step by putting the stored energy in relation to the input energy, after the hydro accumulator is charged. Respectively, the efficiency of the discharging step can be calculated by the ratio of energy output and stored energy.

$$\eta_c = \frac{E_{st}}{E_{in}}, \qquad \eta_d = \frac{E_{out}}{E_{st}} \qquad \text{3.2.2-2}$$

η_c efficiency of the charging process

η_d efficiency of the discharging process

E_{st} stored energy [kWh]

Volumetric energy density W'

The volumetric energy density was already defined in chapter 2.2.1 (2.2.1-6). It is the stored energy per volume, which allows the comparison with other storage technologies. It also can be used to scale up the observed ESS.

Due to the simplifications and assumptions for the basic model, the mentioned parameters may be less meaningful for first simulations. In the further course of the project, however, they can be complemented and used for comparison purposes.

3.3 Dimensioning of the key components

This chapter provides the basics for the dimensioning of the key components of the hydro accumulator system dependent on the framework, which was illustrated in chapter 3.2.1. The results will be used to feed the basic simulation models with appropriate parameters in the next step.

3.3.1 Dimensioning of the pump and motor

The input power serves as a starting point for the dimensioning of the pump. The prototype of the wind turbine provides 500W, which is the mechanical power that the pump is able to convert into hydraulic power in the (assumed) best case ($P_{wt} = P_p$). The power of a hydrostatic displacement machine can be calculated as follows (Murrenhoff 2014, p. 35):

$$P = \omega \cdot T = Q \cdot \Delta p = V_D \cdot \frac{n}{60} \cdot \Delta p \qquad \text{3.3.1-1}$$

P power [W]

ω angular velocity [1/s]

T torque [Nm]

Q volume flow [m^3/s]

Δp pressure difference between inlet p_i and outlet p_o [N/m^2]

V_D volumetric displacement [m^3/rev]

n rotational speed [rev/min]

(rev/min = rpm; rev = revolution = 1; the stated SI units are used for the calculation. However, the pressure is usually displayed in [bar], the volume flow in [l/min] and the volumetric displacement in [cm^3/rev])

Consequently, the power of the pump is:

$$P_p = \omega_p \cdot T_p = Q_p \cdot \Delta p = V_{D,p} \cdot \frac{n_p}{60} \cdot \Delta p \quad = \mathbf{500W} \qquad \text{3.3.1-2}$$

For the basic model, a fixed displacement pump will be integrated. The volumetric displacement must be determined so that the pump operates within a proper speed range by a given storage pressure. On the one hand, operation at too low speed results in low efficiency and can cause problems regarding self-lubrication and overheating (Murrenhoff 2014, p. 218). Too high speeds, on the other hand, can cause damage to the mechanics of the pump. Manufacturers usually recommend rotational speeds above 150-700rpm dependent on the pump design (Bosch Rexroth AG 2019, Moog Inc. 2016). Thus, the minimum speed of the applied pump is set to 750rpm for the simulation ($n_{p,min} = 750\,\frac{rev}{min}$).

The minimum speed of the pump appears at the highest operating pressure. Hence, the volumetric displacement at 100bar can be calculated according to 3.3.1-2. As mentioned before, the pressure at the pump inlet is assumed to be zero, so that $\Delta p = p_2 = p_o = 100bar$:

$$P_p = V_{D,p} \cdot \Delta p \cdot \frac{n_p}{60} \Leftrightarrow V_{D,p} = \frac{P_p}{\Delta p \cdot \frac{n_p}{60}}$$

$$\Rightarrow V_{D,p} = \frac{500W}{100 \cdot 10^5\,\frac{N}{m^2} \cdot \frac{750\,\frac{rev}{min}}{60}} = \mathbf{4 \cdot 10^{-6}\,\frac{m^3}{rev}} = \mathbf{4\,\frac{cm^3}{rev}}$$

With the volumetric displacement, the maximum pump speed at the pre-charge pressure state can be determined according to 3.3.1-2 ($\Delta p = p_1 = p_o = 35bar$):

$$P_p = V_{D,p} \cdot \Delta p \cdot \frac{n_{p,max}}{60} \Leftrightarrow n_{p,max} = \frac{P_p \cdot 60}{\Delta p \cdot V_{D,p}}$$

$$\Rightarrow n_{p,max} = \frac{500W \cdot 60}{35 \cdot 10^5\,\frac{N}{m^2} \cdot 4 \cdot 10^{-6}\,\frac{m^3}{rev}} \approx \mathbf{2150\,\frac{rev}{min}}$$

It can be seen that the pump operates in an appropriate speed range between 750 and 2150rpm. The maximum speed of the pump results in a maximum volume flow of (Murrenhoff 2014, p. 35):

$$Q = n \cdot V_D \Rightarrow Q_{p,max} = n_{p,max} \cdot V_{D,p} = 2150\,\frac{rev}{min} \cdot 4\,\frac{cm^3}{rev} = 8600\,\frac{cm^3}{min} \qquad \text{3.3.1-3}$$

$$= \mathbf{8.6\,\frac{l}{min}} \approx \mathbf{143 \cdot 10^{-6}\,\frac{m^3}{s}}$$

Respectively, the minimum volume flow at the minimum speed yields: $Q_{p,min} = \mathbf{3\,\frac{l}{min}}$.

It is assumed that the hydraulic motor has the same dimensions as the pump. This makes sense regarding the variability of the system. Having the same characteristics for both, the pump and the motor, allows replacing both components with one pump-motor unit. If deviations during the discharging process occur, which affect the motor in a way that the dimensions become unrealistic, adjustments can still be made afterwards.

Consequently, the dimensions of the power components, i.e. the pump and the hydraulic motor, can be summarised as follows:

Table 5: Dimensions of the pump and the motor of the basic model

Pump and motor of the basic model	
Power: P_p, P_m [W]	500
Volumetric displacement: $V_{D,p}$, $V_{D,m}$ [cm^3/rev]	4
Speed range: n_{min} – n_{max} [rev/min]	750-2150
Volume flow range : Q_{min} – Q_{max} [l/min]	3-8.6

There is the opportunity to replace the fixed displacement units by variable displacement units. They allow the adjustment of the volumetric displacement (e.g. manual, electric or hydraulic adjustment) (Bauer 2016, pp. 75&102-103). Consequently, the provided volume flow can be regulated with a higher level of flexibility in combination with the torque-dependent control (cf. Chapter 3.4.1), which then can increase the overall efficiency of the system. For example, the Krisch-Dienst GmbH Fluidtechnik offers different kinds of “Janus” variable axial piston pumps and motors. They solely run with water, operate up to 160bar and displace between 1 and 70.3cm^3/rev dependent on their design (Krisch-Dienst GmbH Fluidtechnik n.d.). This might be a potential supplier for the implementation of a prototype. However, for the basic model this thesis initially stays with the fixed displacement units.

3.3.2 Dimensioning of the hydro accumulator

The first value of interest is the storage size of the hydro accumulator. According to the framework, the accumulator is charged for 30min with an ideally power input of 500W. That corresponds to an energy input of ($E_{in} = W_c,\ P_{wt} = P_p$):

$$W_c = P_p \cdot t_c = 500W \cdot 1800s = 900000J = \mathbf{0.25kWh}$$

Referring to the volumetric energy density, calculated for the ideal isothermal change of state (Chapter 2.2.1), the storable amount of energy with 200bar storage pressure was 2.04kWh/m^3 (2.2.1-7). With 100bar storage pressure, this value is halved: **1.02kWh/m^3**.

Hence, the air in the accumulator will store 1.02kWh of energy per cubic metre in the best case (W'). Together with W_c, the required volume of the storage medium can be derived:

$$V_{air} = (W')^{-1} \cdot W_c = \frac{1m^3}{1.02kWh} \cdot 0.25kWh \approx \mathbf{0.245}\boldsymbol{m^3} = \mathbf{245}\boldsymbol{l}$$

Since the isothermal storage process is idealistic, the actual amount of storable energy per volume (W') will be lower. Thus, the air volume is slightly increased for the simulation and the total accumulator volume is set according to the following assumption:

$$V_{acc} = \mathbf{250}\boldsymbol{l}$$

$$V_{air} = V_{acc} - 1l = \mathbf{249}\boldsymbol{l}$$

As a potential component, a standard bladder accumulator from HYDAC (Type SB330-200) could be selected. This accumulator has a slightly lower storage volume of 200l but can operate with pressures up to 330bar (HYDAC INTERNATIONAL GmbH n.d.). Thus, HYDAC's accumulator has roughly the same characteristics as the hydro accumulator defined in this thesis. It is used as a reference for some parameters, which are needed in the following section.

The thermal time constant is another important parameter that has to be determined. It allows the consideration and modelling of heat exchange processes between the hydro accumulator and its surrounding. It is defined as the ratio of heat storage capacity and heat exchange capacity of the storage gas and can be described by the following equation (Rotthäuser 1993, p. 46):

$$\tau = \frac{m_g \cdot c_v}{\alpha_g \cdot A_g} \qquad \text{3.3.2-1}$$

τ thermal time constant [s]

m_g mass of the gas [kg]

c_v gas specific heat capacity at constant volume [J/kgK]

α_g overall heat transfer coefficient [W/m^{2}K]

A_g thermal exchange area of the gas [m^2]

(α_g ≙ combination of heat conduction through the surface area and heat convection between the gas and the hydro accumulator and the hydro accumulator and its surrounding)

With the assumption of ideal gas behaviour (2.2-2) at pre-charge state, the mass of the gas can be replaced as follows:

$$\tau = \frac{p_1 \cdot V_1 \cdot c_v}{T_1 \cdot R_g \cdot \alpha_g \cdot A_g} \qquad \text{3.3.2-2}$$

The exact calculation of τ is laborious and very complex, since it is related to various parameters, like the design of the accumulator, the storage medium, applied pressures, etc. (Rotthäuser 1993, p. 66; Korkmaz 1982, p. 29). Additionally, some influencing factors, like the heat transfer coefficient and the effective thermal exchange area, change during operation (Pourmovahed & Otis 1990, p. 117). This is the reason why the thermal time constant is usually determined experimentally in practice (cf. Pourmovahed & Otis 1990).

For the sake of simplicity, the thermal time constant is, therefore, only roughly calculated. It can serve as a reference for later investigations. Referring to the values defined in the framework and the dimensioning section, the state variables as well as the properties of the air are already known:

$$p_1 = 35bar, \qquad V_1 \approx 250l, \qquad T_1 = 293K, \qquad R_{air} = 287\,{}^{J}/_{kgK}, \qquad c_{v,air} = 718\,{}^{J}/_{kgK}$$

In order to calculate the thermal time constant, two parameters are missing: α_g, A_g. Actually, the total heat transfer coefficient α_g depends on various parameters. These include, for instance, the material properties (e.g. viscosity of the air, thermal conductivity characteristics of the water, the pressure vessel and the separator, etc.) as well as the flow and convection characteristics of the air (cf. Cerbe & Wilhelms 2013, pp. 371-380). For this calculation, only the heat transfer coefficient (i.e. the heat exchange between the gas and the surface area) is taken into account. A practical approximate value for gases is provided by Cerbe & Wilhelms (2013, p. 530): $\alpha_g \approx \mathbf{45\,W/m^2K}$.

The thermal exchange area A_g (i.e. surface area where heat transfer occurs) depends on the accumulator type, shape and state of charge. For the calculation, the surface area will be simplified assumed to be constant. The bladder accumulator SB330-200 from HYDAC serves as a reference to calculate A_g. Since the air volume was assumed to be nearly the accumulator volume in pre-charge state ($V_{air} = V_{acc} - 1l$), the shape and size of the flexible bladder is close to the actual accumulator's shape and size ($A_{acc} \approx A_g, V_{acc} \approx V_g = V_1$). Consequently, the form of the bladder can be simplified as a cylinder, which is capped at both ends with a half-sphere (cf. Figure 6). Thus, the surface area yields (geometric formulas: Hering, Martin & Stohrer 2017, p. 25):

$$A_g = A_c + 2A_{hs} = A_c + A_s$$

$$\Rightarrow A_g = 2\pi \cdot r \cdot h + 4\pi \cdot r^2 \qquad \text{3.3.2-3}$$

The height h of the cylindrical part is assumed to be 10 times the radius r, which is acceptable when comparing the radius and the height of the SB330-200: $r = 205mm$, $h \approx 2100mm$. Hence, equation 3.3.2-3 can be simplified as follows.

$$A_g = 2\pi \cdot r \cdot 10 \cdot r + 4\pi \cdot r^2 = 24\pi \cdot r^2 \qquad \text{3.3.2-4}$$

In order to reach the defined volume of 250l (V_g), the values of the referenced accumulator need to be slightly adapted for the hydro accumulator used in this thesis.

$$V_g = V_c + V_s = \pi \cdot r^2 \cdot h + \frac{4}{3}\pi \cdot r^3 = 10\pi \cdot r^3 + \frac{4}{3}\pi \cdot r^3 = \frac{34}{3}\pi \cdot r^3 \qquad \text{3.3.2-5}$$

$$\Leftrightarrow r = \sqrt[3]{\frac{3 \cdot V_g}{34\pi}} \quad \Rightarrow r = \sqrt[3]{\frac{3 \cdot 0.25m^3}{34\pi}} \approx 0.19m = \boldsymbol{190mm} \qquad \text{3.3.2-6}$$

As a result, the thermal exchange area of the hydro accumulator (with the dimensions: $r = 190mm$ & $h = 1900mm$) yields (3.3.2-4):

$$A_g = 24\pi \cdot r^2 = 24\pi \cdot (0.190m)^2 \approx \boldsymbol{2.722m^2}$$

By inserting all previously defined values in equation 3.3.2-2, the thermal time constant can finally be calculated (based on the set of assumptions):

$$\tau = \frac{p_1 \cdot V_1 \cdot c_v}{T_1 \cdot R_g \cdot \alpha_g \cdot A_g} = \frac{35 \cdot 10^5 \frac{N}{m^2} \cdot 0.25m^3 \cdot 718 \frac{J}{kgK}}{293K \cdot 287 \frac{J}{kgK} \cdot 45 \frac{W}{m^2K} \cdot 2.772m^2} \approx \boldsymbol{60s}$$

A thermal time constant with the above value means that the gas temperature reaches 63.2% of the system's final temperature after 60s (Pourmovahed & Otis 1990, p. 118).

Based on practical measurements made by Rupprecht, the thermal time constant can also be approximated with the following equations (cf. Rupprecht 1988):

Table 6: Approximation equations for the thermal time constant

Bladder accumulator	Piston accumulator
$\tau = 1.338 \cdot p \cdot V^{0.313}$	$\tau = 0.3 \cdot p \cdot V^{0.22} + 86.2 \cdot V^{0.49}$
p [bar] at 20°C, V [m^3]	

Using these equations results in a thermal time constant of either 30s (bladder-type) or 51s (piston-type) for the dimensioned hydro accumulator. The real value for τ will lie somewhere in between the calcualtion results of this section. Consequently, an initial thermal time constant of $\tau = \boldsymbol{50s}$ is sufficiently accurate for the simulation. It is also the practice-oriented default value of the software AMESim.

The comparison of the (dis-) charge time with the thermal time constant allows the characterisation of the change of state. For example, utilising charge times, which are much shorter than the thermal time constant ($t_c \ll \tau$), results in a rather isentropic change of state. On the other hand, much longer charging ($t_c \gg \tau$) result in a nearly

isothermal change of state (Korkmaz 1982, p. 29). The charge time for the simulation is predefined with 1800s which is, by far, greater than the thermal time constant. Therefore, the assumption of nearly isothermal operation is entirely justified.

The specification of the inlet of the hydro accumulator is the final step of this dimensioning. During the storage process, flow resistances occur at the inlet. For example, the poppet at the bladder accumulator (cf. Figure 6), necessary to prevent the bladder to get pushed out, restricts the volume flow and leads to pressure losses. Consequently, inlet behaviour and losses can be modelled with the orifice law, which represents a narrowing of the cross section between connecting pipe and hydro accumulator (Murrenhoff 2014, p. 51):

$$Q = \alpha_D \cdot A_0 \sqrt{\frac{2 \cdot \Delta p}{\rho}} \qquad 3.3.2\text{-}7$$

α_D flow coefficient (depends on geometry)

A_0 orifice cross section [m^2]

ρ density of the liquid [kg/m^3]

However, orifice effects only gain importance when high flow rates are utilised. Since the volume flows are very low for this storage system, resulting losses will be marginal and can be neglected in the first step. Hence, the required orifice parameters (α_D & A_0) can be assumed as follows for the simulation:

- $\alpha_D = \mathbf{0.7}$ (≙ reference value according to Murrenhoff 2014, p. 52)
- $A_0 = \frac{A_{pipe}}{2}$, with $d_0 = \frac{d_{pipe}}{2} = \mathbf{10mm}$ (cf. Chapter 3.3.3)

The results of the dimensioning of the hydro accumulator are summarised in table 7.

Table 7: Dimensions of the hydro accumulator of the basic model

Hydro accumulator of the basic model	
Accumulator volume V_{acc} [l]	250
Thermal time constant τ [s]	50
Orifice diameter d_0 [mm] & flow coefficient α_D	10 & 0.7
Storage medium (air)	
Pre-charge volume V_1 [l]	249
Pre-charge pressure p_1 [bar]	35
Higher operating pressure p_2 [bar]	100
Pre-charge temperature T_1 [K]	293

3.3.3 Dimensioning of further components

Hydraulic pipes

At first, the dimensioning of the hydraulic pipe is limited to its diameter and its wall thickness. Additional specifications, like the pipe length and the surface roughness, can be added in further steps. While the flow rate is the parameter that determines the necessary diameter, the maximum operating pressure determines the required wall thickness (Murrenhoff 2014, p. 301).

To find an appropriate pipe diameter for the basic model, the Reynolds number plays an important role. The dimensionless number Re marks the point at which the flow behaviour of fluids changes from laminar to turbulent (Murrenhoff 2014, p. 50). Generally, laminar flows are preferred because, in this case, the pressure losses along the pipe only increase linearly with the volume flow (quadratic increase for turbulent flows) (Bauer 2016, pp. 15-16). For liquids, Re is defined as follows (Bauer 2016, p. 13):

$$Re = \frac{v \cdot d_{hyd}}{\nu} \qquad \text{3.3.3-1}$$

v average flow velocity [m/s]
d_{hyd} hydraulic diameter [m]
ν kinematic viscosity (“ny”) of the fluid [m^2/s]

The hydraulic diameter is equivalent to the internal diameter of the pipe ($d_{hyd} = d_{in}$) (Bauer 2016, p. 13). With some transformations, the Reynolds number of hydraulic pipes can be displayed as (Bauer 2016, p. 14):

$$Re = \frac{v \cdot d_{in}}{\nu}, \qquad Q = v \cdot A = v \cdot \pi \cdot \frac{{d_{in}}^2}{4}$$

$$\Rightarrow Re = \frac{Q \cdot d_{in}}{\nu \cdot A} = \frac{4 \cdot Q \cdot d_{in}}{\nu \cdot \pi \cdot {d_{in}}^2} = \frac{4 \cdot Q}{\nu \cdot \pi \cdot d_{in}} \qquad \text{3.3.3-2}$$

Q flow rate / volume flow [m^3/s]
A cross section of the pipe [m^2]
d_{in} internal diameter of the pipe [m]

The diameter should be defined, so that a critical Reynold number Re_{cr} is not exceeded, i.e. the flow type remains laminar. For pipes, the critical value lies between 2300-2400 (Sigloch 2017, p. 456). This value is likely to be surpassed with high volume flows.

Consequently, the operating state, at which the maximum volume flow occurs, is the reference point (cf. Chapter 3.3.1): $Q_{max} = 8.6\frac{l}{min}$, $p_1 = 35bar$, $T_1 = 293K$. By using these values, the kinematic viscosity of water can be approximated according to a table provided by Herbert Sigloch (2017, p. 454): $\nu_{wa} \approx \mathbf{1.002 \cdot 10^{-6}\,\frac{m^2}{s}}$.

By selecting the lower value $Re_{cr} = 2300$, the diameter of the pipe can now be calculated:

$$Re_{cr} > \frac{4 \cdot Q}{\nu_{wa} \cdot \pi \cdot d_{in}} \Leftrightarrow d_{in} > \frac{4 \cdot Q}{\nu_{wa} \cdot \pi \cdot Re_{cr}} \qquad \text{3.3.3-3}$$

$$\Rightarrow d_{in} > \frac{4 \cdot 143 \cdot 10^{-6}\,\frac{m^3}{s}}{1.002 \cdot 10^{-6}\,\frac{m^2}{s} \cdot \pi \cdot 2300} \approx 0.079m = \mathbf{79mm}$$

It can be seen that the internal diameter should be bigger than around 8cm in order to have laminar flow in the pipe. This is a pretty high value, which is not technically sensible for such a small-scale system. The reason for the large diameter is the characteristically low kinematic viscosity of water.

As a comparison, the use of HLP 46, a standard hydraulic oil with a viscosity of 46mm²/s at 40°C (Bauer 2016, p. 50), would result in a minimum diameter of only 1.7mm under the same conditions. Consequently, laminar flows are difficult to realise when utilising water as the hydraulic liquid in small-scale systems.

Choosing a different approach provided by Murrenhoff, the required pipe diameter can be calculated as follows (2014, p. 301):

$$A = \pi \cdot {r_{in}}^2 = \pi \cdot \frac{{d_{in}}^2}{4} = \frac{Q}{v} \Leftrightarrow d_{in} = \sqrt{\frac{4 \cdot Q}{\pi \cdot v}} \qquad \text{3.3.3-4}$$

A	cross section of the pipe [m^2]
r_{in}	internal radius of the pipe [m]
d_{in}	internal diameter of the pipe [m]
Q	flow rate / volume flow [m^3/s]
v	average flow velocity [m/s]

With $Q = Q_{max} = 143 \cdot 10^{-6} \frac{m^3}{s}$ and a recommended average flow velocity of around 4m/s for operation pressures between 50 and 100bar (Murrenhoff 2014, p. 301), the internal diameter is given with (3.3.3-4):

$$d_{in} = \sqrt{\frac{4 \cdot Q}{\pi \cdot v}} = \sqrt{\frac{4 \cdot 143 \cdot 10^{-6} \frac{m^3}{s}}{\pi \cdot 4 \frac{m}{s}}} \approx 0.00675m = \mathbf{6.75mm}$$

The result shows a recommendation for the pipe diameter of around 6.75mm. This is comparably small regarding the previous calculation and would result in a Reynolds number of around 27,000, which represents by far a turbulent flow. Fortunately, the lengths of the pipes, utilised for the prototype, are rather short. This means that occurring pressure losses remain low despite turbulent flow.

As a consequence, the pipe's initial diameter can be set to an appropriate mean value of **20mm** (≈ **3/4inch**) for the basic model. This value can be adapted in later steps to minimise efficiency losses in the connecting elements. The wall thickness can be determined according to the DIN EN 10305. For example, seamless steel pipes with an internal diameter of 20mm and a wall thickness of **1mm** allow operating pressures up to 128bar (safety factor 1.5, temperature range: -40°C – +120°C), which would be a convenient component for the prototype system (Bauer 2016, p. 204).

Valves and sensors

For the basic model, the valves and the sensors of the hydro accumulator system are dimensioned in a way that they just provide their functionality and have no negative impact on the storage process. Thus, the dynamic characteristics of the named components are being ignored for convenient analysing and modelling. For example, the check valve only restricts the direction of flow without causing any pressure losses due to friction. These impacts can be taken into account in further steps of the project.

At this stage, the framework for the simulation of the basic model is set and the dimensioning of the utilised components is done according to a subset of initial assumptions. This allows the setup and investigation of the basic model with AMESim, which is done in the following chapter.

3.4 Setup of the basic simulation model

In order to understand the results of further simulations, the model of the hydro accumulator system will initially be subdivided into the charging and discharging process. The separated models will be illustrated and their functionality will be explained. Subsequently, the simulation of the models will be executed, evaluated and checked against the results of the dimensioning.

3.4.1 Setup and simulation of the basic charging model

Figure 17 shows the AMESim basic model of the charging process of the hydro accumulator system. The green icons represent the input interface, the red icons the control scheme and the blue icons illustrate the system's storage components. More details are provided in the HTML report of the charging model (Appendix A).

Figure 17: Setup of the basic charging model

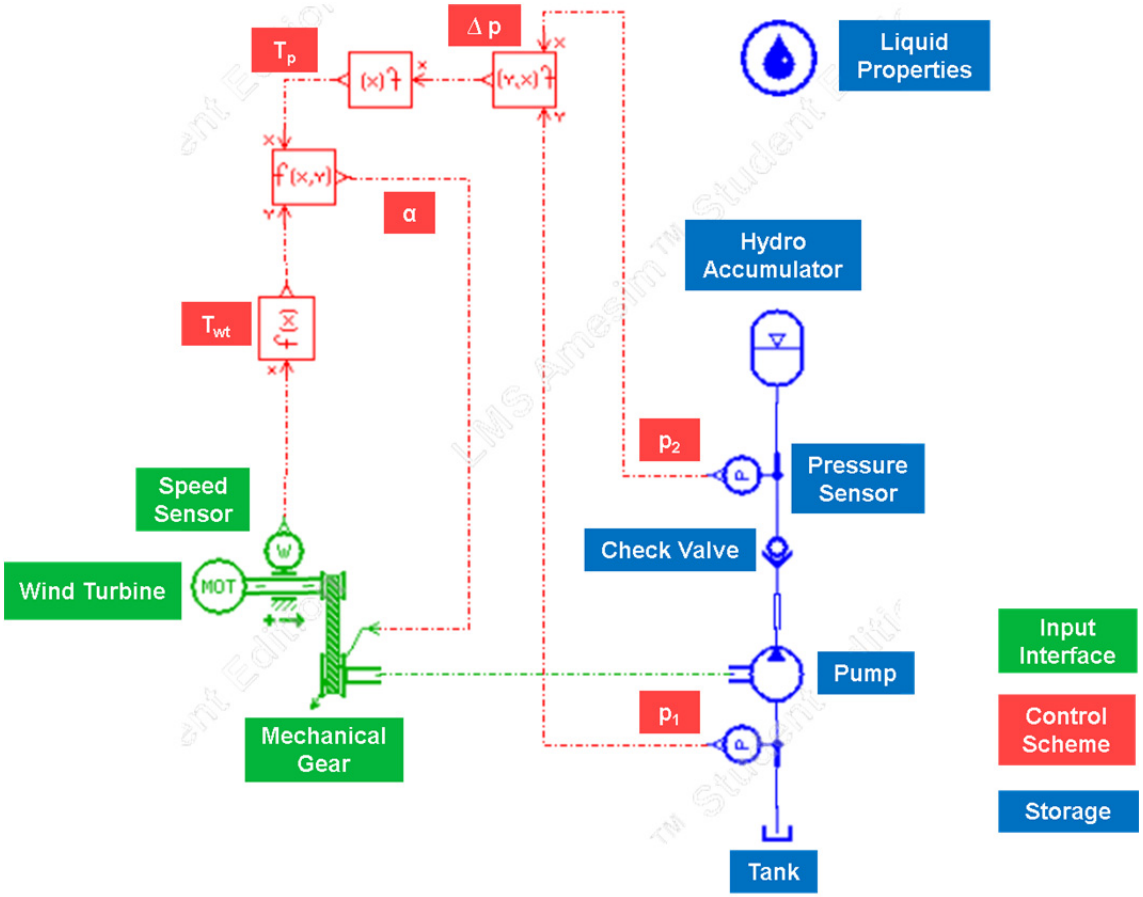

Input Interface

Since the input of the wind turbine is assumed to be constant ($n_{wt} = 300 rev/min$, $P_{wt} = 500W$), it can be represented in a simplified way with a constant-speed motor which applies the same characteristics. A variable wind input can replace the motor in later steps. Furthermore, the wind turbine and the hydraulic pump are coupled mechanically. For the simulation model, an ideal (i.e. efficiency of 100%) stepless mechanical gearbox (MGB) is implemented. Stepless MGBs provide continuously variable transmission (CVT). Normally, these MGBs operate with a maximum efficiency of 90 to 95% (Ruan, Zhang & Walker 2015, p. 2; AïtTaleb, Chaâba & Sallaou 2013, p. 156). However, for the practical implementation in the WESSPA project the translation of power is most likely done electrically with a generator and frequency converter, since electrical transmission components are cheaper and improve the regulation flexibility by having comparable efficiency. Consequently, the MGB is only applied to provide its key function: To control the power at the interface by providing the (lossless) conversion of torque and speed. Thus, the MGB maintains the power equality at its input and output ports. More precisely, the wind turbine is only able to provide a specific amount of power to the storage system (500W). The MGB regulates the pump's speed via the gear ratio alpha (α) so that the pump also operates with 500W of power during the charging process. The underlying control scheme is illustrated below.

Control scheme

The base equation for the control of the charging process is the power equality at the input interface:

$$P_{wt} = P_p$$

$$\omega_{wt} \cdot T_{wt} = \omega_p \cdot T_p \qquad \text{3.4.1-1}$$

P_{wt} Power of the wind turbine [W]

P_p Power of the pump [W]

ω_{wt} angular velocity of the wind turbine [1/s]

T_{wt} torque of the wind turbine [Nm]

ω_p angular velocity of the pump [1/s]

T_p torque of the pump [Nm]

(with $\omega = 2\pi \cdot f = 2\pi \cdot \frac{n}{60}$; frequency f [1/s], rotational speed n [1/min])

The gear ratio α is the ratio of speed or of torque, which is needed as an input for the MGB:

$$\alpha = \frac{T_{wt}}{T_p} = \frac{\omega_p}{\omega_{wt}} \qquad \text{3.4.1-2}$$

In the applied control scheme, the gear ratio is calculated with the torque of the wind turbine and the torque of the pump. The torque of the wind turbine is given with 3.4.1-1, whereby the actual speed is captured with a speed sensor:

$$T_{wt} = \frac{P_{wt}}{\omega_{wt}} = \frac{P_{wt}}{2\pi \cdot \frac{n_{wt}}{60}} = \frac{30}{\pi} \cdot \frac{P_{wt}}{n_{wt}} \qquad \text{3.4.1-3}$$

According to 3.3.1-2, the torque of the pump is stated with:

$$T_p = \frac{V_D \cdot \Delta p}{2\pi} = \frac{V_D \cdot (p_2 - p_1)}{2\pi} \qquad \text{3.4.1-4}$$

The volumetric displacement V_D is a fixed value (cf. Chapter 3.3.1), while the pressure difference Δp is variable and thus recorded with two pressure sensors. During the charging process, the pressure of the air and consequently the pressure in the hydraulic system continuously increase. This results in an increasing resistance, which restricts the volume flow provided by the pump. As a consequence, the torque at the pump rises simultaneously with the increasing Δp over time. To maintain power equality, the speed of the pump must be reduced accordingly (cf. 3.4.1-1), which is done with the MGB by feeding the torque ratio T_{wt}/T_p as the gear ratio.

Storage

The simulation of the loading process is conducted according to the specifications established in the framework and dimensioning section. The hydro accumulator, with a volume of 250l and a pre-charge pressure of 35bar, is loaded under ambient temperature conditions for 30 minutes with 500W. The hydraulic power is provided by a pump which displaces 4cm^3 of water per revolution (see Chapter 3.2 & 3.3 or Appendix A for the remaining values). A check valve restricts the liquid to flow back into the pump. The liquid icon determines the water's properties (cf. Chapter 3.2.1) and the tank, as an idealised infinite liquid source, provides the required amounts of water.

The execution of the simulation allows the validation of the control method and illustrates the working process of the ESS.

Simulation results of the input interface and the pump

Figure 18 summarises the simulation results of the input interface and the pump. The graph on the bottom right displays the constant torque of around 16Nm, which is provided by the wind turbine. The results for the pump show that the implemented control scheme works correctly. The pump's shaft torque rises during the charging process (from roughly 2 to 6 Nm). Consequently, the gear ratio permanently reduces the pumps shaft speed to maintain the system's power.

Figure 18: Simulation results of the input interface & pump (charging model)

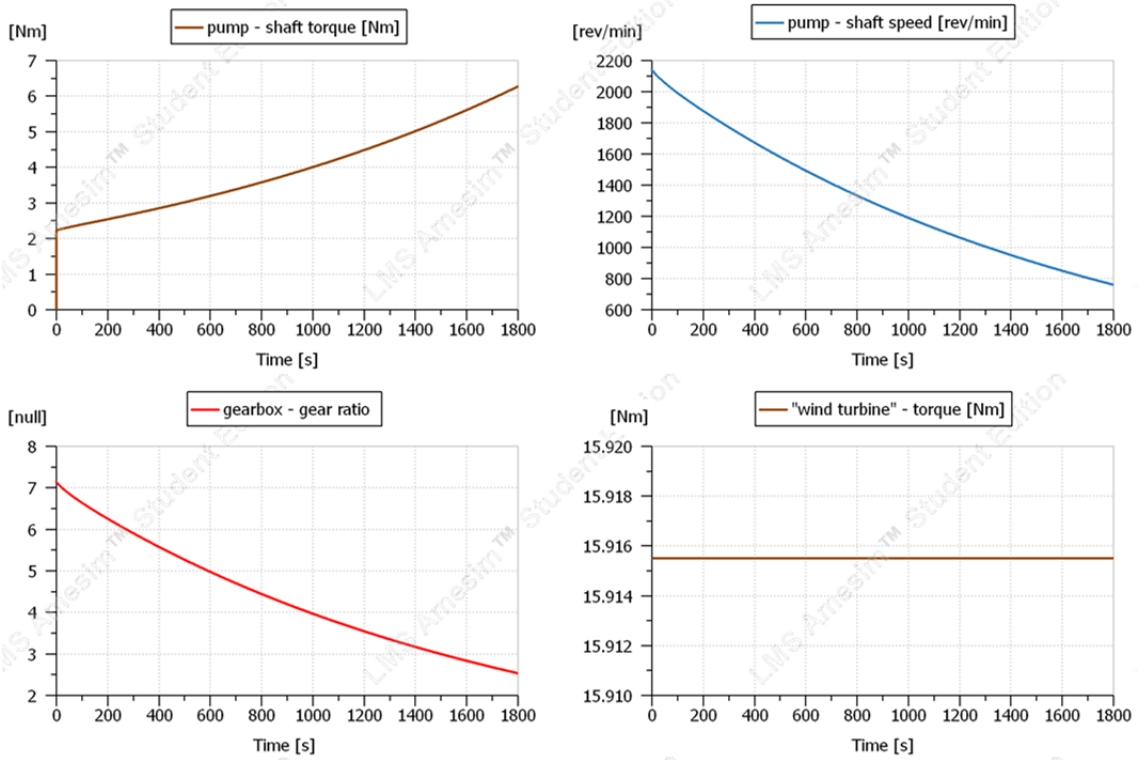

The pump operates in a speed range between 760 and 2140 rev/min, which is very close to the speed range determined in the dimensioning section (cf. Chapter 3.3.1). The initial speed of 2140rev/min is derived from the pre-charge pressure of 35bar in the system. Under real conditions, the pump would adequately be accelerated up to the operating speed before the charging starts. The resulting impacts on the hydro accumulator are illustrated in the following graphs.

Simulation results of the hydro accumulator

Figure 19 summarises the simulation results of the hydro accumulator. The volume flow into the hydro accumulator is equal to the flow rate provided by the pump. The reason for this is that the basic model represents an idealistic storage system with nearly no dissipation. It can be seen that the maximum flow rate of 8.6l/min is the same as calculated in the dimensioning section. It is reduced, due to the decreasing shaft speed of the pump, to a minimum value of roughly 3l/min.

The incoming water pressurises the air in the accumulator from the pre-charge pressure of 35bar to a final storage pressure of around 98bar. That nearly matches the previously defined storage pressure of 100bar. As a result, the volume of the gas is reduced from its initial volume of 249l to its final storage volume of around 91l. Consequently, the hydro accumulator keeps 158l of water under pressure (98bar) at the end of the charging process (≙ effective volume ΔV).

Figure 19: Simulation results of the hydro accumulator (charging model)

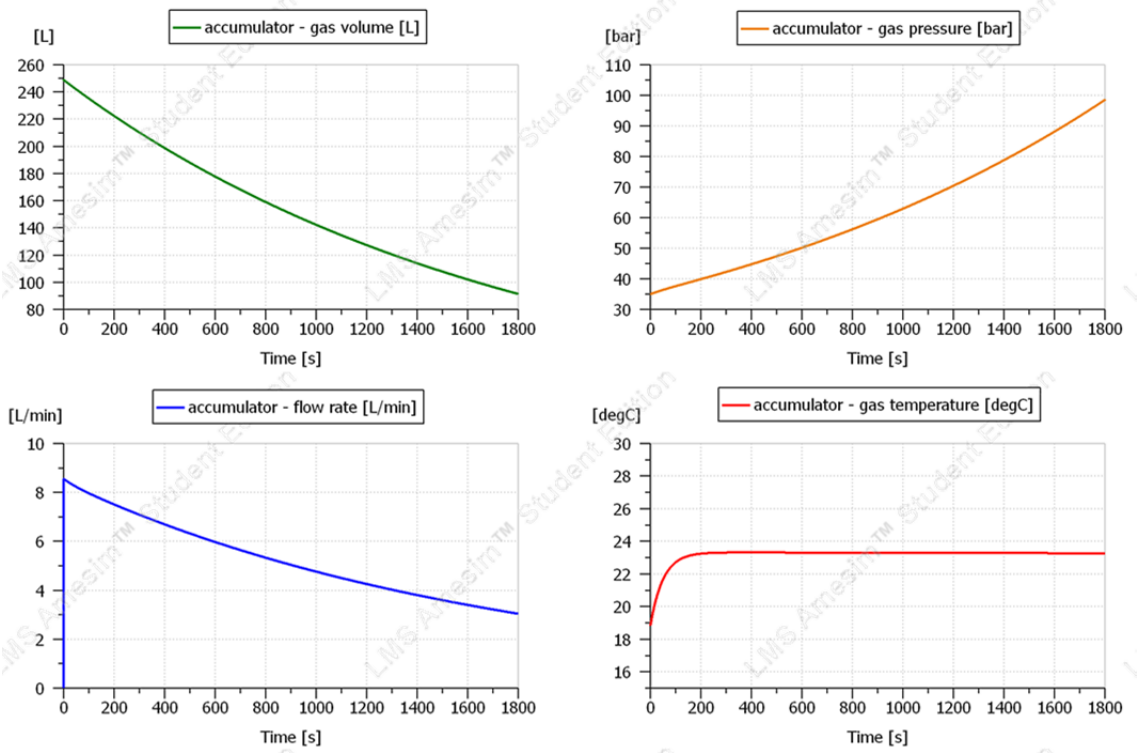

Normally, the temperature of the gas should start at the ambient temperature of 20°C (≙ 293K). For some reason, the underlying equations of the simulations calculate an initial temperature of around 19°C. As mentioned in chapter 3.3.2, the development of the gas temperature is influenced by the thermal time constant (50s). It can be seen that the temperature of the gas rises during the first 140s and finds its equilibrium at around 23°C (≙ 296K). The compression heat dissipates across the system boundary, so that an almost constant temperature difference of 3°C between the gas and its surrounding settles in. The waste heat is mostly absorbed and removed by the water.

It can be concluded that the long charging period (i.e. nearly isothermal compression) allows proper heat exchange, which results in a stable temperature range of the working and storage medium during compression.

Due to the idealised conditions, the amount of energy stored in the accumulator is close to the input energy ($W_C = 0.25kWh$). The stored energy can be calculated with the equation 2.2.1-1 and yields around 0.249kWh. The tiny difference arises from heat losses occurring during compression. Hence, the volumetric energy density (W') is more or less the optimum with 1.001kWh/m^3 (optimum: 1.02kWh/m^3, cf. Chapter 3.3.2). There will be more deviations from the ideal storage when the initial assumptions are iteratively replaced with more realistic values.

The final properties of the hydro accumulator are the initial inputs for the basic discharging model. Therefore, the values of interest are summarised in table 8.

Table 8: Characteristics of the charged hydro accumulator

Charged hydro accumulator	
Accumulator volume V_{acc} [l]	250
Thermal time constant τ [s]	50
Orifice diameter d_0 [mm] & flow coefficient α_D	10 & 0.7
Storage medium (air)	
Storage volume V_2 [l]	**91**
Storage pressure p_2 [bar]	**98**
Storage temperature T_2 [K]	**296**

3.4.2 Setup and simulation of the basic discharging model

Figure 20 shows the AMESim basic model of the discharging process of the hydro accumulator system. It is the “counterpart” of the charging model which was described in detail in chapter 3.4.1. More details regarding the discharging model are displayed in Appendix B.

Figure 20: Setup of the basic discharging model

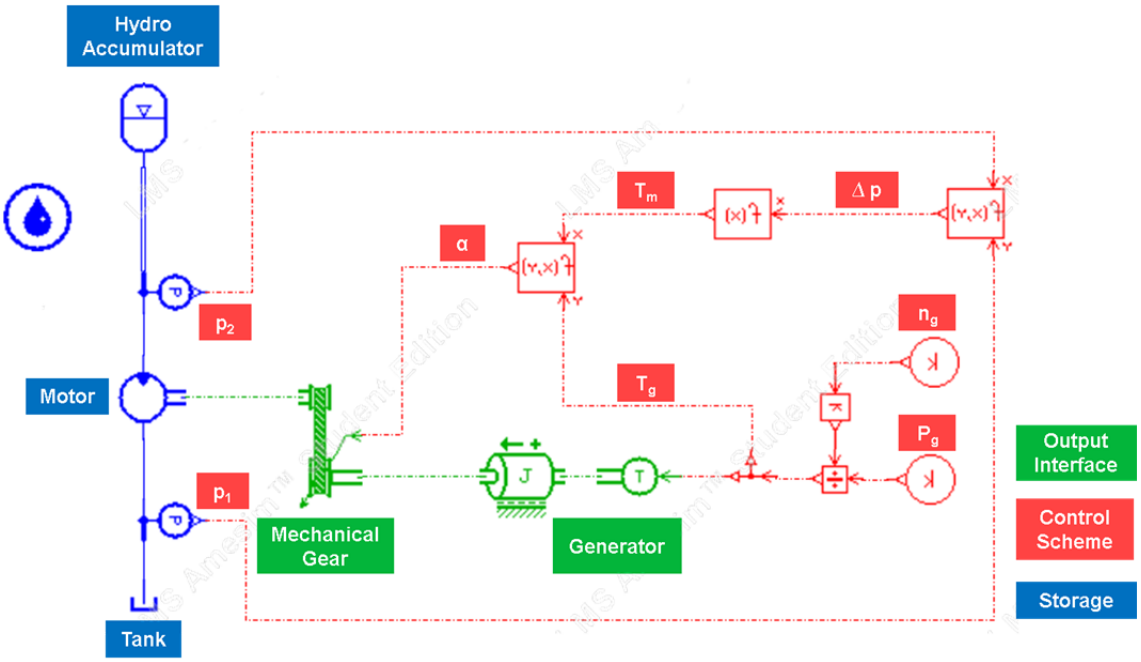

Output Interface

The model for the electrical consumer, i.e. the generator, is strongly simplified in order to realise the discharging of the hydro accumulator system. The generator is represented by an (idealised) constant mechanical load, which discharges the stored energy with the previously assumed characteristics: $P_g = 500W$, $f_g = 50Hz$ ($\triangleq \mathrm{n}_g = 3000rev/min$). Likewise the charging model, the generator is coupled mechanically to the accumulator system, more specifically to the hydraulic motor, via an ideal stepless MGB to regulate the power relevant variables. Here, the hydraulic energy is converted into mechanical energy, which is required by the generator. Thus, the same specifications, made for the input interface, also apply for the discharging model.

Control Scheme

The control scheme of the discharging process is based on the same prerequisites and equations as the control scheme of the charging process (cf. Chapter 3.4.1).

For this reason, the description of the control scheme during discharging is kept short. Here, the gear ratio α yields (with T_g & T_m according to 3.4.1-3 &-4):

$$\alpha = \frac{T_g}{T_m} \qquad \text{3.4.2-1}$$

T_g torque of the generator [Nm]

T_m torque of the motor [Nm]

Analogous to the pump, the torque of the motor depends on the pressure difference Δp, which is captured with two pressure sensors. During discharging, the air in the hydro accumulator expands continuously and thus the pressure at the motor inlet decreases, which consequently reduces Δp. This results in a declining torque of the motor. In order to be able to provide a constant power to the generator, the MGB regulates the motor by increasing its shaft speed (reverse regulation as it happens for the charging). Overall, the control scheme enables the generator to drive at constant speed and power, by using the stored energy within the system's operating range.

Besides, other regulation solutions exist. One option is, for example, to keep the pressure at the motor inlet constant by utilising a PRV. This consequently restricts the motor's speed to a certain value (i.e. resistance control with impressed pressure, cf. Murrenhoff 2014, pp. 329-330). In this application, no transmission would be necessary, since the generator shaft could be coupled directly to the constant-speed shaft of the hydraulic motor. However, this approach is associated with significant shortcomings. In particular, huge efficiency losses at the PRV diminish the performance of the storage system, since excess amounts of liquid, provided by the hydro accumulator, must be bypassed into a tank to maintain the pressure. Hence, the regulation and con-

trol of the discharging process, provided in this thesis, have the advantage of reduced losses and higher efficiency.

Storage

The outcome of the charging model serves as a starting point for the parameters of the basic discharging model (cf. Table 8). In particular, the hydro accumulator ($V_{acc} = 250l$) is in the charged state with an air storage pressure of 98bar, a corresponding air volume of 91l and temperature of 23°C. The air expands and forces the water out of the accumulator to drive the motor ($V_{D,m} = 4cm^3/rev$) with 500W. The discharging process lasts until the pre-charge pressure state is reached, i.e. lower system pressure of 35bar. This consequently determines the discharge time t_d. The final system's state is equal to the initial state of the charging step. The results of the simulation are visualised below.

Simulation results of the output interface and the motor

Figure 21: Simulation results of the output interface & motor (discharging model)

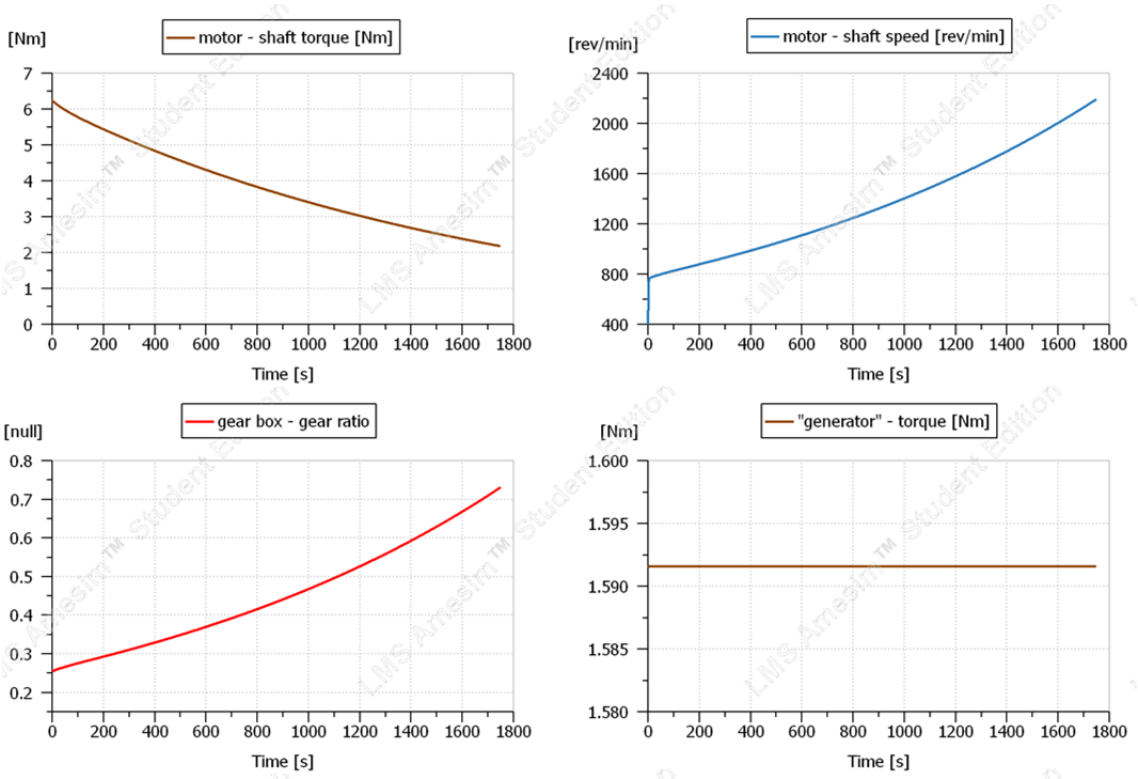

The results only show the discharging process during the actual operating phase. The ramp-up phase, during which the generator and motor are accelerated to system speed, is not displayed. The generator must be continuously supplied with 500W. The corresponding load, applied at the storage system, is roughly 1.6Nm. As already described in the control section, the motor shaft torque falls with the declining storage pressure, here, from approximately 6Nm to 2Nm. As a reaction, the MGB regulates the

motor speed gradually from around 765rev/min up to 2190rev/min by adjusting the gear ratio alpha. It can be seen that the operational parameters (i.e. torque- and speed-range) of the motor are nearly equal to the pump's parameters; an indicator that the control scheme works for both interfaces. As a result, the motor power is equal to the required consumer power at any point during operation. The changes in the hydraulic accumulator are illustrated below.

Simulation results of the hydro accumulator

Figure 22: Simulation results of the hydro accumulator (discharging model)

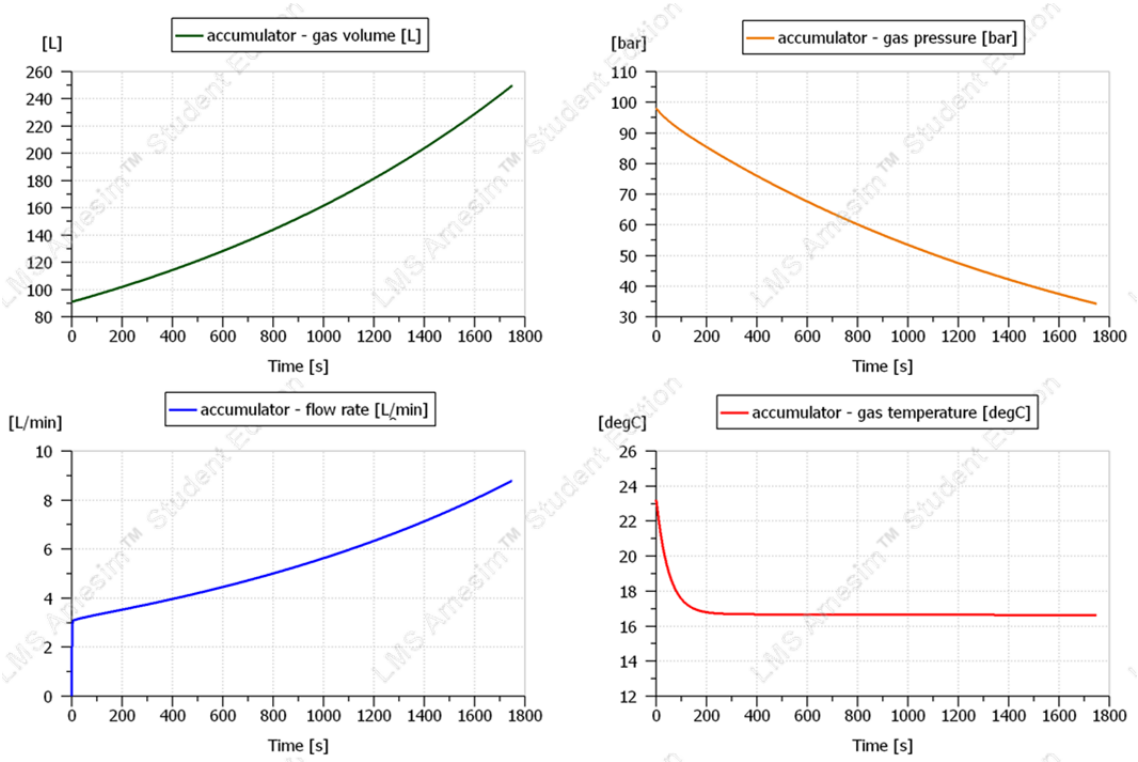

The graphs above show that the pressurised air gradually expands from 98bar, and a corresponding volume of 91l, back to pre-charge conditions: 35bar and 249l. That forces the stored water out of the hydro accumulator (Q_{acc}) and drives the motor ($Q_{acc} \approx Q_m$). The flow rate increases continuously from roughly 3l/m to 8.8l/min. This is necessary to compensate the decreasing system pressure and therefore torque at the motor (cf. Figure 21). As a reminder, the gas pressure is equal to the pressure at the motor inlet and also to Δp (= system pressure, cf. Chapter 3.3.1).

Due to the expansion with the related thermal time constant, the gas temperature drops sharply from 23°C to roughly 17°C in the first 140s and remains at this value for the rest of the discharging process. When the gas temperature becomes lower than the surrounding's temperature (i.e. water temperature: $T_{wa} = 20°C$), heat transfer occurs from the water into the gas and stabilises the temperature during expansion. Combined

with the slow operation, this leads to a total temperature difference of only 6°C (nearly isothermal) during expansion.

Besides the volumetric energy density W', it is possible to determine other parameters defined in chapter 3.2.2. The total efficiency η_s of the storage cycle can be derived from the ratio of discharge and charge time, because the input power and the output power are equal (cf. 3.2.2-1). A closer look at the graphs shows that the time period for discharging is shorter than for the charging process. In fact, the discharging process only lasts around 1750s. For the idealised basic model, the following efficiency can be stated ($P_{in} = P_{out} = 500W$):

$$\eta_s = \frac{P_{out} \cdot t_d}{P_{in} \cdot t_c} = \frac{t_d}{t_c} = \frac{1750s}{1800s} \approx 97.2\%$$

The efficiency is less than 100% because a small amount of energy is lost as heat and cannot be reused as volumetric change work. As a consequence, less energy is available to drive the hydraulic motor and hence the generator. Currently, the calculation of the system's efficiency is rather representative, since both models represent idealistic systems (i.e. no dissipation, idealised components, etc.). Nevertheless, the efficiency of the storage system can be determined by following this approach. By taking additional losses (e.g. mechanical and hydraulic frictions) into account, the discharge time and thus the efficiency of one storage cycle are further reduced. The final efficiency cannot precisely be determined at this stage, but it is expected that the system is able to reach efficiencies between 60-80%.

Overall, the presented simulation results demonstrate the functionality of the (idealistic) basic charging and discharging models of the hydro accumulator system. The outcome is in line with the dimensioning and the underlying control schemes. The models can be adapted and optimised to become more realistic. In the following step, both models are merged in one basic storage model which represents a full storage cycle.

3.4.3 Merging of the charging and discharging model

In this chapter, the charging model and discharging model (cf. Chapter 3.4.1 &-2) are merged to one basic model that is capable of the representation of full storage cycles. It can be used for further simulation and examination purposes in the research project WESSPA. The structure of the model is described, followed by a qualitative representation of its functionality. Figure 23 depicts the merged model which was also set up with the AMESim software. The HTML report, attached in Appendix C, provides more detailed information.

Figure 23: Merged basic model

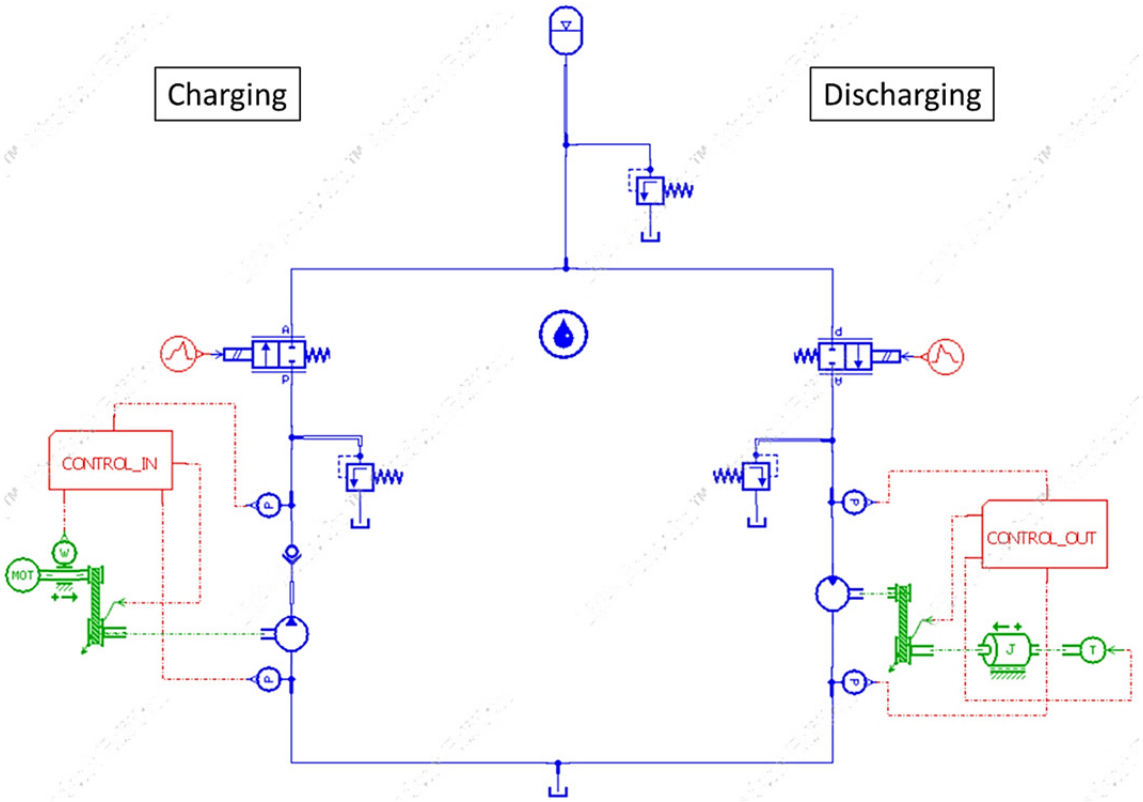

It can be seen that the structure of the model is based on the previously separated dis- and charging model. The left side represents the charging process (charging side), while the right side implements the discharging process (discharging side). Consequently, the same components (i.e. the same characteristics and dimensions) are applied according to the separated models. For the sake of clarity, the control schemes are merged into so called “Supercomponents”, which basically fulfil the same function as the control schemes of the separated models.

The model is extended by two different kinds of valves (cf. Chapter 2.3): DCVs and PRVs. As already mentioned in chapter 3.3.3, the valves are dimensioned so that they have, at first, no negative influence on the system’s performance. The three PRVs, at the pump, the motor and the hydro accumulator are integrated for safety reasons. They limit the pressure in the hydraulic system to avoid damages caused by unexpected pressure peaks. They are configured to open slightly over the targeted storage pressure at 105bar. This makes sense because the storage pressure was one design criterion in the dimensioning section (cf. Chapter 3.3). The two DCVs are utilised to separate the charging and discharging side. They are triggered time-dependent and distinct three different phases in the storage cycle.

1. *Charging phase:* The left DCV is open and the right DCV is closed, so that the water only flows from the pump into the hydro accumulator (i.e. the discharging side is shut off). The charging phase represents a time period when the wind turbine generates surplus energy, which is stored by the hydro accumulator system.
2. *Storage phase*: Both DCVs are closed. Thus, the liquid flow is interrupted and the hydro accumulator is shut off from the system. The storage phase represents a time period when the stored energy is not required.
3. *Discharging phase*: The left DCV is closed and the right DCV is open, so that the stored liquid can exit the hydro accumulator and drive the hydraulic motor (i.e. the charging side is shut off). The discharging phase is active when the wind turbine does not provide enough power due to the lack of wind.

The merging of the models has caused some complications. Hence, the following adjustments had to be made.

Required changes for the merging

The first adjustment concerns the orifice of the hydro accumulator. The diameter had to be adapted from 10mm to 5mm. For some reasons, a “large” orifice diameter led to uncontrolled incoming and outgoing flows of water during the storage phase. This made the simulation extremely slow and prevented appropriate investigations. Consequently, the orifice diameter was reduced. Nevertheless, related pressure losses at the accumulator inlet remain negligible due to the low flow rates. The impact of the orifice diameter on the simulation is illustrated below.

Figure 24: Impact of the orifice diameter on the simulation

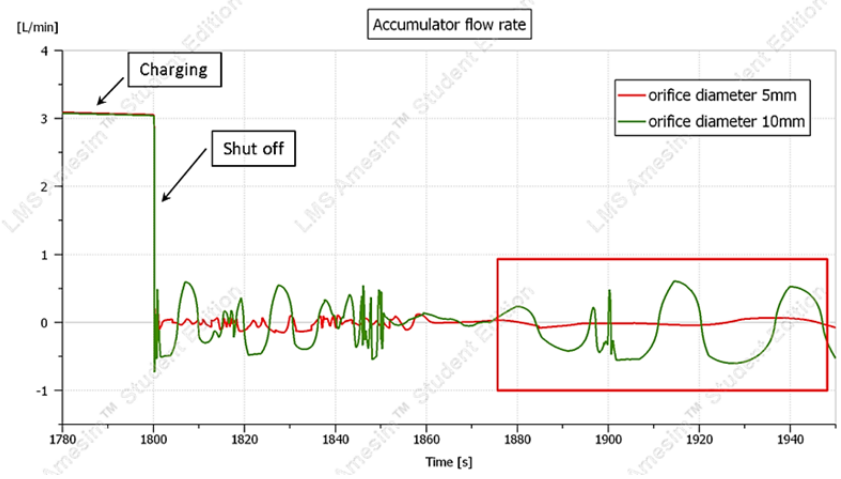

It can be seen that a smaller diameter results in less flow fluctuations at the accumulator inlet which levels off in the further course of the storage phase. That is not the case for a diameter of 10mm.

Secondly, the control schemes of the charging and discharging side needed to be extended. Under real conditions, the storage system would be coupled or decoupled to the input and output interface according to the current supply and demand situation. This was realised in the model by activating or deactivating the charging and discharging side for a defined period. Accordingly, related components are only active for their respective time period. As a result, charging and discharging of the storage system do not occur at the same time.

Simulation results

Since the merged model is a combination of the charging and discharging model, the general conditions (framework, dimensions, parameters, etc.) are exactly the same as explained in detail in the previous chapters. For this reason, the simulation results are only presented concisely and qualitatively. Resulting values will not be discussed in detail, as these correspond to the previous simulation results. However, it was not possible to model the storage phase with the single models, so this phase receives more attention in this section. Overall, the aim is to illustrate the functionality of the merged model.

The hydro accumulator system is charged for 30min, followed by a storage phase of 10min (600s) and then discharged to pre-charge conditions. The execution of the simulation shows the following results.

Simulation results of the pump and motor

Figure 25: Simulation results of the pump & motor (merged model)

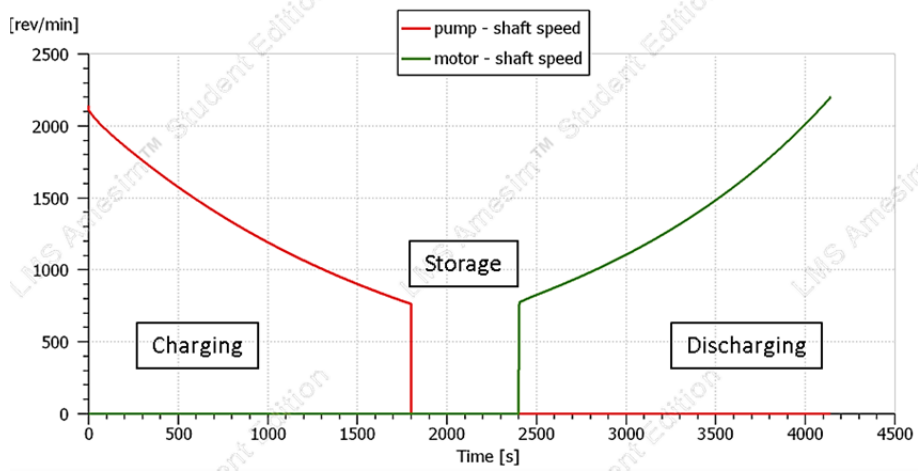

Figure 25 shows that the total simulation time period is set to 4500s. However, the motor stops after roughly 4140s. This is because the hydro accumulator reaches its pre-charge state at this point. Since the charge time and storage time is fixed, it can be concluded that the discharge time is slightly shorter in comparison to the results of chapter 3.4.2. The reason for this is described in the following sections. For the

demonstration of the functionality, the shaft speed of the pump and the motor serve as an example. It can be seen that the power components only operate when they are required. There is a downtime of 10min during the storage phase. The direct interruption, when the storage process changes from one phase to another, is a simplification. In real applications the transition would be more continuous.

Simulation results of the hydro accumulator

Figure 26: Simulation results of the air volume (merged model)

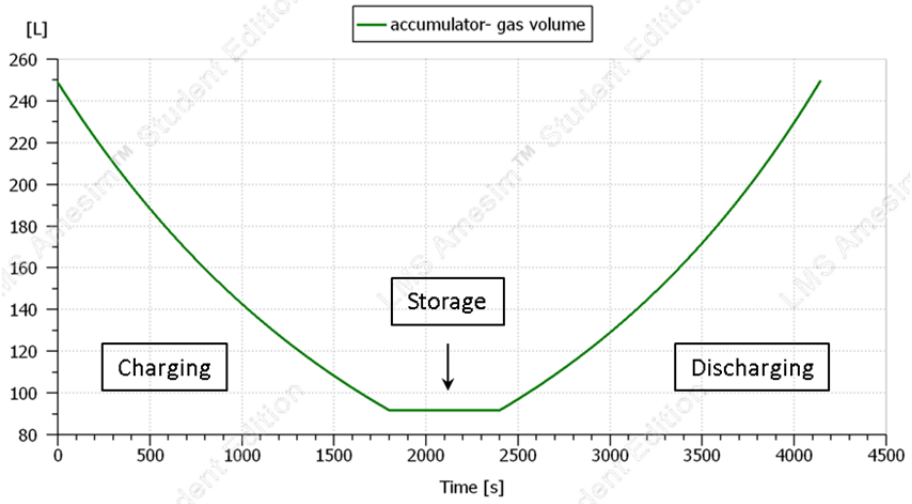

The three different phases of the storage cycle can be easily identified by examining the volume of the air (Figure 26). The charging phase, i.e. compression, is followed by the storage phase where the volume remains constant. When the discharging is induced, the air continuously expands to the initial volume. The development of the air volume during charging and discharging is similar to the separated simulation models of the previous chapters.

Figure 27: Simulation results of the air pressure (merged model)

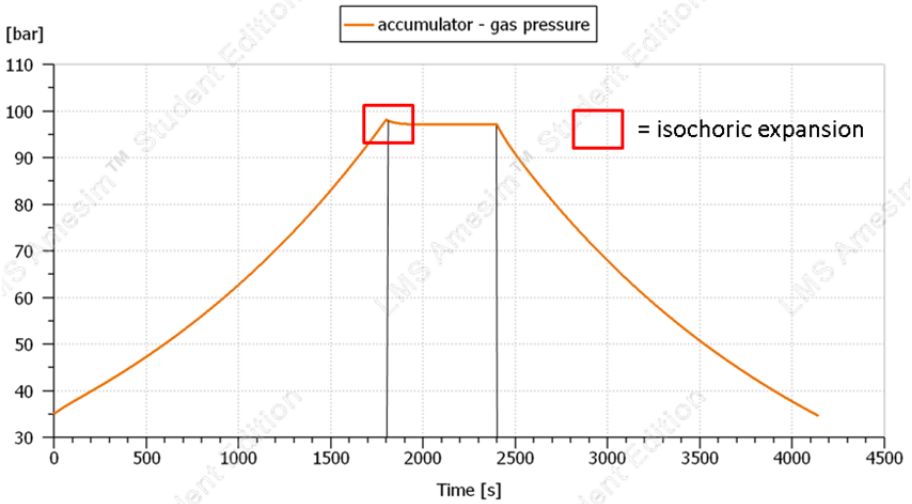

The pressure development is displayed in Figure 27. In this graph, the pressure behaves in exact contrast to the volume, but also represents the phases of the storage cycle. When the storage pressure is reached after 30min, a slight pressure drop can be noted right after the accumulator is shut off from the system. Here, the air expands isochorically (cf. Chapter 2.2) because the air temperature deviates from the temperature of its surrounding. This means the accumulator loses some of its storage pressure without performing usable work, which consequently reduces the discharge time and the efficiency a tiny bit. After that, the hydro accumulator is in equilibrium for the remaining storage period from the thermodynamic point of view. It is interrupted when the discharging side opens and the stored potential energy is used to push the water out of the hydro accumulator, which steadily reduces the systems pressure back to precharge conditions. Hence, this storage cycle represents three changes of state: isothermal compression, isochoric expansion and isothermal expansion.

Figure 28: Simulation results of the air temperature (merged model)

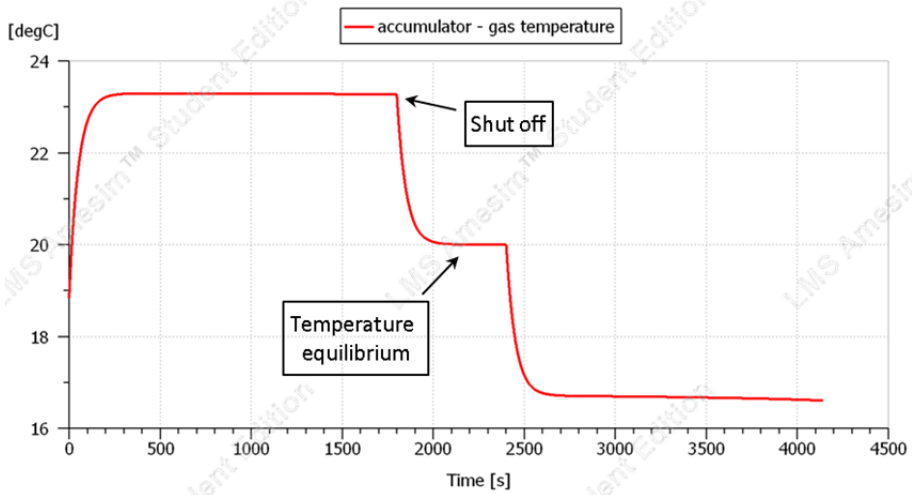

By taking a closer look at the development of the air temperature, it can be seen that there is only one time period where no heat transfer occurs between the storage medium and the surrounding components (Figure 28). This is when the air temperature has balanced to the ambient temperature during the storage phase. During charging and discharging, the compression and expansion results in heating and cooling of the gas, which leads to a temperature gradient and heat flows over the system boundary. At the moment when the hydro accumulator is shut off, the cooling of the gas leads to isochoric expansion (cf. Figure 27). Nevertheless, the total change of temperature is very low, which keeps thermal effects and resulting efficiency losses marginal in the presented storage system. Moreover, the stable temperature has the positive effect that some properties of the working and storage medium also remain relatively constant during operation. As already mentioned, the viscosity, heat capacity and density are, for instance, temperature dependent characteristics. As a result, the system's perfor-

mance is easier to calculate and to predict and deviations from the initial assumptions are kept small.

To sum it up, this chapter represented the functionality of the merged basic model. The combination of the charging and discharging models additionally allows the investigation of effects, which occur during the storage phase. In the following chapter, the findings and results of this thesis are compared with the work of Jan Molter who investigated a purely pneumatic CAES system within the research framework.

3.4.4 Comparison of the hydro accumulator and CAES system

The main working principle and characteristics of CAES is part of chapter 1.4. General similarities and differences between the purely pneumatic CAES system and the hydro-pneumatic accumulator system were already discussed in chapter 2.3. While both systems utilise air as the storage medium, the hydro accumulator system does not use air as the working medium but uses a liquid (water) instead. This chapter provides a comparison of the results of this thesis with the results of Jan Molter. The aim is to highlight important differences of the examined system parameters and characteristics (e.g. temperature or pressure behaviour) in order to identify potential difficulties and sticking points for subsequent tasks in the WESSPA project.

From the start, the authors ensured comparability of both concepts when defining the framework with its underlying assumptions, the dimensioning criteria and the setup of the simulation models. For example, the applied control schemes as well as the input and output requirements for the storage system are equal. Moreover, the applied storage medium is dry air in both cases. The structure of the models is similar and the simulations are executed according to the same general conditions. That means, for instance, that the charge time, the operating pressure range and the initial temperature are equal.

To get a quick overview, the main parameters of interest are summarised in the table below. These mainly consist of the results of the thermodynamic calculations and the simulation results of the separated basic models. The results of the merged models are compared qualitatively. Some values are rounded for the sake of clarity. Again, the simulation results should be treated with caution due to the set of assumptions made for first research purposes. Currently, the available data for evaluation is limited, since both systems are still in their pre-development phase. Hence, further examination is necessary for more meaningful comparisons.

Table 9: Comparison of the hydro accumulator and CAES system

Parameter	Hydro accumulator system	CAES system
Isothermal energy density [kWh/m^3] (p_1=35bar, p_2=100bar)	1.02	2.9
Isentropic energy density [kWh/m^3] (p_1=35bar, p_2=100bar)	0.86	2.5
Storage volume [l]	249	21
Storage pressure (achieved) [bar]	98	96
Minimum storage temperature [°C]	17	-9
Maximum storage temperature [°C]	23	67
Discharge time [s]	1750	420
Efficiency [%]	97	23

Source of CAES data: Jan Molter 2020

The first parameter of interest is the (volumetric) energy density for both storage concepts. It can be seen that the isothermal and isentropic energy density is roughly three times lower for hydro accumulator systems. Consequently, CAES systems are able to provide the same storage capacity as hydro accumulators with less volume or a lower storage pressure. Hence, CAES systems generally allow a more space-saving design than hydro accumulator systems. For this reason, the required storage volume, to reach the aimed 100bar, is considerably lower for the CAES system, only 21l, while the dimensioning of the hydro accumulator leads to a required storage volume of 249l. Furthermore, the dimensioning of the CAES storage volume relies on slightly different equations (mass specific dimensioning), which is another reason for the deviation of storage sizes.

After the charging process, both storage systems nearly reach the aimed storage pressure of 100bar, while the CAES system's storage pressure is slightly lower with 96bar than the hydro accumulator system's pressure (98bar). From the thermodynamic point of view, this means that both systems nearly achieve the optimum of storable energy. However, a closer look at the temperature of the storage medium emphasises the main difference between CAES and hydro accumulator system (Figure 29).

While the temperature of the air in the hydro accumulator only deviates a few degrees from the ambient temperature (17-23°C), the thermal effects in the CAES system are enormous during the storage process. Even with slow operation (30min charge time), the temperature rises up to 67°C in the storage tank.

Figure 29: Comparison of the storage temperature during the charging process

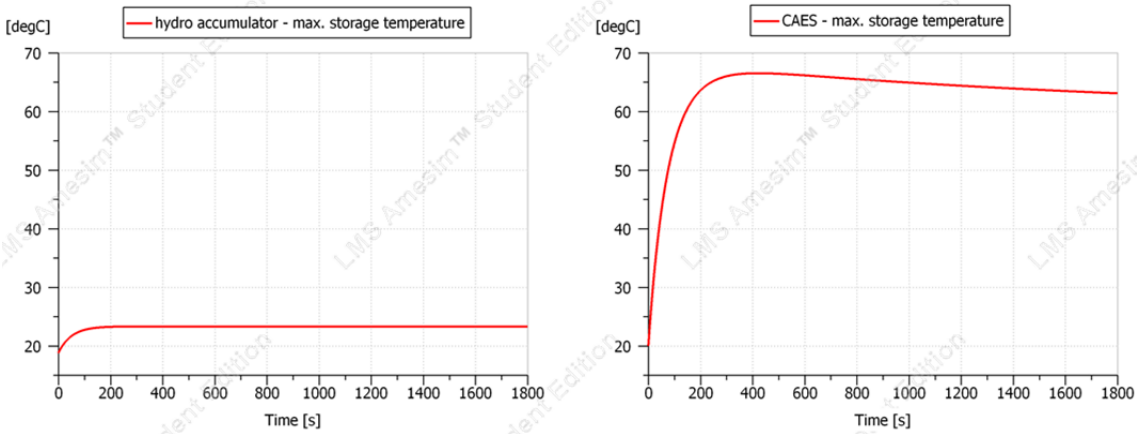

Source of CAES data: Jan Molter 2020

Discharging from this state results in a minimum temperature of minus 9°C. The simulation results, thus, substantiate the complications of heat management that CAES systems have to challenge, as it was already mentioned in chapter 2.3. This is additionally highlighted when the temperature of the compressor is examined. Here, the simulation shows a maximum temperature of 467°C. That would result in serious damage at the compressor unit in real applications.

The large temperature variation has several negative impacts on the performance of the CAES system, which the hydro accumulator system does not have to deal with to this extent. Firstly, temperature dependent properties of the air (e.g. viscosity and density) are more variable. Consequently, the calculation of the system's outcome gets more complex and deviations from initial assumptions are more severe. Secondly, occurring thermal effects have an adverse impact on the total efficiency. This becomes clear when comparing the discharge times. While the hydro accumulator system is able to provide 500W of power for 1750 seconds, the discharge period of the CAES system only lasts 420 seconds. Hence, the discharge time is roughly four times shorter compared to the discharge time of the hydro accumulator system. This in turn leads to a total efficiency of only 23%, whereas the efficiency of the hydro-pneumatic system is roughly 97%. Since both concepts utilise idealised components (e.g. 100% efficiency of the power units and transmission system), the logical conclusion is that thermal losses (i.e. waste heat during compression and cooling during expansion) are the main reason for the poor efficiency of the purely pneumatic system.

The influence of the temperature development on the system's performance is even more serious when the simulations of the merged models are being compared. As it was described in the previous chapter, the stable temperature range of the hydro accumulator system keeps differences between the results of the separated models and the merged model low. The addition of the storage phase only leads to a slight pres-

sure drop and therefore a small amount of lost energy. However, the storage phase in the CAES system results in a considerable temperature drop of the air (from 67°C to 20°C), which is followed by a huge pressure decrease. Hence, the amount of reusable energy is further reduced and with it the already modest discharge time and efficiency.

Overall, even though CAES systems achieve higher energy densities, the complexity and impact of thermal effects crucially influence the system's performance. The hydro accumulator system circumvents this problem by utilising an almost incompressible liquid with a higher heat capacity as the working medium. Consequently, the hydro accumulator system achieves better efficiencies and more feasible simulation results than the CAES system at the current research state. As a reminder, the efficiency is only 23%, although idealised conditions are assumed. Opportunities to enhance the efficiency of the CAES system are, on the one hand, to compress the air in several stages (followed by a cooling phase) up to the storage pressure and, on the other hand, the integration of a TES solution to reduce thermal losses (cf. Chapter 1.4). The TES stores waste heat, which is generated during compression, and returns it during the expansion step to minimise the temperature decrease. These are necessary steps before the CAES system can be implemented as a real application.

4 Conclusion & Outlook

As a conclusion, the following can be claimed about the outcome of this bachelor thesis. For a basic understanding, important theoretical and physical principles of the hydro accumulator concept were illustrated and classified within the current state of energy storage technologies. Particularly the hydro accumulator, as the key component of the storage system, was discussed with its existent designs, working principle and current state of research. For the requirements of the WESSPA project, a hydro accumulator system was designed based on various parameters and general conditions. In the next step, the system was modelled, parameterised and then simulated with the software tool AMESim. The evaluation of the simulation results showed that the functionality of the models is in accordance with the outcome of the dimensioning. The dimensioning, modelling and simulation was sufficiently documented for subsequent investigations.

Thus, this work provides a theoretical framework as well as several storage models to the project team, which can easily be understood, used and adapted according to specific requirements. Consequently, the task of the conception, modelling and dimensioning of an energy storage system for wind energy with hydro accumulators is successfully completed.

The following difficulties and complications emerged during the working process. The familiarisation with the simulation software was more difficult than expected. The understanding of the interrelations of parameters, the underlying calculation methods as well as the selection and adjustment of the system components were very time-consuming. Another challenge was the development of a proper functioning control scheme which works for the input and the output interface.

In addition, the high complexity of the system led to a number of simplifying assumptions, made for the dimensioning and simulation, which do not apply in reality. These assumptions limit the informative value of the obtained simulation results. Detailed statements about final system’s efficiency and technical feasibility are therefore destined for later stages of the project. Hence, this thesis rather serves as a foundation for further research purposes.

Consequently, the author suggests the following steps in the further course of the research project. The basic models should be enhanced by systematically replacing the initial assumptions with more realistic values. This includes, for instance, the following implementations.

- consideration of the efficiencies of the power units (pump & motor) and the transmission system (η_{vol}, η_{hm}, η_{mech}, ...)
- adjustments of integrated valves to consider losses caused by system control and regulation
- replacement of an ideal gas by a real gas to examine realistic behaviour of the storage medium
- consideration of dissolved air in the hydraulic liquid and of dissolved water in the storage medium (air) to investigate resulting impacts on the fluid's characteristics during operation (e.g. compressibility, temperature, etc.)
- replacement of a constant power input by a variable wind input to model effects of storage dynamics
- consideration of pressure losses at the pipes by taking wall roughness, pipe length and geometries (i.e. junctions, connectors, etc.) into account
- …

The improved models can then be used to optimise the storage system further. This is done by parameter variations, such as the variation of the accumulator's storage pressure, volume and charge time. This approach creates more usable data to drive scientific insights related to the hydro accumulator system. The next logical step is the selection of proper system components for a first prototype, whereby the dimensioning and simulation results serve as a reference point. The prototype of the hydro accumulator system can then be coupled to the prototype of the small-scale wind turbine of the WESSPA project and be investigated in the wind tunnel of htw saar. The models and related simulation results are suitable for comparison with the experimental outcomes.

The hydro accumulator technology, with its versatile applicability and environmentally friendly characteristics, will play an important role in the future of energy storages. Therefore, research projects, such as the WESSPA project, are indispensable to push the technical progress for a sustainable and long-term energy supply.

V. List of references

AïtTaleb, A., Chaâba A., Sallaou, M. (2013). Efficiency Evaluation of Continuously Variable Transmissions Including a Planetary Gear Train. *Energy and Power Engineering* [Online], 5(2), 153-160. Available from: https://www.scirp.org/journal/paperinformation.aspx?paperid=29425 [Accessed 2 March 2020].

Arani, A. A. K. et al. (2017). Review of Flywheel Energy Storage Systems structures and applications in power systems and microgrids. *Renewable and Sustainable Energy Reviews* [Online], 69(1), 9-18. Available from: https://www.researchgate.net/publication/310451921_Review_of_Flywheel_Energy_Storage_Systems_structures_and_applications_in_power_systems_and_microgrids [Accessed 13 January 2020].

Bauer, G. (2016). *Ölhydraulik: Grundlagen, Bauelemente, Anwendungen*. 11th edn. Wiesbaden: Springer Vieweg.

Bocklisch, T. (2014). Intelligente dezentrale Energiespeichersysteme. *uwf UmweltWirtschaftsForum*, 22(1), 63-70.

Bosch Rexroth AG (2019). *Mobile Hydraulics and Electronics: Pumps* [Online]. Available from: https://www.boschrexroth.com/en/xc/products/product-groups/mobile-hydraulics/pumps [Accessed 28 February 2020].

Buhagiar, D., Sant, T. (2017). Modelling of a novel hydro-pneumatic accumulator for large-scale offshore energy storage applications. *Journal of Energy Storage,* 14(2), 283-294.

Carr, G. J. (1975). *Hydro Pneumatic Flexible Bladder Accumulator.* No. 3,907,000 (Patent). Available from: https://patentimages.storage.googleapis.com/1f/75/1d/41986d5b00681f/US3907000.pdf [Accessed 10 January 2020].

Cerbe, G., Wilhelms, G. (2013*). Technische Thermodynamik: Theoretische Grundlagen und praktische Anwendungen.* 17th edn. München: Carl Hanser Verlag.

Chang, C. (2019). Factors Affecting Capacity Design of Lithium-Ion Stationary Batteries. *Batteries* [Online], 5(3), 58. Available from: https://www.mdpi.com/2313-0105/5/3/58 [Accessed 15 January 2020].

Cosford, J. (2014). *Accumulators add functionality to hydraulic circuits* [Online]. Hydraulics & Pneumatics. Available from: https://www.hydraulicspneumatics.com/technologies/accumulators/article/21883813/accumulators-add-functionality-to-hydraulic-circuits [Accessed 17 January 2020].

Eder, S. W., Hartbrich, I., Reckter, B. (2020a). Dauerbrenner. *VDI Nachrichten,* No. 1/2/3, 10 January, p. 1.

Eder, S. W., Hartbrich, I., Reckter, B. (2020b). Die Energie der Zukunft. *VDI Nachrichten,* No. 1/2/3, 10 January, pp. 20-21.

Environmental Protection Agency (EPA) (2018). *Electricity Storage* [Online]. Available from: https://www.epa.gov/energy/electricity-storage [Accessed 30 January 2020].

Euronews (2020). *2020 sets record for Europe's hottest January, Copernicus data shows* [Online]. Available from: https://www.euronews.com/2020/02/05/2020-sets-record-for-europe-s-hottest-january-copernicus-data-shows [Accessed 3 February 2020].

European Commission (2017). *Commission Staff Working Document: Energy storage – the role of electricity* [Online]. Brussels. Available from: https://ec.europa.eu/energy/sites/ener/files/documents/swd2017_61_document_travail_service_part1_v6.pdf [Accessed 6 January 2020].

European Commission (2019). *Communication from the Commission to the European Parliament, The European Council, The Council, The European Economic and Social Committee and the Committee of the Region: The European Green Deal* [Online]. Brussels. Available from: https://ec.europa.eu/info/sites/info/files/european-green-deal-communication_en.pdf [Accessed 15 January 2020].

Eurostat (2018). *Primary energy consumption* [Online]. Available from: https://ec.europa.eu/eurostat/tgm/table.do?tab=table&plugin=1&language=en&pcode=sdg_07_10 [Accessed 13 March 2020].

Eurostat (2020). *Renewable energy statistics* [Online]. Available from: https://ec.europa.eu/eurostat/statistics-explained/index.php?title=Renewable_energy_statistics [Accessed 13 March 2020].

Fan, Y., Mu, A., Ma, T. (2016). Study on the application of energy storage system in offshore wind turbine with hydraulic transmission. *Energy Conversion and Management*, 110(1), 338-346.

Federal Ministry for Economic Affairs and Energy (FMEAE) (2020). *Renewable Energy* [Online]. Available from: https://www.bmwi.de/Redaktion/EN/Dossier/renewable-energy.html https://www.bmwi.de/Redaktion/DE/Dossier/erneuerbare-energien.html [Accessed 5 January 2020].

Geissbühler, L. et al. (2018). Pilot-scale demonstration of advanced adiabatic compressed air energy storage, Part 1: Plant description and tests with sensible thermal-energy storage. *Journal of Energy Storage* [Online], 17(1), 129-139. Available from: https://api.nfp-energie.ch/api/de/content/file/d3b7858ad4749d9e5f27178aac55b85c [Accessed 13 January 2020].

Gomoll, W. (2014). *Luft-Hybrid von Peugeot und Citroën: Fahren wir bald alle mit heißer Luft? Das kann der neue Wunder-Hybrid* [Online]. Online Focus. Available from: https://www.focus.de/auto/fahrberichte/luft-hybrid-von-peugeot-und-citroen-fahren-wir-bald-alle-mit-heisser-luft-das-kann-der-neue-wunder-hybrid_id_3966146.html [Accessed 23 January 2020].

Groupe PSA (2016). *Hybrid Air: An innovative full-hybrid petrol solution for the car of the future* [Online]. Available from: https://www.groupe-psa.com/en/newsroom/automotive-innovation/hybrid-air/ [Accessed 23 January 2020].

Grünweg, T. (2014). *Druckluft-Hybrid von PSA: Peugeot geht die Pumpe* [Online]. Spiegel Mobilität. Available from: https://www.spiegel.de/auto/aktuell/hydraulik-hybrid-im-peugeot-2008-ersetzt-druckluft-den-akku-a-979662.html# [Accessed 23 January 2020].

Hartbrich, I. (2020). Knistern in der Luft – und auch überall sonst. *VDI Nachrichten,* No. 1/2/3, 10 January, p. 23.

Hau, E. (2016). *Windkraftanlagen: Grundlagen · Technik · Einsatz · Wirtschaftlichkeit*. 6th edn. Berlin: Springer Vieweg.

Hering, E., Martin, R., Stohrer, M. (2017). *Taschenbuch der Mathematik und Physik*. 6th edn. Berlin: Springer Vieweg.

Hübner, D. (2019). *WESSPA – Wind Energy Storage System with Pressurized Air*. Forschungs- und Entwicklungsantrag. Saarbrücken: htw saar.

Hübner, D., Ortwig, H., Zimmermann, U. (2016). *Investigations on Fluid Dynamics of Hydraulic Accumulators* [Online]. 12th International Conference on Heat Transfer, Fluid Mechanics and Thermodynamics, Malaga, Spain. Available from: https://repository.up.ac.za/handle/2263/61858 [Accessed 16 February 2020]

HYDAC INTERNATIONAL GmbH (n.d.). *Standard/High pressure bladder acc*. [Online]. Available from: https://www.hydac.com/de-en/products/hydraulic-accumulators/bladder-accumulator/standardhigh-pressure-bladder-acc.html [Accessed 16 February 2020].

Institute for Power Electronics and Electrical Drives (ISEA) (2012). *Technology Overview on Electricity Storage: Overview on the potential and on the deployment perspectives of electricity storage technologies* [Online]. RWTH Aachen. Available from: https://www.sefep.eu/activities/projects-studies/120628_Technology_Overview_Electricity_Storage_SEFEP_ISEA.pdf [Accessed 2 January 2020].

International Energy Agency (IEA) (2005). *Energy Technology Analysis: Prospects for Hydrogen and Fuel Cells* [Online]. OECD Publishing, Paris. Available from: https://www.oecd-ilibrary.org/energy/prospects-for-hydrogen-and-fuel-cells_9789264109582-en [Accessed 12 January 2020].

International Energy Agency (IEA)-Energy Technology Systems Analysis Programme (ETSAP), International Renewable Energy Agency (IRENA) (2013). *Thermal Energy Storage: Technology Brief* [Online]. Available from: https://www.irena.org/publications/2013/Jan/Thermal-energy-storage [Accessed 12 January 2020].

International Renewable Energy Agency (IRENA) (2017). *Electricity storage and renewables: Costs and markets to 2030* [Online]. Abu Dhabi. Available from: https://www.irena.org/-/media/Files/IRENA/Agency/Publication/2017/Oct/IRENA_Electricity_Storage_Costs_2017.pdf [Accessed 7 January 2020].

International Renewable Energy Agency (IRENA) (2018). *Hydrogen from Renewable Power: Technology Outlook for the Energy Transition* [Online]. Abu Dhabi. Available from: https://www.irena.org/publications/2018/Sep/Hydrogen-from-renewable-power [Accessed 11 January 2020].

Jorio, L. (2016). *Energiespeicher im Berg: Eine unterirdische Batterie aus Druckluft* [Online]. SWI swissinfo.ch. Available from: https://www.swissinfo.ch/ger/wirtschaft/energiespeicher-im-berg_eine-unterirdische-batterie-aus-druckluft/42324670 [Accessed 4 January 2020].

Kalide, W. (2005). *Energieumwandlung in Kraft- und Arbeitsmaschinen: Kolbenmaschinen – Strömungsmaschinen – Kraftwerke*. 9th edn. München, Wien: Carl Hanser Verlag.

Kaspar, F., Friedrich, K. (2020). *Rückblick auf die Temperatur in Deutschland im Jahr 2019 und die langfristige Entwicklung* [Online]. Deutscher Wetterdienst (DWD). Available from: https://www.dwd.de/DE/klimaumwelt/aktuelle_meldungen/200103/temperatur_d_2019_langfristig.html;jsessionid=ED92C65EF86DCC4BF5B6D7B72EF4EDF8.live11043?nn=344870 [Accessed 10 January 2020].

Korkmaz, F. (1982). *Hydrospeicher als Energiespeicher.* Berlin, Heidelberg: Springer-Verlag.

Krisch-Dienst GmbH Fluidtechnik (n.d.). *Pumpen* [Online]. Available from: http://wasser-hydraulik.de/html/pumpen.html [Accessed 2 February 2020].

Labor Windenergietechnik htw saar (n.d.). *Windkanäle* [Online]. Available from: http://www.htw-saar-windlab.de/index.php/de/Ausstattung.html [Accessed 2 February 2020].

Leiva, L. (2017). *Wie stark belastet die Batterieherstellung die Ökobilanz von Elektroautos?* [Online]. Energie Experten. Available from: https://www.energie-experten.ch/de/mobilitaet/detail/wie-stark-belastet-die-batterieherstellung-die-oekobilanz-von-elektroautos.html [Accessed 7 January 2020].

Liu, C., Neale, Z. G., Cao, G. (2016). Understanding electrochemical potentials of cathode materials in rechargeable batteries. *Materials Today* [Online], 19(2), 109-123. Available from: https://www.sciencedirect.com/science/article/pii/S1369702115003181 [Accessed 12 January 2020].

Liu, Z. et al. (2017). Variable speed and constant frequency control of hydraulic wind turbine with energy storage system. *Advances in Mechanical Engineering* [Online], 9(8), 1-10. Available from: https://www.researchgate.net/publication/318905320_Variable_speed_and_constant_frequency_control_of_hydraulic_wind_turbine_with_energy_storage_system [Accessed 16 January 2020].

Luo, X. et al. (2015). Overview of current development in electrical energy storage technologies and the application potential in power system operation. *Applied Energy* [Online], 137(1), 511-536. Available from: https://www.sciencedirect.com/science/article/pii/S0306261914010290 [Accessed 11 January 2020].

Matthies, H. J., Renius, K. T. (2014). *Einführung in die Ölhydraulik: Für Studium und Praxis*. 8th edn. Wiesbaden: Springer Vieweg.

Max Bögl Wind AG (2017). *Gaildorf pioneers electricity storage* [Online]. Available from: https://www.mbrenewables.com/en/pilot-project/ [Accessed 4 January 2020].

Molter, J. (2020). *Conception, modelling and dimensioning of an energy storage system for wind energy with pressurized air*. Saarland: Hochschule für Technik und Wirtschaft des Saarlandes. Bachelor Thesis.

Moog Inc. (2016). *Drehzahlgeregelte Pumpe: Energieeffizienz und Flexibilität für anspruchsvolle Anwendung* [Online]. Available from: https://www.moog.de/literature/ICD/Moog-Pumps-SpeedControlledPumpSystem-Overview-de.pdf [Accessed 28 February 2020].

Murrenhoff, H. (2014). *Fundamentals of Fluid Power: Part 1: Hydraulics.* 7th edn. Trans. Pongratz, S., Theissen, H. Aachen: Shaker Verlag.

Ogawa, T., Takeuchi, M., Kajikawa, Y. (2018). Analysis of Trends and Emerging Technologies in Water Electrolysis Research Based on a Computational Method: A Comparison with Fuel Cell Research. *Sustainability* [Online], 10(2), 478. Available from: https://www.mdpi.com/2071-1050/10/2/478 [Accessed 8 January 2020].

Park, M. et al. (2016). Material design and engineering of next-generation flow-battery technologies. *Nature Reviews Materials* [Online], 2(16080), 1-18. Available from: https://www.nature.com/articles/natrevmats201680 [Accessed 10 January 2020].

Pfleger, N. et al. (2015). Thermal energy storage – overview and specific insight into nitrate salts for sensible and latent heat storage. *Beilstein Journal of Nanotechnology* [Online], 6(1), 1487-1497. Available from: https://www.beilstein-journals.org/bjnano/articles/6/154 [Accessed 3 January 2020].

Pimm, A. J., Garvey, S. D., Jong, D. M. (2014). Design and testing of Energy Bags for underwater compressed air energy storage. *Energy*, 66(1), 469-508.

Pourmovahed, A., Otis, D. R. (1990). An Experimental Thermal Time-Constant Correlation for Hydraulic Accumulators. *Journal of Dynamic Systems, Measurement, and Control* [Online], 112(1), 116-121. Available from: https://www.semanticscholar.org/paper/An-Experimental-Thermal-Time-Constant-Correlation-Pourmovahed-Otis/581f5d2038e1c605fc38ccada16dd0b7a231ec8b [Accessed 22 February 2020].

Rehman, S., Al-Hadhrami, L. M., Alam, M. M. (2015). Pumped hydro energy storage system: A technological review. *Renewable and Sustainable Energy Reviews*, 44(1), 586-598.

Roddeck, W. (2016). *Einführung in die Mechatronik.* 5th edn. Wiesbaden: Springer Vieweg.

Rotthäuser, S. (1993). *Verfahren zur Berechnung und Untersuchung hydropneumatischer Speicher*. Faculty of Mechanical Engineering. Aachen: Rheinisch-Westfälische Technische Hochschule (RWTH) Aachen. PhD Thesis.

Ruan, J., Zhang, N., Walker, P. (2015). *Comparing of single reduction and CVT based transmissions on battery electric vehicle* [Online]. 14th IFToMM World Congress, Taipei, Taiwan. Available from: https://www.researchgate.net/publication/282996810_Comparing_of_single_reduction_and_CVT_based_transmissions_on_battery_electric_vehicle [Accessed 5 March 2020]

Runkel, W. (2014). *Hydro-Pneumatic Piston Accumulator*. No. US 8,746,661 B2 (Patent). Available from: https://patentimages.storage.googleapis.com/d6/a7/2c/a7b0a18ba14ed8/US8746661.pdf [Accessed 12 January 2020].

Rupprecht, K. R. (1988). *Hydrospeicher: experimentelle und analytische Untersuchungen zur Energiespeicherung*. Aachen: Rheinisch-Westfälische Technische Hochschule (RWTH) Aachen. PhD Thesis.

RWE Power (2010). ADELE – *Der adiabate Druckluftspeicher für die Elektrizitätsversorgung* [Online]. Available from: http://www.rwe.com/app/Pressecenter/Download.aspx?pmid=4004393&datei=1 [Accessed 5 January 2020].

Sabihuddin, S., Kiprakis, A. E., Mueller, M. (2015). A Numerical and Graphical Review of Energy Storage Technologies. *Energies* [Online], 8(1), 172-216. Available from: https://www.mdpi.com/1996-1073/8/1/172 [Accessed 2 January 2020].

Schaaf, T. et al. (2014). Methanation of CO_2 - storage of renewable energy in a gas distribution system. *Energy, Sustainability and Society* [Online], 4(2), 1-14. Available from: https://link.springer.com/article/10.1186/s13705-014-0029-1 [Accessed 16 January 2020].

Shnaid, I., Weiner, D., Brokman, S. (1996). *Compressed Air Energy Storage Method and System*. No. 5,537,822 (Patent). Available from: https://patentimages.storage.googleapis.com/ac/d5/34/a5dfb5fdef1169/US5537822.pdf [Accessed 3 January 2020].

Siemens Industry Software Inc. (2019). *Simcenter Amesim* [Online]. Siemens. Available from: https://www.plm.automation.siemens.com/global/en/products/simcenter/simcenter-amesim.html [Accessed 24 January 2020].

Siemens Industry Software NV. (2017). *LMS Imagine.Lab AMESim Student Edition Rev 13 SL3.* [Downloadable programme]. Windows version. Siemens Industry Software Inc. Available from: https://www.plm.automation.siemens.com/plmapp/education/simcenter/en_us/free-software/student/ [Accessed 02 January 2020].

Sigloch, H. (2017). *Technische Fluidmechanik*. 10th edn. Berlin: Springer Vieweg.

Slocum, A. et al. (2013). Ocean Renewable Energy Storage (ORES) System: Analysis of an Undersea Energy Storage Concept. *Proceedings of the IEEE,* 101(4), 906-924.

Statistisches Bundesamt (2019). *Schätzung für 2018: Bevölkerungszahl auf 83,0 Millionen gestiegen* [Online]. Available from: https://www.destatis.de/DE/Presse/Pressemitteilungen/2019/01/PD19_029_12411.html [Accessed 28 January 2020].

Stierstadt, K. (2018). *Thermodynamik für das Bachelorstudium.* 2nd edn. Berlin : Springer Spektrum.

Tagesschau.de (2020). *Brände in Australien: Canberra schließt Flughafen* [Online]. Available from: https://www.tagesschau.de/ausland/australien-braende-127.html [Accessed 25 January 2020].

Tixador, P. (2008). Superconducting Magnetic Energy Storage: Status and Perspective. *IEEE/CSC & ESAS European Superconductivity News Forum (SNF)* [Online], 2(3), 1-14. Available from: https://snf.ieeecsc.org/abstracts/cr5-superconducting-magnetic-energy-storage-status-and-perspective [Accessed 3 January 2020].

Umweltbundesamt (UBA) (2019a). *Umweltbewusstsein in Deutschland* [Online]. Available from: https://www.umweltbundesamt.de/themen/nachhaltigkeit-strategien-internationales/gesellschaft-erfolgreich-veraendern/umweltbewusstsein-in-deutschland [Accessed 19 January 2020].

Umweltbundesamt (UBA) (2019b). *Trends der Lufttemperatur* [Online]. Available from: https://www.umweltbundesamt.de/daten/klima/trends-der-lufttemperatur#textpart-1 [Accessed 19 January 2020].

Uniper SE (n.d.). *Druckluftspeicherkraftwerk Huntorf* [Online]. Available from: https://www.uniper.energy/de/kraftwerk-wilhelmshaven [Accessed 4 February 2020].

University of Innsbruck (n.d.). *Buoyant Energy: Smart Concepts for Energy Storage* [Online]. Available from: http://www.buoyant-energy.com/english/home.html [Accessed 24 January 2020].

Vaezi, M., Izadian, A. (2014). *Energy Storage Techniques for Hydraulic Wind Power Systems* [Online]. International Conference on Renewable Energy Research and Application (ICRERA), Milwakuee, WI, USA. Available from: https://ieeexplore.ieee.org/document/7016514 [Accessed 11 January 2020].

Wang, J. et al. (2017). Overview of Compressed Air Energy Storage and Technology Development. *Energies* [Online], 10(7), 991. Available from: https://www.mdpi.com/1996-1073/10/7/991 [Accessed 13 January 2020].

Watter, H. (2017). *Hydraulik und Pneumatik: Grundlagen und Übungen – Anwendungen und Simulation.* 5th edn. Wiesbaden: Springer Vieweg.

Wei, L. et al. (2018). Modeling and Control of a 600 kW Closed Hydraulic Wind Turbine with an Energy Storage System. *Applied Sciences* [Online], 8(8), 1314. Available from: https://www.mdpi.com/2076-3417/8/8/1314 [Accessed 8 January 2020].

Wiesinger, J. (2015). *Hydraulik-Hybrid von Bosch und PSA* [Online]. kfztech.de. Available from: https://www.kfztech.de/kfztechnik/alternativ/hydraulik-hybrid.htm [Accessed 22 January 2020].

Wietschel, M. et al. (2015). *Energietechnologien der Zukunft: Erzeugung, Speicherung, Effizienz und Netze*. Wiesbaden: Springer Vieweg.

Wilming, W. (2019). Schreckgespenst Dunkelflaute. *VDI Nachrichten,* No. 51/52, 20 December, pp. 12-13.

Wraneschitz, H. (2020). Netztechniker mahnen Verteilnetzausbau an. *VDI Nachrichten,* No. 1/2/3, 10 January, p. 11.

VI. Appendices

Appendix A: HTML report of the charging model

HTML Report generated by LMS Imagine.Lab AMESim Rev13 SL3 (*Sa 7. Mrz 17:54:13 2020*)

Circuit name

BasicModel_ChargingProcess

Circuit schematics

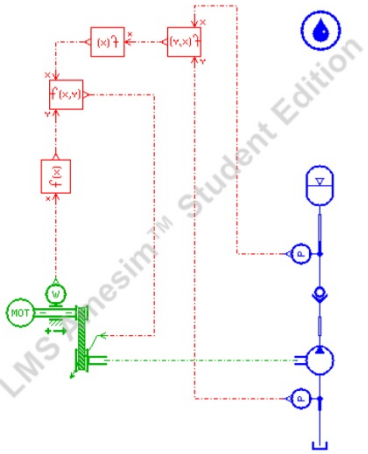

Component submodels

accumulator [HA0010-1]

hydraulic accumulator with heat exchange and with inlet orifice

HA0010-1 : All internal variables with startvalues	Unit	Value
gas volume	L	249
gas pressure	bar	35
liquid pressure in accumulator	bar	35

HA0010-1 : All real parameters	Unit	Value
accumulator volume	L	250
gas precharge pressure	bar	35
gas precharge temperature	degC	20
environment (liquid) temperature	degC	20
time constant for heat exchange	s	50
gas constant R	J/kg/K	287
heat capacitance Cv	J/kg/K	718
accumulator orifice diameter	mm	10
critical flow number	null	1000
maximum flow coefficient for orifice	null	0.7

HA0010-1 : All integer parameters	Value
index of hydraulic fluid	0

elementaryhydraulicprops [FP04-1]

indexed hydraulic fluid properties

FP04-1 : All real parameters	Unit	Value
density	kg/m**3	1000
bulk modulus	bar	20000
slope of bulk modulus [bar] in function of pressure [bar] (in percentage)	null	0
absolute viscosity	cP	1.002
absolute viscosity of air/gas	cP	0.02
saturation pressure (for dissolved air/gas)	bar	1000
air/gas content	%	0.1
temperature	degC	20
temperature T1	degC	40
kinematic viscosity at (Patm, T1)	cSt	56.47
temperature T2	degC	100
kinematic viscosity at (Patm, T2)	cSt	9.71
coefficient for temperature viscosity characteristic	null	0.8
polytropic index for air/gas/vapor content	null	1.4
(advanced user) high saturated vapor pressure	bar	-0.5
(advanced user) low saturated vapor pressure	bar	-0.6
(advanced user) absolute viscosity of vapor	cP	0.02
(advanced user) effective molecular mass of vapor	null	200
(advanced user) air/gas density at atmospheric pressure 0 degC	kg/m**3	1.2
saturation pressure (for dissolved air/gas)	bar	0

FP04-1 : All integer parameters	Value
type of fluid properties	elementary
fuel type	ISO 4113
fluid property file	user data file
bulk modulus type	adiabatic
index of hydraulic fluid	0

FP04-1 : All text parameters	Value
name of fluid	Water
name of file specifying fluid properties	$AME/tutorial/tblprop1.txt

fofx [FX00-1]

output a prescribed function of input

FX00-1 : All text parameters	Value
T(p)	(displ/1000000)*x/(2*PI)

fofx_1 [FX00-2]

output a prescribed function of input

FX00-2 : All text parameters	Value
n(wt) to T(wt)	500/(2*PI*(x/60))

fofxy [FXY0-2]

signal function of inputs x and y

FXY0-2 : All text parameters	Value
gear ratio alpha	y/x

fofxy_1 [FXY0-1]

signal function of inputs x and y

FXY0-1 : All text parameters	Value
delta p [N/m^2]	((x+0.0001)-y)*100000

pmover01 [PM000-1]

constant speed prime mover

PM000-1 : All external variables with startvalues	Unit	Value
n(wt)	rev/min	300

presscontrol02 [CV000-1]

hydraulic check valve with linear characteristic

CV000-1 : All real parameters	Unit	Value
check valve cracking pressure	bar	0
check valve flow rate pressure gradient	L/min/bar	500
hysteresis for opening/closing	bar	0

CV000-1 : All integer parameters	Value
index of hydraulic fluid	0

pressuresensor [PT002-1]

hydraulic pressure sensor with offset and gain

PT002-1 : All real parameters	Unit	Value
offset to be subtracted from pressure	bar	0
gain for signal output	1/bar	1

pressuresensor_1 [PT003-1]

hydraulic pressure sensor with offset and gain

PT003-1 : All real parameters	Unit	Value
offset to be subtracted from pressure	bar	0
gain for signal output	1/bar	1

pump01 [PU001-1]

ideal fixed displacement hydraulic pump

PU001-1 : All real parameters	Unit	Value
pump displacement	cc/rev	displ
typical speed of pump	rev/min	1000

PU001-1 : All integer parameters	Value
index of hydraulic fluid	0

reducerv [VRR000-1]

variable gear ratio (velocity port 1 input)

rotaryspeedsensor2 [MECRSS0A-1]

rotary speed sensor with offset and gain

MECRSS0A-1 : All real parameters	Unit	Value
offset to be subtracted from angular velocity	rev/min	0
gain for signal output	min/rev	1

MECRSS0A-1 : All integer parameters	Value
sign convention: positive from	port 3 to 1

tank01 [TK000-1]

tank modelled as constant pressure source

TK000-1 : All external variables with startvalues	Unit	Value
tank pressure	bar	0

Line submodels

hydraulic_1 [HL000-2]

simple compressibility hydraulic line (C)

HL000-2 : All external variables with startvalues	Unit	Value
pressure at port 1	bar	35

HL000-2 : All real parameters	Unit	Value
diameter of pipe	mm	20
pipe length	m	1
wall thickness	mm	1
Young's modulus for material	bar	2.06e+06
user specified effective bulk modulus	bar	8000

HL000-2 : All integer parameters	Value
1 for calculated bulk modulus value 2 for user specified value	1
index of hydraulic fluid	0

hydraulic_4 [HL000-1]

simple compressibility hydraulic line (C)

HL000-1 : All external variables with startvalues	Unit	Value
pressure at port 1	bar	0

HL000-1 : All real parameters	Unit	Value
diameter of pipe	mm	20
pipe length	m	1
wall thickness	mm	1
Young's modulus for material	bar	2.06e+06
user specified effective bulk modulus	bar	8000

HL000-1 : All integer parameters	Value
1 for calculated bulk modulus value 2 for user specified value	1
index of hydraulic fluid	0

Global parameters

Name	Title of real global parameter	Value	Unit
displ	pump displacement	4	cc/rev

Run Parameters

Run parameter	Value	Unit
Run type	Single	
Integrator type	Standard	
Start time	0	s
End time	1800	s
Communication interval	0.1	s
Tolerance	1e-005	
Maximum time step	1e+030	s
Solver type	Regular	
Error type	Mixed	
Simulation mode	Stabilizing + Dynamic	
Discontinuity printout	Off	
Activity index calculation	Off	
Power calculation	Off	
Energy calculation	Off	
Holds input constant	Off	

Appendix B: HTML report of the discharging model

HTML Report generated by LMS Imagine.Lab AMESim Rev13 SL3($a 7. Mrz 18:57:17 2020)

Circuit name

BasicModel_DischargingProcess

Circuit schematics

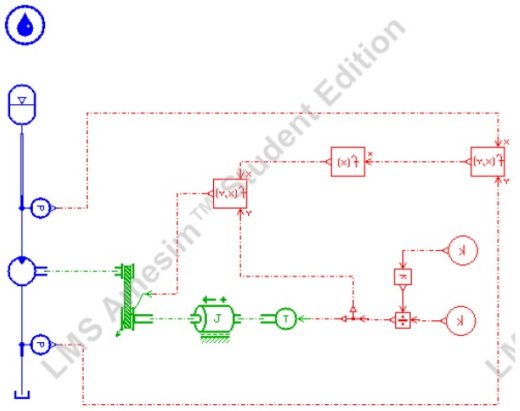

Component submodels

accumulator [HA0010-1]

hydraulic accumulator with heat exchange and with inlet orifice

HA0010-1 : All internal variables with startvalues	Unit	Value
gas volume	L	91
gas pressure	bar	98
liquid pressure in accumulator	bar	98

HA0010-1 : All real parameters	Unit	Value
accumulator volume	L	250
gas precharge pressure	bar	35
gas precharge temperature	degC	23
environment (liquid) temperature	degC	20
time constant for heat exchange	s	50
gas constant R	J/kg/K	287
heat capacitance Cv	J/kg/K	718
accumulator orifice diameter	mm	10
critical flow number	null	1000
maximum flow coefficient for orifice	null	0.7

HA0010-1 : All integer parameters	Value
index of hydraulic fluid	0

constant [CONS00-1]

constant signal

CONS00-1 : All real parameters	Unit	Value
P(G)	null	500

constant_1 [CONS00-2]

constant signal

CONS00-2 : All real parameters	Unit	Value
n(G)	null	3000

control04 [SPLT0-1]

splitter junction

division [DIV00-1]

divides input 3 by input 1

elect01 [GA00-1]

gain

GA00-1 : All real parameters	Unit	Value
n(G) to w(G)	null	2*PI/60

motor01 [MO001-1]

ideal fixed displacement hydraulic motor

MO001-1 : All real parameters	Unit	Value
motor displacement	cc/rev	displ1
typical speed of motor	rev/min	1000

MO001-1 : All integer parameters	Value
index of hydraulic fluid	0

pressuresensor [PT002-1]

hydraulic pressure sensor with offset and gain

PT002-1 : All real parameters	Unit	Value
offset to be subtracted from pressure	bar	0
gain for signal output	1/bar	1

elementaryhydraulicprops [FP04-1]

indexed hydraulic fluid properties

FP04-1 : All real parameters	Unit	Value
density	kg/m**3	1000
bulk modulus	bar	20000
slope of bulk modulus [bar] in function of pressure [bar] (in percentage)	null	0
absolute viscosity	cP	1.002
absolute viscosity of air/gas	cP	0.02
saturation pressure (for dissolved air/gas)	bar	1000
air/gas content	%	0.1
temperature	degC	23
temperature T1	degC	40
kinematic viscosity at (Patm, T1)	cSt	56.47
temperature T2	degC	100
kinematic viscosity at (Patm, T2)	cSt	9.71
coefficient for temperature viscosity characteristic	null	0.8
polytropic index for air/gas/vapor content	null	1.4
(advanced user) high saturated vapor pressure	bar	-0.5
(advanced user) low saturated vapor pressure	bar	-0.6
(advanced user) absolute viscosity of vapor	cP	0.02
(advanced user) effective molecular mass of vapor	null	200
(advanced user) air/gas density at atmospheric pressure 0 degC	kg/m**3	1.2
saturation pressure (for dissolved air/gas)	bar	0

FP04-1 : All integer parameters	Value
type of fluid properties	elementary
fuel type	ISO 4113
fluid property file	user data file
bulk modulus type	adiabatic
index of hydraulic fluid	0

FP04-1 : All text parameters	Value
name of fluid	Water
name of file specifying fluid properties	$AME/tutorial/tblprop1.txt

fofx [FX00-1]

output a prescribed function of input

FX00-1 : All text parameters	Value
T(M)	(displ1/1000000)*x/(2*PI)

fofxy [FXY0-1]

signal function of inputs x and y

FXY0-1 : All text parameters	Value
delta p [N/m^2]	((x+0.0001)-y)*100000

fofxy_1 [FXY0-2]

signal function of inputs x and y

FXY0-2 : All text parameters	Value
gear ratio alpha	y/x

reducerv [VRR001-1]

variable gear ratio (velocity port 2 input)

rotaryload2ports [RL04-1]

rotary load with two shafts (angle as output)

RL04-1 : All external variables with startvalues	Unit	Value
shaft speed at port 2	rev/min	0
shaft angle at port 2	degree	0

RL04-1 : All real parameters	Unit	Value
offset to be subtracted from angle	degree	0
moment of inertia	kgm**2	0.01
coefficient of viscous friction	Nm/(rev/min)	0.001061
Coulomb friction torque	Nm	0
stiction torque	Nm	0

RL04-1 : All integer parameters	Value
modulo option	no modulo

tank01 [TK000-1]

tank modelled as constant pressure source

TK000-1 : All external variables with startvalues	Unit	Value
tank pressure	bar	0

torquecon [TORQC-1]

conversion of signal to a torque in Nm

pressuresensor_1 [PT003-1]

hydraulic pressure sensor with offset and gain

PT003-1 : All real parameters	Unit	Value
offset to be subtracted from pressure	bar	0
gain for signal output	1/bar	1

Line submodels

hydraulic [HL000-1]

simple compressibility hydraulic line (C)

HL000-1 : All external variables with startvalues	Unit	Value
pressure at port 1	bar	98

HL000-1 : All real parameters	Unit	Value
diameter of pipe	mm	20
pipe length	m	1
wall thickness	mm	1
Young's modulus for material	bar	2.06e+06
user specified effective bulk modulus	bar	8000

HL000-1 : All integer parameters	Value
1 for calculated bulk modulus value 2 for user specified value	1
index of hydraulic fluid	0

Global parameters

Name	Title of real global parameter	Value	Unit
displ1	motor displacement	4	cc/rev

Run Parameters

Run parameter	Value	Unit
Run type	Single	
Integrator type	Standard	
Start time	0	s
End time	1800	s
Communication interval	0.1	s
Tolerance	1e-005	
Maximum time step	1e+030	s
Solver type	Regular	
Error type	Mixed	
Simulation mode	Stabilizing + Dynamic	
Discontinuity printout	Off	
Activity index calculation	Off	
Power calculation	Off	
Energy calculation	Off	
Holds input constant	Off	

Appendix C: HTML report of the merged model

HTML Report generated by LMS Imagine.Lab AMESim Rev13 SL3 (*Sa 7. Mrz 18:58:43 2020*)

Circuit name

BasicModel_Complete

Circuit schematics

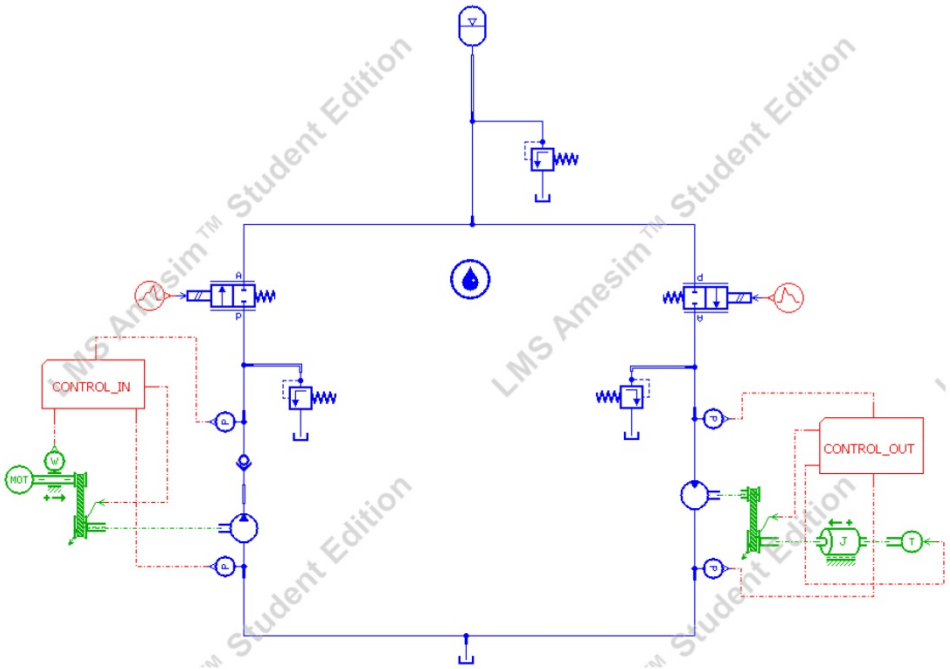

Component submodels

accumulator_1 [HA0010]

hydraulic accumulator with heat exchange and with inlet orifice

HA0010 : All internal variables with startvalues	Unit	Value
gas volume	L	249
gas pressure	bar	35
oil pressure in accumulator	bar	35

HA0010 : All real parameters	Unit	Value
accumulator volume	L	250
gas precharge pressure	bar	35
gas precharge temperature	degC	20
environment (oil) temperature	degC	20
time constant for heat exchange	s	50
gas constant R	J/kg/K	287
heat capacitance Cv	J/kg/K	718
accumulator orifice diameter	mm	5
critical flow number	null	1000
maximum flow coefficient for orifice	null	0.7

component_1 [CONTROL_IN]

component_2 [CONTROL_OUT]

elementaryhydraulicprops [FP04]

indexed hydraulic fluid properties

FP04 : All real parameters	Unit	Value
density	kg/m**3	1000
bulk modulus	bar	20000
slope of bulk modulus [bar] in function of pressure [bar] (in percentage)	null	0
absolute viscosity	cP	1.002
absolute viscosity of air/gas	cP	0.02
saturation pressure (for dissolved air/gas)	bar	1000
air/gas content	%	0.1
temperature	degC	20
temperature T1	degC	40
kinematic viscosity at (Patm, T1)	cSt	56.47
temperature T2	degC	100
kinematic viscosity at (Patm, T2)	cSt	9.71
coefficient for temperature viscosity characteristic	null	0.8
polytropic index for air/gas/vapor content	null	1.4
(advanced user) high saturated vapor pressure	bar	-0.5
(advanced user) low saturated vapor pressure	bar	-0.6
(advanced user) absolute viscosity of vapor	cP	0.02
(advanced user) effective molecular mass of vapor	null	200
(advanced user) air/gas density at atmospheric pressure 0 degC	kg/m**3	1.2
saturation pressure (for dissolved air/gas)	bar	0

FP04 : All integer parameters	Value
type of fluid properties	elementary
fuel type	ISO 4113
fluid property file	user data file
bulk modulus type	adiabatic
index of hydraulic fluid	0

FP04 : All text parameters	Value
name of fluid	Water
name of file specifying fluid properties	$AME/tutorial/tblprop1.txt

hydrnode3 [H3NODE2]

hydraulic junction 3 ports (pressure fixed by port 2)

hydrnode3_1 [H3NODE2]

hydraulic junction 3 ports (pressure fixed by port 2)

hydrnode3_2 [H3NODE3]

hydraulic junction 3 ports (pressure fixed by port 3)

hydrnode3_3 [H3NODE2]

hydraulic junction 3 ports (pressure fixed by port 2)

hydrnode3_4 [H3NODE2]

hydraulic junction 3 ports (pressure fixed by port 2)

motor01 [MO001]

ideal fixed displacement hydraulic motor

MO001 : All real parameters	Unit	Value
motor displacement	cc/rev	displ1
typical speed of motor	rev/min	1000

MO001 : All integer parameters	Value
index of hydraulic fluid	0

pmover01_1 [PM000]

constant speed prime mover

PM000 : All external variables with startvalues	Unit	Value
n(wt)	rev/min	300

presscontrol01 [RV000]

hydraulic relief valve

RV000 : All real parameters	Unit	Value
relief valve cracking pressure	bar	105
relief valve flow rate pressure gradient	L/min/bar	500
valve time constant	s	0.05
valve natural frequency	Hz	20
valve damping ratio	null	1.8
valve hysteresis	bar	0

RV000 : All integer parameters	Value
dynamics	no (static)
index of hydraulic fluid	0

RV000 : All parameter or variable groups	Title
valve dynamics	
integer parameter 1	dynamics
real parameter 3	valve time constant
real parameter 4	valve natural frequency
real parameter 5	valve damping ratio

presscontrol01_1 [RV000]

hydraulic relief valve

RV000 : All real parameters	Unit	Value
relief valve cracking pressure	bar	105
relief valve flow rate pressure gradient	L/min/bar	500
valve time constant	s	0.05
valve natural frequency	Hz	20
valve damping ratio	null	1.8
valve hysteresis	bar	0

RV000 : All integer parameters	Value
dynamics	no (static)
index of hydraulic fluid	0

RV000 : All parameter or variable groups	Title
valve dynamics	
integer parameter 1	dynamics
real parameter 3	valve time constant
real parameter 4	valve natural frequency
real parameter 5	valve damping ratio

presscontrol01_3 [RV000]

hydraulic relief valve

RV000 : All real parameters	Unit	Value
relief valve cracking pressure	bar	105
relief valve flow rate pressure gradient	L/min/bar	500
valve time constant	s	0.05
valve natural frequency	Hz	20
valve damping ratio	null	1.8
valve hysteresis	bar	0

RV000 : All integer parameters	Value
dynamics	no (static)
index of hydraulic fluid	0

RV000 : All parameter or variable groups	Title
valve dynamics	
integer parameter 1	dynamics
real parameter 3	valve time constant
real parameter 4	valve natural frequency
real parameter 5	valve damping ratio

presscontrol02_1 [CV000]

hydraulic check valve with linear characteristic

CV000 : All real parameters	Unit	Value
check valve cracking pressure	bar	0
check valve flow rate pressure gradient	L/min/bar	500
hysteresis for opening/closing	bar	0

CV000 : All integer parameters	Value
index of hydraulic fluid	0

pressuresensor_2 [PT002]

hydraulic pressure sensor with offset and gain

PT002 : All real parameters	Unit	Value
offset to be subtracted from pressure	bar	0
gain for signal output	1/bar	1

pressuresensor_3 [PT003]

hydraulic pressure sensor with offset and gain

PT003 : All real parameters	Unit	Value
offset to be subtracted from pressure	bar	0
gain for signal output	1/bar	1

pressuresensor_4 [PT002]

hydraulic pressure sensor with offset and gain

PT002 : All real parameters	Unit	Value
offset to be subtracted from pressure	bar	0
gain for signal output	1/bar	1

pressuresensor_5 [PT003]

hydraulic pressure sensor with offset and gain

PT003 : All real parameters	Unit	Value
offset to be subtracted from pressure	bar	0
gain for signal output	1/bar	1

pump01_1 [PU001]

ideal fixed displacement hydraulic pump

PU001 : All real parameters	Unit	Value
pump displacement	cc/rev	displ
typical speed of pump	rev/min	1000

PU001 : All integer parameters	Value
index of hydraulic fluid	0

reducerv_1 [VRR000]

variable gear ratio (velocity port 1 input)

reducerv_2 [VRR001]

variable gear ratio (velocity port 2 input)

rotaryload2ports [RL04]

rotary load with two shafts (angle as output)

RL04 : All external variables with startvalues	Unit	Value
shaft speed at port 2	rev/min	0
shaft angle at port 2	degree	0

RL04 : All real parameters	Unit	Value
offset to be subtracted from angle	degree	0
moment of inertia	kgm**2	0.01
coefficient of viscous friction	Nm/(rev/min)	0.001061
Coulomb friction torque	Nm	0
stiction torque	Nm	0

RL04 : All integer parameters	Value
modulo option	no modulo

rotaryspeedsensor2_1 [MECRSS0A]

rotary speed sensor with offset and gain

MECRSS0A : All real parameters	Unit	Value
offset to be subtracted from angular velocity	rev/min	0
gain for signal output	min/rev	1

MECRSS0A : All integer parameters	Value
sign convention: positive from	port 3 to 1

signal03 [UD00]

piecewise linear signal source

UD00 : All real parameters	Unit	Value
time at which duty cycle starts	s	0
output at start of stage 1	null	1
output at end of stage 1	null	1
duration of stage 1	s	tc
output at start of stage 2	null	0
output at end of stage 2	null	0
duration of stage 2	s	1e+06

UD00 : All integer parameters	Value
number of stages	2
cyclic	no

signal03_1 [UD00]

piecewise linear signal source

UD00 : All real parameters	Unit	Value
time at which duty cycle starts	s	0
output at start of stage 1	null	0
output at end of stage 1	null	0
duration of stage 1	s	tc+600
output at start of stage 2	null	1
output at end of stage 2	null	1
duration of stage 2	s	1e+06

UD00 : All integer parameters	Value
number of stages	2
cyclic	no

tank01 [TK000]

tank modelled as constant pressure source

TK000 : All external variables with startvalues	Unit	Value
tank pressure	bar	0

tank01_1 [TK000]

tank modelled as constant pressure source

TK000 : All external variables with startvalues	Unit	Value
tank pressure	bar	0

tank01_2 [TK000]

tank modelled as constant pressure source

TK000 : All external variables with startvalues	Unit	Value
tank pressure	bar	0

tank01_3 [TK000]

tank modelled as constant pressure source

TK000 : All external variables with startvalues	Unit	Value
tank pressure	bar	0

torquecon [TORQC]

conversion of signal to a torque in Nm

valve02 [PV0022]

2 position 2 port hydraulic control valve

PV0022 : All internal variables with startvalues	Unit	Value
fractional spool position	null	0
fractional spool velocity	1/s	0

PV0022 : All real parameters	Unit	Value
saturation of input value	null	1
valve time constant	s	0.05
valve natural frequency	Hz	20
valve damping ratio	null	1.8
characteristic flow rate at maximum opening	L/min	15
corresponding pressure drop	bar	0.01
equivalent cross sectional area at maximum opening	mm**2	20
maximum flow coefficient	null	0.7
critical flow number	null	1000
working density for pressure drop measurement	kg/m**3	850
working kinematic viscosity for pressure drop measurement	cSt	60

PV0022 : All integer parameters	Value
fluid properties for pressure drop measurement	from hydraulic fluid at reference conditions
parameter set for pressure drop	pressure drop/flow rate pair
spool dynamics	2nd order
index of hydraulic fluid	0

valve02_1 [PV0022]

2 position 2 port hydraulic control valve

PV0022 : All internal variables with startvalues	Unit	Value
fractional spool position	null	0
fractional spool velocity	1/s	0

PV0022 : All real parameters	Unit	Value
saturation of input value	null	1
valve time constant	s	0.05
valve natural frequency	Hz	20
valve damping ratio	null	1.8
characteristic flow rate at maximum opening	L/min	15
corresponding pressure drop	bar	0.01
equivalent cross sectional area at maximum opening	mm**2	20
maximum flow coefficient	null	0.7
critical flow number	null	1000
working density for pressure drop measurement	kg/m**3	850
working kinematic viscosity for pressure drop measurement	cSt	60

PV0022 : All integer parameters	Value
fluid properties for pressure drop measurement	from hydraulic fluid at reference conditions
parameter set for pressure drop	pressure drop/flow rate pair
spool dynamics	2nd order
index of hydraulic fluid	0

Line submodels

hydraulic_12 [HL000]

simple compressibility hydraulic line (C)

HL000 : All external variables with startvalues	Unit	Value
pressure at port 1	bar	97

HL000 : All real parameters	Unit	Value
diameter of pipe	mm	20
pipe length	m	1
wall thickness	mm	1
Young's modulus for material	bar	2.06e+06
user specified effective bulk modulus	bar	8000

HL000 : All integer parameters	Value
1 for calculated bulk modulus value 2 for user specified value	1
index of hydraulic fluid	0

hydraulic_2 [HL000]

simple compressibility hydraulic line (C)

HL000 : All external variables with startvalues	Unit	Value
pressure at port 1	bar	0

HL000 : All real parameters	Unit	Value
diameter of pipe	mm	20
pipe length	m	1
wall thickness	mm	1
Young's modulus for material	bar	2.06e+06
user specified effective bulk modulus	bar	8000

HL000 : All integer parameters	Value
1 for calculated bulk modulus value 2 for user specified value	1
index of hydraulic fluid	0

hydraulic_6 [HL000]

simple compressibility hydraulic line (C)

HL000 : All external variables with startvalues	Unit	Value
pressure at port 1	bar	35

HL000 : All real parameters	Unit	Value
diameter of pipe	mm	20
pipe length	m	1
wall thickness	mm	1
Young's modulus for material	bar	2.06e+06
user specified effective bulk modulus	bar	8000

HL000 : All integer parameters	Value
1 for calculated bulk modulus value 2 for user specified value	1
index of hydraulic fluid	0

hydraulic_9 [HL000]

simple compressibility hydraulic line (C)

HL000 : All external variables with startvalues	Unit	Value
pressure at port 1	bar	35

HL000 : All real parameters	Unit	Value
diameter of pipe	mm	20
pipe length	m	1
wall thickness	mm	1
Young's modulus for material	bar	2.06e+06
user specified effective bulk modulus	bar	8000

HL000 : All integer parameters	Value
1 for calculated bulk modulus value 2 for user specified value	1
index of hydraulic fluid	0

Global parameters

Name	Title of real global parameter	Value	Unit
tc	charging time	1800	s
displ1	motor displacement	4	cc/rev
displ	pump displacement	4	cc/rev

Run Parameters

Run parameter	Value	Unit
Run type	Single	
Integrator type	Standard	
Start time	0	s
End time	4300	s
Communication interval	0.1	s
Tolerance	1e-005	
Maximum time step	1e+030	s
Solver type	Regular	
Error type	Mixed	
Simulation mode	Stabilizing + Dynamic	
Discontinuity printout	Off	
Activity index calculation	Off	
Power calculation	Off	
Energy calculation	Off	
Holds input constant	Off	